2013-06-18

A Role for Intraflagellar Transport Proteins in Mitosis: A Dissertation

Alison R. Bright
University of Massachusetts Medical School

A ROLE FOR INTRAFLAGELLAR TRANSPORT PROTEINS IN MITOSIS

A Dissertation Presented

By

ALISON BRIGHT

Submitted to the Faculty of the
University of Massachusetts Graduate School of Biomedical Sciences, Worcester
in partial fulfillment of the requirements for the degree of

DOCTOR OF PHILOSOPHY

JUNE 18TH, 2013

INTERDISCIPLINARY GRADUATE PROGRAM

A ROLE FOR INTRAFLAGELLAR TRANSPORT PROTEINS IN MITOSIS

Dissertation Presented By

Alison Rebecca Bright

The signatures of the Dissertation Committee signify completion and approval as to style and content of the Dissertation

_____
Stephen Doxsey, Ph.D., Thesis Advisor

_____
Jennifer Benanti, Ph.D., Member of Committee

_____
Wei-Lih Lee, Ph.D., Member of Committee

_____
Nicholas Rhind, Ph.D., Member of Committee

_____
William Theurkauf, Ph.D., Member of Committee

The signature of the Chair of the Committee signifies that the written dissertation meets the requirements of the Dissertation Committee

_____
George Witman, Ph.D., Chair of Committee

The signature of the Dean of the Graduate School of Biomedical Sciences signifies that the student has met all graduation requirements of the school.

_____
Anthony Carruthers, Ph.D.,
Dean of the Graduate School of Biomedical Sciences

Interdisciplinary Graduate Program

June 18, 2013

ABSTRACT

Disruption of cilia proteins results in a range of disorders called ciliopathies. However, the mechanism by which cilia dysfunction contributes to disease is not well understood. Intraflagellar transport (IFT) proteins are required for ciliogenesis. They carry ciliary cargo along the microtubule axoneme while riding microtubule motors. Interestingly, IFT proteins localize to spindle poles in non-ciliated, mitotic cells, suggesting a mitotic function for IFT proteins. Based on their role in cilia, we hypothesized that IFT proteins regulate microtubule-based transport during mitotic spindle assembly. Biochemical investigation revealed that in mitotic cells IFT88, IFT57, IFT52, and IFT20 interact with dynein1, a microtubule motor required for spindle pole maturation. Furthermore, IFT88 co-localizes with dynein1 and its mitotic cargo during spindle assembly, suggesting a role for IFT88 in regulating dynein-mediated transport to spindle poles. Based on these results we analyzed spindle poles after IFT protein depletion and found that IFT88 depletion disrupted EB1, γ-tubulin, and astral microtubule arrays at spindle poles. Unlike IFT88, depletion of IFT57, IFT52, or IFT20 did not disrupt spindle poles. Strikingly, the simultaneous depletion of IFT88 and IFT20 rescued the spindle pole disruption caused by IFT88 depletion alone, suggesting a model in which IFT88 negatively regulates IFT20, and IFT20 negatively regulates microtubule-based transport during mitosis. Our work demonstrates for the first time that IFT proteins function with dynein1 in mitosis, and it also raises the important possibility that mitotic defects caused by IFT protein disruption could contribute to the phenotypes associated with ciliopathies.

COPYRIGHTED MATERIAL

TABLE OF CONTENTS

LIST OF FIGURES

ABBREVIATIONS

IFT	Intraflagellar transport
Dynein1	Cytoplasmic dynein 1
Dynein2	Cytoplasmic dynein 2 aka Cytoplasmic dynein 1b
Basal body	Mother centriole of centrosome, base of primary cilium
Spindle pole	Mitotic centrosome
APC	Antigen presenting cell
TCR	T cell receptor complex
PKD	Polycystic kidney disease
Transport-complex	Appears in Chapter IV. Refers to complexes containing IFT proteins, microtubule motor, and cargo

MULTIMEDIA OBJECTS

The following are supplementary movies associated with the work presented in Chapter II. They can be viewed by following this link:

http://www.nature.com/ncb/journal/v13/n4/full/ncb2202.html#supplementary-information

Movie II-S1
Time-lapse movie of a control GFP-α tubulin LLC-PK1 prometaphase cell showing minus-end directed motion of peripheral MT clusters (arrows) toward spindle pole.

Movie II-S2
Time-lapse movie of a control GFP-α tubulin LLC-PK1 metaphase cell showing minus-end directed motion and subsequent integration of a peripheral MT cluster (arrow) into a spindle pole.

Movie II-S3
Time-lapse movie of an IFT88-depleted GFP-α tubulin LLC-PK1 prometaphase cell showing peripheral MT clusters accumulation in the cytoplasm. These clusters (arrow) are not moving toward spindle poles.

Movie II-S4
Time-lapse movie of an IFT88-depleted GFP-α tubulin LLC-PK1 metaphase cell, showing a peripheral MT cluster not moving toward spindle pole.

Movie II-S5
Time-lapse movie of a GFP-IFT88 LLC-PK1 metaphase cell showing one of the IFT88 foci (arrow) moving toward a spindle pole.

PREFACE

Chapter II represents co-authored work. Please see Chapter II, page 24 for a detailed list of author contributions. Appendix A represents a small but important data set that provides perspective on topics discussed in Chapter IV.

CHAPTER I

GENERAL INTRODUCTION

Cilia are involved in movement, sensation, and signaling[1,2], while mitotic spindles are required for chromosome segregation and orientation of the cell division axis during mitosis[3,4]. Although their functions are different, both structures form around centrosomes, and both are assembled and maintained through the action of microtubule-based, motor-driven transport. Strikingly, we found that IFT proteins, known regulators of microtubule-based cargo transport within cilia, also regulate microtubule-mediated transport of spindle pole cargo. The IFT protein driven bidirectional transport mechanisms for both spindle pole cargo in dividing cells and ciliary cargo in differentiated tissue (non-dividing cells) suggests that some (if not all) ciliary proteins may have extra-ciliary functions. Here I will introduce findings supporting ciliary proteins having non-ciliary (e.g. mitotic) mechanisms and argue that these non-ciliary mechanisms may underlie the genesis of ciliopathies.

The centrosome is the root of two cellular structures

The centrosome, the primary microtubule-organizing center (MTOC) in the cell, regulates cell motility, polarity, adhesion, and shape (reviewed in [5–7]). At different stages of the cell cycle the centrosome initiates the generation of different cellular structures. In interphase (G_1) cells, or cells that have exited the cell cycle (G_0), the mother centriole (basal body) of the centrosome can template, and become the base of the primary

cilium[1,5–7]. In cycling cells, the centrosome duplicates during S phase so that during mitosis the duplicated centrosomes (spindle poles), can move to opposite sides of the cell where they nucleate, organize, and anchor microtubules, which form the mitotic spindle[7]. With roles in both cilia and spindle formation, the centrosome is the common link between previous studies of ciliary IFT proteins and the work I will present in this thesis, characterizing IFT protein regulation of spindle assembly.

Cilia and spindles are assembled through similar processes

Cilia, which can form on almost every cell type in the body, function in movement, sensation, and signaling (reviewed in [1,2,8]). They are assembled when the centrosome in a G_1 or G_0 cell docks at the cell cortex. Nine doublet microtubules are extended from the basal body to form the long ciliary axoneme which projects out of the cell body, encased by a ciliary membrane that is continuous with the cell's plasma membrane[1,2]. Cilia are assembled through a microtubule-based bidirectional transport system called intraflagellar transport (IFT). Within this system a microtubule plus end-directed motor, kinesin-II propels ciliary cargo along the microtubule axoneme from the base of the cilium to the tip (anterograde movement). Cytoplasmic dynein 2 (dynein2), a microtubule minus end-directed motor powers movement from the tip of the cilium to the base (retrograde movement, Figure I-1). Ciliary cargoes are proteins required for cilia growth or function that need to be transported to the appropriate place within the cilium for incorporation after their synthesis within the cell body. IFT particles, that consist of two IFT protein complexes, A and B, are required for IFT and ciliogenesis, and are

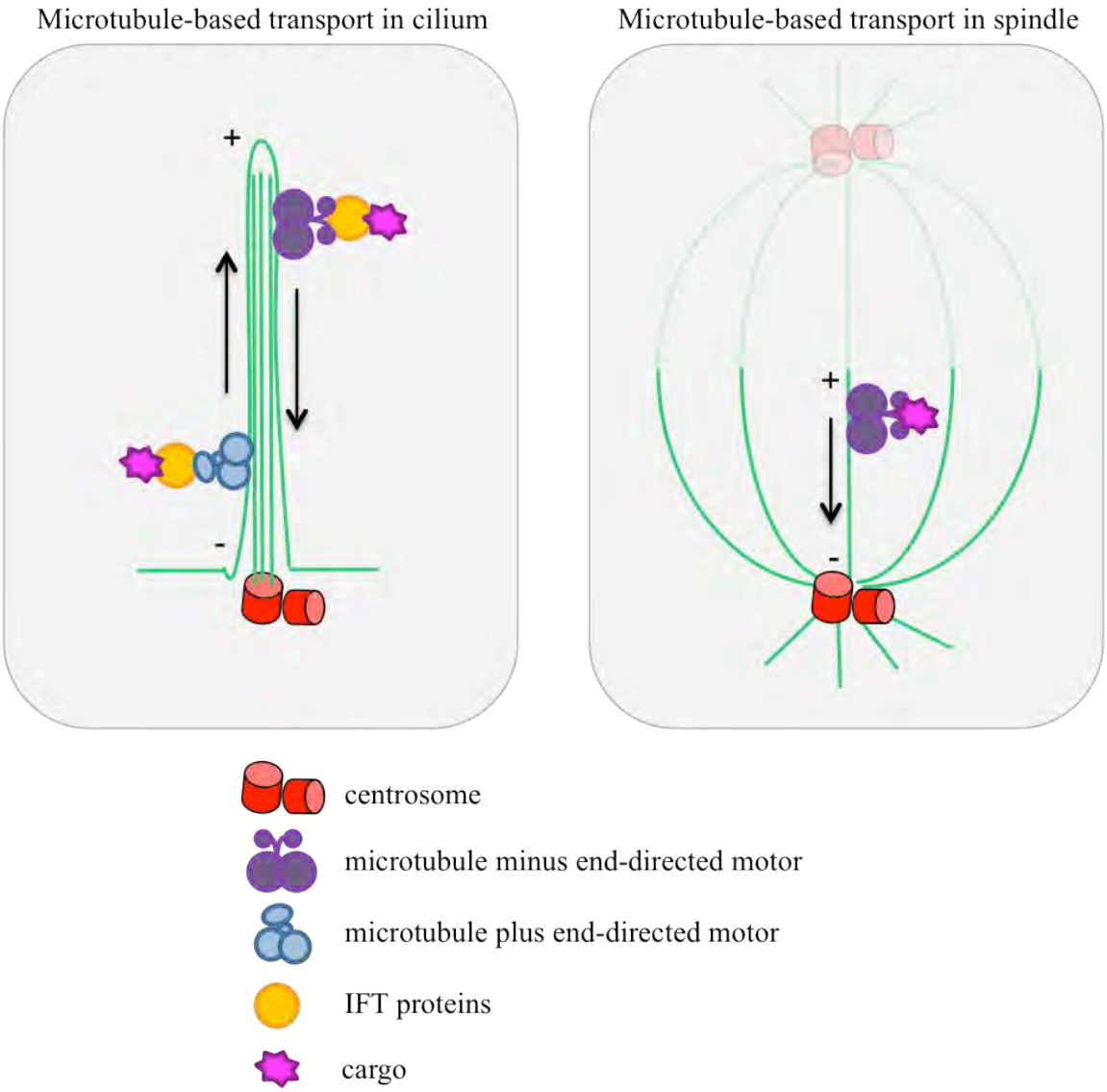

Figure I-1 Cilium and spindle are assembled and maintained through microtubule-based transport.
In cilia, a microtubule plus end-directed motor (kinesin-II) carries ciliary cargo from the base of the cilium to the tip. A microtubule minus end-directed motor (dynein2) carries cargo from the tip of the cilium back to the base. IFT proteins are thought to act as cargo adaptors that link cilia cargo with cilia motors. In mitotic spindles, a microtubule minus end-directed motor (dynein1) carries cargo from the cytoplasm to the spindle pole, for example during centrosome maturation and spindle assembly.

proposed to function as adaptors that link ciliary cargo with ciliary motors. Thus, cilia are built and maintained through a microtubule-based transport system.

Like cilia, the mitotic spindle is another cellular structure composed of an organized network of microtubules focused around centrosomes, which relies on microtubule motors for assembly and maintenance. The mitotic spindle provides a physical platform for accurate chromosome segregation and sets the orientation for cell division during mitosis (reviewed in [3,4]). The main microtubule motor involved in spindle assembly is the microtubule minus-end directed motor, dynein1. Although dynein1 performs many mitotic functions, its role in centrosome maturation as cells transition from G_2 to mitosis, is most reminiscent of ciliary IFT. In this role, dynein1 transports spindle pole cargo (contributors to microtubule nucleation) from the cytoplasm to the microtubule minus ends anchored at spindle poles, increasing the microtubule nucleating capacity at spindle poles (Figure I-1). The parallels between cilia and spindle formation suggest the possibility that the two processes may share key components.

“Cilia” proteins versus “centrosome” proteins

Over the years, many proteins have been classified as “cilia” or “centrosome” proteins based on their first-characterized localization and/or function within the cell. A previous study by Jurczyk *et al*[9], highlights the shortcomings of this classification system. This study focused on pericentrin, originally characterized as a centrosome protein based on its localization to MTOCs and its importance for microtubule nucleation and spindle assembly[10], and IFT proteins, classically considered cilia proteins based on their

discovery within the IFT complex purified from *Chlamydomonas* flagella[11]. Despite its centrosomal classification, Jurczyk *et al* found that pericentrin purifies with IFT complexes from mouse testes, forms a complex with cilia proteins IFT20 and IFT88, and is required for ciliogenesis. A later study supports this work, demonstrating that ten of eleven examined centrosome proteins are required for ciliogenesis[12]. Thus, regulation of ciliogenesis by a centrosome protein is not specific to pericentrin, but is a conserved feature amongst many centrosome proteins. Not only do centrosome-associated proteins have roles in ciliogenesis, but cilia-associated proteins also contribute to centrosome function. The same study from Jurczyk *et al* found cilia-associated IFT88 in purified centrosome preparations, and demonstrated that cilia-associated IFT20 contributes to centrosome integrity, as it is required for pericentrin's localization to the centrosome[9]. Furthermore, three cilia-localized[13–17] transmembrane proteins, polycystin-1, polycystin-2, and fibrocystin have recently been implicated in centrosome amplification[18–20]. Several mechanisms can contribute to centrosome amplification, including over-duplication of centrioles during S phase, cytokinesis (the final step of mitosis during which daughter cells are separated) failure, and cell fusion[21]. Further experiments are required to determine how polycystin-1, polycystin-2, or fibrocystin disruption results in increased numbers of centrosomes, but interestingly polycystin-2 and fibrocystin localize to spindle poles and spindles, and polycystin-2 depends on diaphanous, a protein important for cytokinesis[22], for its localization to the spindle[23]. This suggests that at least in the case of polycystin-2, centrosomes may accumulate via cytokinesis failure. Whether these ciliary transmembrane proteins remain membrane-bound at the spindle, if they function as

intracellular channels, and how their disruption ultimately contributes to centrosome accumulation are questions that still need to be answered.

Together these studies demonstrate that centrosome-associated proteins contribute to ciliogenesis, and cilia-associated proteins contribute to centrosome integrity. They also suggest the likelihood that additional roles for "cilia" proteins in centrosome function, and "centrosome" proteins in cilia function, exist and should be identified. This along with the similarities between the assembly pathways for cilia and mitotic spindles, as well as the localization of IFT proteins to spindle poles[24–27] spurred our investigation of IFT protein function in spindle assembly.

Roles for IFT proteins outside of cilia

IFT proteins have traditionally been characterized as members of IFT particles, involved in the bidirectional IFT transport process required for cilia generation and maintenance. In this context IFT proteins are organized into two complexes, IFT complex A and IFT complex B, which dissociate from one another under high salt conditions[11]. IFT complex A is composed of six known proteins: IFT144, IFT140, IFT139, IFT122, IFT121, and IFT43; and IFT complex B is composed of 14 known proteins: IFT172, IFT88, IFT81, IFT80, IFT74 (aka IFT72), IFT70, IFT57, IFT54, IFT52, IFT46, IFT27, IFT25, IFT22, and IFT20[2]. In addition to their association with ciliary IFT, several studies implicate functions for IFT proteins as well as the IFT microtubule plus end-directed motor, kinesin-II, outside of cilia.

One IFT protein with characterized extra-ciliary function is IFT88. Before IFT88 was identified as a member of the IFT complex required for ciliogenesis, mutations within Tg737, the gene that encodes IFT88, were associated with over-proliferation of liver progenitor cells in mice[28]. Based on the high rate of mutations found within the Tg737 gene in human liver tumors and tumor cell lines, and the rescue incurred by Tg737 re-expression, the gene was classified as a tumor suppressor[29]. In line with this early work, more recent studies in non-ciliated cells demonstrate a role for IFT88 in cell-cycle progression[25]. IFT88 depletion results in an increase in cell-cycling, while over-expression of IFT88 causes a cell-cycle arrest in G_1[25]. The G_1 arrest is instituted by an interaction between IFT88 and Che-1 that competitively inhibits Che-1's ability to interact with the tumor suppressor Rb, leaving Rb free to repress E2F1, a transcription factor whose activation is required for the G_1/S transition[25]. Our work also suggests that IFT88 affects cell-cycle progression through its role in mitotic spindle assembly and orientation. Together these findings demonstrate multifaceted roles for IFT88 in the regulation of cell-cycle. Further experiments are necessary to identify all the mechanisms by which IFT88 influences cell-cycle progression, and how those mechanisms may feedback upon one another.

While IFT20 was first discovered for its function in intraflagellar transport, research has since identified roles for IFT20 outside of cilia. For example, IFT20 has been shown to co-localize with the cis-Golgi complex in a GMAP210 dependent manner[26,30]. When IFT20 is depleted in cells, the ciliary membrane protein, polycystin-2, is reduced in cilia, suggesting that IFT20 may be involved in trafficking polycystin-2

from its synthesis site in the ER to the cilium[26]. IFT20 maintains its localization at the Golgi and post-Golgi compartments in lymphoid cells[31], one of the few cell types that do not form cilia. When lymphoid T cells make contact with antigen presenting cells (APCs) bearing cognate peptide antigen, an immune synapse rich with T cell receptors (TCRs) is formed between the two cells. To create the immune synapse, the T cell undergoes a dramatic cytoskeletal rearrangement, with the centrosome and Golgi apparatus reorienting to the cell cortex in contact with the APC. TCRs are targeted to the immune synapse through a combination of polarized recycling, lateral diffusion, and cytoskeleton-driven movement[32]. In response to T cell activation, IFT20 reorients toward the immune synapse along with the Golgi apparatus, and is induced to form a complex with members of the TCR/CD3 complex (CD3 molecules form a complex with TCRs and are responsible for TCR signal transduction[33]). Furthermore, IFT20 is required for the clustering of TCR/CD3 complexes to the synapse via polarized recycling. In this capacity, IFT20 interacts with two other IFT complex members, IFT88 and IFT57[31], suggesting that not just IFT20, but IFT complex B participates in TCR/CD3 trafficking to the immune synapse. Together these data define a role for IFT20 in intracellular trafficking that is conserved in ciliated and non-ciliated cells.

Two more proteins involved in ciliary IFT, IFT27 and kinesin-II, have also been implicated in roles outside of the cilium, but their mechanisms of action are not yet clear. IFT27, a Rab-like GTPase, causes a growth delay when depleted in *Chlamydomonas*[34]. Further inspection revealed an increase in multinucleated cells after IFT27 depletion[34], suggesting the protein may function in cytokinesis. Additionally, the IFT microtubule

plus end-directed motor, kinesin-II localizes to the mitotic spindle[35,36], and when mutated induces chromosome loss in *Chlamydomonas,* and aneuploidy and multipolar spindles in NIH3T3 cells[36,37]. These findings suggest that both IFT27 and kinesin-II function during mitosis, however further investigation is required to understand how they are mechanistically involved in cell division.

Possible mechanisms underlying ciliopathies

Over the past 10-15 years primary (sensory) cilia dysfunction has become associated with several human disorders, collectively termed ciliopathies. Primary cilia form on almost every cell type in the body, thus the phenotypes that result from their disruption are often syndromic, and can include cystic kidneys, polydactyly, *situs inversus*, obesity, and encephalocele[38]. Research aimed at understanding how cilia dysfuntion causes ciliopathies has produced several enticing hypotheses that include the disruption of Hh signaling leading to polydactyly, and defects in Ca^{2+} or PCP signaling contributing to cystogenesis. However, these hypotheses have led to few solid answers, particularly in relation to the etiology of cystic kidneys, a phenotype shared by many ciliopathies. This lead me to propose an alternative hypothesis based on my findings in Chapters II and III: that the direct role for IFT88 and IFT20 in regulating spindle assembly and orientation may cause cystogenesis when these proteins are disrupted.

Indeed, the study of normal kidney tubule development supports the idea that cystic kidneys may be a result of misoriented cell divisions[39]. Kidney tubules are formed through a strictly organized, massive, cellular proliferation during nephron

morphogenesis, in which daughter cells insert themselves into the growing tissue layer such that tubules are specifically elongated, but not widened[40]. This directional growth pattern is made possible by the intrinsic polarity of dividing kidney cells, which align their mitotic spindles parallel with the developing kidney tubule[39]. However, in ciliopathy animal models for polycystic kidney disease (PKD) the intrinsic polarity normally exhibited during kidney tubule elongation is lost. Misoriented cell divisions have been observed in cystic kidney tubules, and have also been found prior to cyst formation, suggesting that misoriented cell division is the underlying cause of cystic kidneys[39].

One ciliopathy, polycystic kidney disease (PKD), was first associated with primary cilia dysfunction when the mutated gene within the Oak Ridge Polycystic Kidney (ORPK) mouse model was identified as IFT protein, IFT88 and disruption of cilia within cystic kidney tubules was observed[41]. It has been proposed that the non-canonical Wnt signaling pathway, also known as the planar cell polarity (PCP) pathway, is the link between cilia dysfunction and spindle misorientation observed in cystogenesis. This signaling cascade dictates organ shape in *Drosophila* through its regulation of spindle orientation during development[42]. It also contributes to stereocilia bundle organization within hair cells of the vertebrate inner ear[43]. Several studies have implicated cilia in the transduction of PCP signaling. One cilia protein, Inversin, behaves like a molecular switch between the canonical Wnt and PCP signaling pathways[44]. Other studies show that in the absence of cilia, the canonical Wnt pathway is hypersensitive to activation by Wnt ligands[45,46]. Because the PCP pathway is important for tissue organization, and cilia are important for PCP signaling, and both tissue organization and cilia are disrupted in PKD

mouse models, it was hypothesized that the kidney cysts associated with PKD are a result of defective PCP signaling caused by disrupted cilia. However, a more recent study has shown that cilia and retrograde IFT are not required for canonical Wnt signaling, or for appropriate switching between canonical Wnt and PCP signaling pathways, calling into question defective PCP signaling as the primary cause of cystic kidneys[47]. Future studies that examine kidney tubule formation in PCP mutant mice, as well as the ability of PKD animal models to transduce PCP signals, will help to clarify the possible contributions of PCP signaling and cilia disruption to cyst formation.

In light of the many roles that cilia proteins perform outside of cilia, it may be important to think outside the cilium to understand how ciliopathies occur. Intriguingly, in Chapters II and III we show that IFT88 and IFT20 co-regulate mitotic progression, and that IFT88 in particular, directly regulates spindle orientation through its role in the formation of robust astral microtubule arrays. Thus, it's possible that kidney cysts arise from mitotic dysfunction associated with IFT88 disruption. Renal cysts are a conserved phenotype amongst many ciliopathy syndromes including Bardet-Biedl, Oral-Facial-Digital, Senior-Loken, Meckel, and Joubert sydnromes[48]. Future experiments are required to assess the possible contribution of the many cilia proteins whose disruption is associated with these ciliopathy syndromes, to the regulation of mitotic spindle assembly and orientation. Perhaps a mitotic mechanism for cyst formation will also be a conserved feature amongst these ciliopathies.

In summary, we are interested in the cross talk between "cilia" and "centrosome" protein functions. The established role for centrosome-associated proteins in ciliogenesis

and for cilia-associated proteins in centrosome function, the parallels between cilia and mitotic spindle assembly, and the continued localization of IFT proteins at spindle poles in non-ciliated cells inspired us to investigate roles for IFT proteins during mitosis. In Chapter II I will describe IFT88's role in the regulation of spindle assembly and spindle orientation in non-ciliated, mitotic cells. In Chapter III I will investigate a role for three additional IFT proteins in mitosis, and describe a novel regulatory relationship between IFT88 and IFT20, which together mediate mitotic progression.

CHAPTER II

THE CILIA PROTEIN IFT88 IS REQUIRED FOR SPINDLE ORIENTATION IN MITOSIS

Delaval B, Bright A, Lawson ND, Doxsey S

Author contributions

Main figures:
Contributions by Alison Bright
Figure II-1a, Figure II-1b (disrupted poles and misaligned chromosomes categories), Figure II-1 e and f, Figure II-2d (disrupted γ-tubulin category), Figure II-2 f-h, Figure II-3 f-g, Figure II-4 b-e, Figure II-5a, Figure II-5 e-f

Contributions by Dr. Benedicte Delaval
Figure II-1b (spindle tilt category), Figure II-1 c and d, Figure II-1 g and h, Figure II-2 a-c, Figure II-2d (disrupted EB1 category), Figure II-2e, Figure II-3 a-e, Figure II-4a, Figure II-4f , Figure II-5 b-d, Figure II-5g

Supplementary Figures:
Contributions by Alison Bright
Figure II-S1a, Figure II-S1 c-e, Figure II-S8 e-f

Contributions by Dr. Benedicte Delaval
Figure II-S1b, Figure II-S2, Figure II-S3, Figure II-S4, Figure II-S5, Figure II-S6, Figure II-S7, Figure II-S8 a-d, Moveies II-S1-5

Abstract

Cilia dysfunction has long been associated with cyst formation and ciliopathies[49]. More recently, misoriented cell division has been observed in cystic kidneys[39], but the molecular mechanism leading to this abnormality remains unclear. Proteins of the intraflagellar transport (IFT) machinery are linked to cystogenesis and are required for cilia formation in non-cycling cells[41,50]. Several IFT proteins also localize to spindle poles in mitosis[24–27], indicating uncharacterized functions for these proteins in dividing cells. Here, we show that IFT88 depletion induces mitotic defects in human cultured cells, in kidney cells from the IFT88 mouse mutant *Tg737*^{orpk} and in zebrafish embryos. In mitosis, IFT88 is part of a dynein1-driven complex that transports peripheral microtubule clusters containing microtubule-nucleating proteins to spindle poles to ensure proper formation of astral microtubule arrays and thus proper spindle orientation. This work identifies a mitotic mechanism for a cilia protein in the orientation of cell division and has important implications for the etiology of ciliopathies.

Results and Discussion

In non-cycling cells, centrosomes (basal bodies) contribute to the assembly of primary cilia[51] through intraflagellar transport, an intra-cellular motility system in which protein complexes are transported bidirectionally along the cilium[1,52,53]. During mitosis, centrosomes (spindle poles) participate in the organization and orientation of the spindle[54–56]. In this context, astral microtubules interact with spindle microtubules to facilitate chromosome segregation[54] and with the cell cortex to orient the spindle[55,56]. One

of the best-studied IFT proteins, IFT88, which was first characterized for its role in cilia formation and polycystic kidney disease[41,57–60], also localizes to spindle poles during mitosis[25].

To test for mitotic functions of IFT88, the protein was depleted in several experimental systems. In HeLa cells, defects in mitosis were first indicated by an increased mitotic index and delayed mitotic progression (Supplementary Figure. II-S1a–e). Closer inspection revealed spindle pole disruption, chromosome misalignment and spindle misorientation (Figure II-1a,b). The spindle angle relative to the cell–substrate adhesion plane[56] (Figure II-1c,d) of most IFT88-depleted cells (~80%) was greater than 10°, whereas control spindles were usually parallel to the substratum (Figure II-1d), demonstrating a critical role for IFT88 in spindle orientation. Time-lapse microscopy imaging showed that spindle misorientation resulted in misoriented cell divisions, where one daughter cell divided outside the plane of the substratum, thus delaying adherence to the substrate (Figure II-1e,f). Despite misorientation, spindles were largely bipolar (Figure II-1a) and cells ultimately progressed through division (Figure II-1f and Supplementary Figure II-S1d). Given the role of IFT88 in cystic kidney formation[41], IFT88 disruption was examined in kidney cell lines by siRNA (porcine LLC-PK1; Supplementary Figure II-S2a–c) and by mutation (murine *Tg737*^{orpk} ; Figure II-1g and Supplementary Figure II-S2d) and showed similar mitotic defects. In zebrafish embryos, IFT88 depletion by morpholino oligonucleotides known to induce

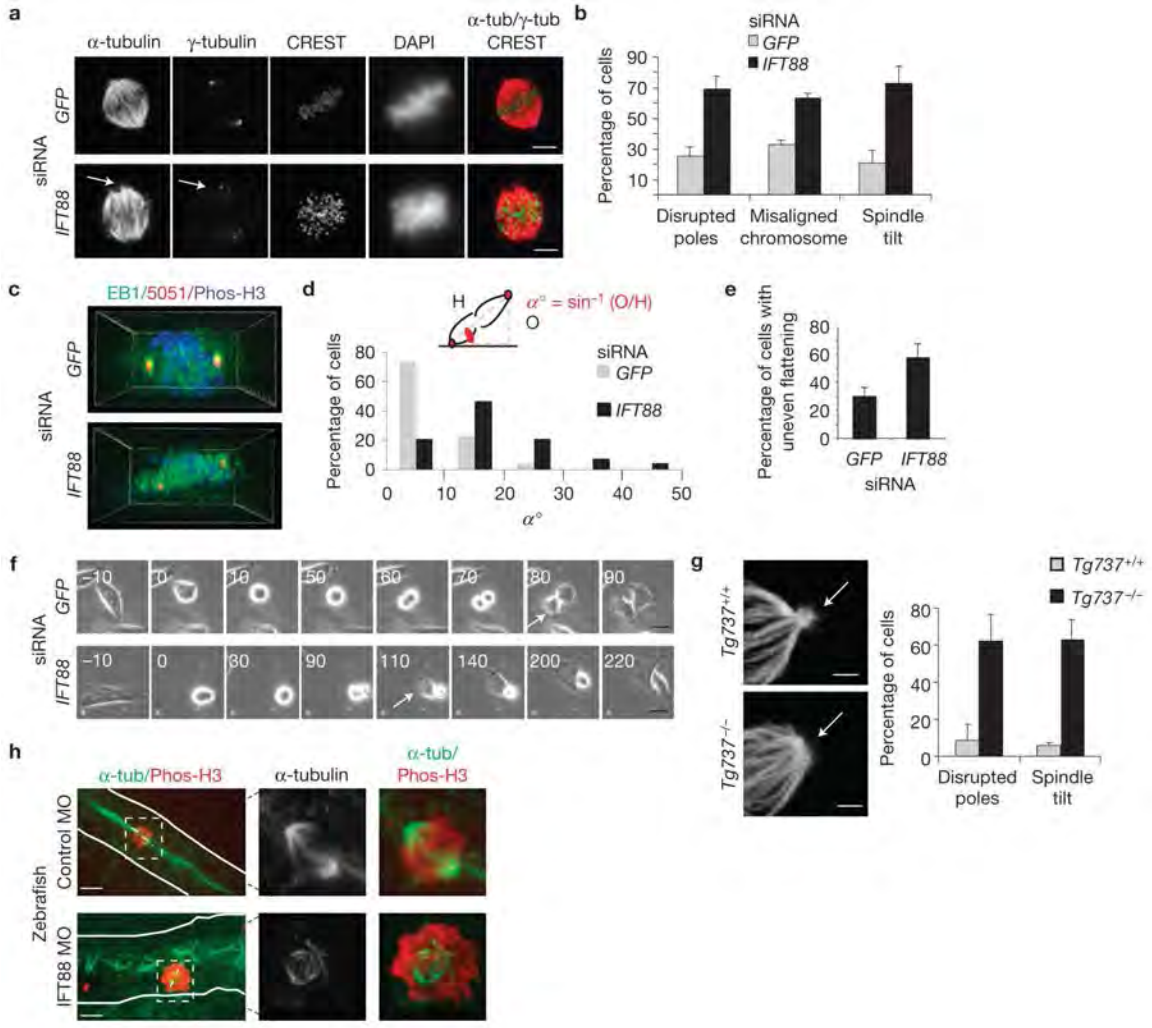
a
α-tubulin
γ-tubulin
CREST
DAPI
α-tub/γ-tub CREST
siRNA
GFP
IFT88
b
siRNA
GFP
IFT88
Percentage of cells
Disrupted poles
Misaligned chromosome
Spindle tilt
c
EB1/5051/Phos-H3
d
H
O
α° = sin⁻¹ (O/H)
Percentage of cells
α°
e
Percentage of cells with uneven flattening
f
g
Tg737+/+
Tg737−/−
h
α-tub/Phos-H3
α-tubulin
α-tub/ Phos-H3
Zebrafish
Control MO
IFT88 MO

Figure II-1

Figure II-1 IFT88 depletion leads to mitotic defects in HeLa cells, kidney cells from the *Tg737 ^{orpk}* mouse mutant and zebrafish.
(a) Immunofluorescence microscopy images of control (GFP) and IFT88-siRNA-treated mitotic HeLa cells. α-tubulin (microtubules) and γ-tubulin (spindle poles, arrow) staining show spindle pole defects. CREST (kinetochores) or DAPI (DNA) staining shows misaligned chromosomes. Scale bars, 5 μm. **(b)** Quantification of mitotic defects following IFT88- or control (GFP)-siRNA treatment in HeLa cells. Defects include disrupted poles (α- and γ-tubulin), misaligned chromosomes (DAPI staining) and spindle misorientation (spindle tilt, spindle poles in different focal planes). *n* = 70 mitotic cells per experiment. **(c)** Side views of 3D reconstructed immunofluoresence images showing misoriented mitotic spindles in IFT88- versus control-siRNA-treated HeLa cells. Spindle (EB1), centrosomes (5051) and DNA (Phos-H3). **(d)** Histogram showing metaphase spindle-angle distribution in control- and IFT88-siRNA-treated cells. *n* = 30 mitotic spindles. Schematic (top) showing spindle angle (α) measurement. H, hypotenuse. O, opposite. **(e,f)** Quantification (e) and time-lapse microscopy images (f) showing uneven timing of daughter-cell flattening onto the substrate after mitosis (misoriented cell division) in IFT88-siRNA-treated HeLa cells, compared with control. *n* = 50 mitotic cells per experiment. Arrows, time when the first daughter cell begins flattening. Time, min. Scale bar, 10 μm. **(g)** Immunofluorescence microscopy images (left) showing a disrupted spindle pole (α-tubulin, arrow) in kidney cells derived from the IFT88 mouse mutant *Tg737 ^{orpk}* (*Tg737 $^{-/-}$*), compared with wild type (*Tg737 $^{+/+}$*). Scale bars, 2 μm. Graph (right), quantification of mitotic defects in wild-type and *Tg737 ^{orpk}* mutant cells. **(h)** Immunofluorescence microscopy images of mitotic spindles from the pronephric ducts of whole-mount zebrafish embryos. Control embryo, cell with aligned chromosomes and mitotic spindle oriented in the longitudinal plane of the duct. IFT88-depleted embryo, cell with non-aligned chromosomes and misoriented spindle. Lines, pronephric duct border. Dashed lines, spindle orientation. MO, morpholino. Right, enlargements of spindles outlined by dashed rectangles. Scale bar, 5 μm.

ciliopathies[59] also resulted in mitotic defects including misoriented spindles (Figure II-1h and Supplementary Figure II-S2e). These results demonstrate a conserved mitotic role for IFT88 in spindle and cell-division orientation.

We next examined the structural underpinnings of spindle misorientation induced by IFT88 depletion. The most notable defect was a significant loss and shortening of astral microtubules, which did not contact the cell cortex, a requirement for force generation during spindle orientation (Figure II-2a,b). This phenotype was consistently observed in different experimental systems (Figures II-1g and II-2a,b), demonstrating a conserved role for IFT88 in the formation of astral microtubule arrays.

In centrosome-containing cells, astral microtubule arrays arise from both centrosome-based nucleation and transport of microtubule clusters to the poles from the periphery[61,62]. To define the role of IFT88 in the assembly of astral microtubule arrays, we tested the contribution of the protein in both processes. A role for IFT88 in microtubule nucleation was first indicated by loss of microtubule-nucleating components, γ-tubulin and end-binding protein 1 (EB1; [54,63–66]) from spindle poles following IFT88 depletion (Figure II-2c,d and Supplementary Figure II-S3a,b); EB1 depletion did not affect IFT88 pole localization (Supplementary Figure II-S3c). The similarities in mitotic phenotypes induced by depletion of IFT88, EB1 or γ-tubulin (spindle pole defects, reduced astral microtubules and misoriented spindle; Figure II-1; refs [56,64–66]) and the mitotic interaction of IFT88 with EB1 and γ-tubulin (Figure II-2e) supported the idea that these proteins may co-function in mitosis. More specifically, the impaired recruitment of γ-tubulin to spindle

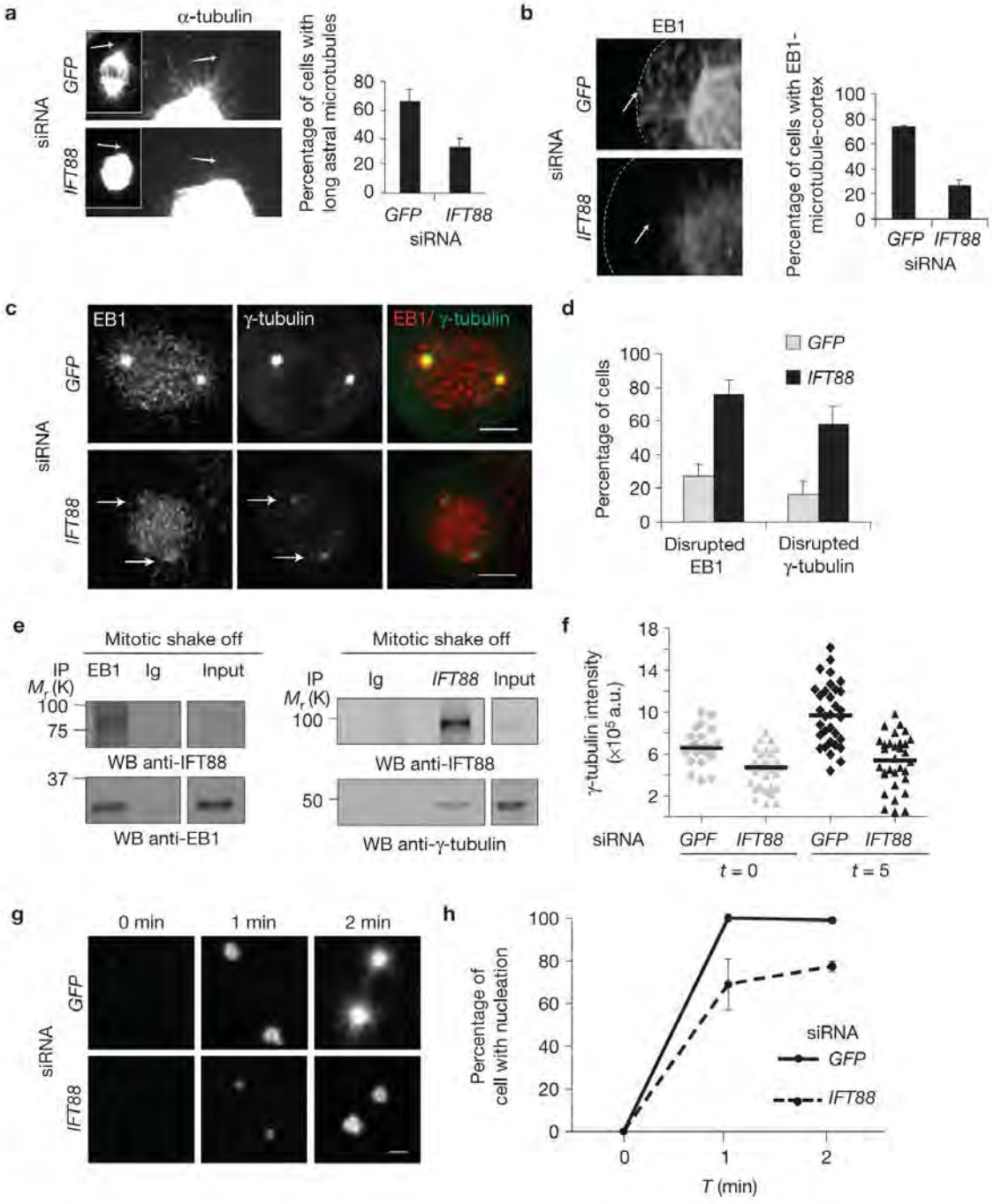
a
α-tubulin
siRNA
GFP
IFT88
Percentage of cells with long astral microtubules
80
60
40
20
0
GFP IFT88
siRNA
b
EB1
siRNA
GFP
IFT88
Percentage of cells with EB1-microtubule-cortex
100
80
60
40
20
0
GFP IFT88
siRNA
c
EB1
γ-tubulin
EB1/ γ-tubulin
siRNA
GFP
IFT88
d
GFP
IFT88
Percentage of cells
100
80
60
40
20
0
Disrupted EB1
Disrupted γ-tubulin
e
Mitotic shake off
IP
EB1 Ig Input
Mr (K)
100
75
WB anti-IFT88
37
WB anti-EB1
Mitotic shake off
IP
Ig IFT88 Input
Mr (K)
100
WB anti-IFT88
50
WB anti-γ-tubulin
f
γ-tubulin intensity (×10^5 a.u.)
18
14
10
6
2
siRNA
GPF IFT88 GFP IFT88
t = 0
t = 5
g
0 min
1 min
2 min
siRNA
GFP
IFT88
h
Percentage of cell with nucleation
100
80
60
40
20
0
siRNA
GFP
IFT88
0
1
2
T (min)

Figure II-2

Figure II-2 IFT88 depletion disrupts astral microtubules and the spindle pole localization of proteins involved in microtubule nucleation in HeLa cells.
(a) Immunofluoresence microscopy images (left) of mitotic spindles showing disrupted astral microtubules (α-tubulin) at spindle poles of IFT88-depleted cells, compared with control. Pixel intensity range increased to visualize astral microtubules (arrow). Enlargements, spindle pole region. Graph (right), quantification of cells with long astral microtubules (>3 μm). *n* = 70 mitotic spindles per experiment. **(b)** Side view of 3D reconstructed images (left) showing astral microtubules (EB1 staining) contacting the cortex in control cells (arrow, upper panel) and astral microtubules that fail to contact the cell cortex in IFT88-depleted cells (arrow, lower panel). Dotted lines, cell cortex. Graph (right), quantification of cells with both poles showing astral microtubules contacting cortex. n = 50 mitotic spindles per experiment. **(c,d)** Immunofluorescence microscopy images **(c)** and quantification **(d)** of mitotic spindles showing loss of EB1 and γ-tubulin from spindle poles (arrow) in IFT88-depleted cells, compared with control. Graph **(d)**, percentage of cells with disrupted pole localization of EB1 or γ-tubulin. *n* = 50 mitotic spindles per experiment. Scale bar, 5 μm. **(e)** Immunoblots (WB) showing that IFT88 co-immunoprecipitates with EB1 (left) and that γ-tubulin co-immunoprecipitates with IFT88 (right) from lysates of mitotic HeLa cells, demonstrating a mitotic interaction between the proteins, either direct or indirect. Ig, rabbit antibody, negative immunoprecipitation (IP) control. Input, 5% of total lysate used for immunoprecipitation. For full scan of immunoblots, see Supplementary Fig. S8. **(f)** Quantification of γ-tubulin intensity at spindle poles of mitotic cells showing γ-tubulin recruitment to poles in a microtubule regrowth experiment. *t* , time after nocodazole washout (min). Bar, median. Experiment shown is representative of three independent experiments. a.u., arbitrary unit. **(g)** Immunofluoresence microscopy images showing microtubule regrowth (α-tubulin) at mitotic spindle poles 0, 1 and 2 min after nocodazole washout in IFT88- or GFP-depleted mitotic cells. *t* = 0 min shows no nucleation in GFP- and IFT88-depleted cells, and *t* = 1 min and 2 min show decreased nucleation in IFT88-depleted cells, compared with control cells. Scale bar, 2 μm. (h) Percentage of cells showing detectable nucleation (aster size ≥1 μm) 0, 1 and 2 min after nocodazole washout. *n* = 50 mitotic cells per experiment; error bars, mean of at least three experiments ± s.d.

poles in IFT88-depleted cells following microtubule regrowth (Figure II-2f) indicated a role for IFT88 in the recruitment of microtubule-nucleating components to spindle poles. Consistent with the polar loss of microtubule-nucleating proteins, IFT88 depletion decreased microtubule nucleation, but the effect was modest when compared with the marked disruption of astral microtubules (Figure II-2g,h and Supplementary Figure II-S3d). This observation and the known role of IFT proteins in the transport of components in cilia[1,52] indicated that IFT88 might function in microtubule transport to poles during mitosis rather than directly participating in microtubule nucleation at poles.

To test this, we examined the role of IFT88 in the transport of peripheral microtubule clusters towards spindle poles during the prophase-to-metaphase transition using green fluorescent protein (GFP)–α-tubulin-expressing LLC-PK1 cells previously optimized for this purpose[62]. In prometaphase, IFT88 localized to foci at the minus end of peripheral microtubule clusters where the dynein motor was previously localized[61] (Figure II-3a and Supplementary Figure II-S4a). In IFT88-depleted cells, peripheral microtubule clusters accumulated in the cytoplasm (Figure II-3b), indicating that they were unable to integrate into spindle poles during the prometaphase-to-metaphase transition. The ectopic microtubule clusters contained the microtubule-nucleating proteins γ-tubulin and EB1, and the microtubule-associated motor dynein1 (Figure II-3c,d). To directly test whether IFT88 is required for the movement of microtubule clusters, we examined the recruitment of peripheral microtubules to poles by time-lapse microscopy imaging (Figure II-3e; Supplementary Movies S1–S4). In control cells, peripheral microtubules moved poleward in prometaphase and contributed to the

formation of robust spindle poles, as seen previously[61,62] (Figure II-3e top panel and Supplementary Movie S1). By metaphase, most clusters were cleared from the periphery and incorporated into spindle poles (Supplementary Movie S2). In IFT88-depleted cells, peripheral microtubule clusters did not move towards spindle poles in prometaphase (Figure II-3e lower panel and Supplementary Movie S3) and by metaphase, they were still not cleared from the periphery (Supplementary Movie S4), indicating a defect in transport. An independent strategy that directly tests the movement of microtubule clusters from periphery to poles during spindle reassembly[67] also revealed a defect in relocalization of microtubule clusters to poles following IFT88 depletion (Figure II-3f). These results uncover a new role for IFT88 in the movement and subsequent integration of microtubule clusters containing microtubule-nucleating proteins into spindle poles. They further indicate that IFT88 may be part of a transport complex in mitosis.

Microtubule cluster transport towards spindle poles requires the minus-end-directed motor dynein1[62]. In cilia, the movement of IFT88-containing particles is also motor dependent[1]. We thus investigated whether IFT88 was part of a microtubule-based, motor-driven transport system in mitosis as it is in ciliated cells. Consistent with this model, IFT88 co-pelleted with taxol-stabilized microtubules from mitotic cell lysates (Figure II-4a). Moreover, the spindle pole localization of IFT88 was dependent on microtubules, as shown by the marked reduction of IFT88 at spindle poles following microtubule depolymerization, and its restoration after nocodazole washout (Figure II-4b). During spindle reassembly, a remarkable redistribution of IFT88 was observed. Within 5 min, IFT88 redistributed from a diffuse cytoplasmic location to numerous

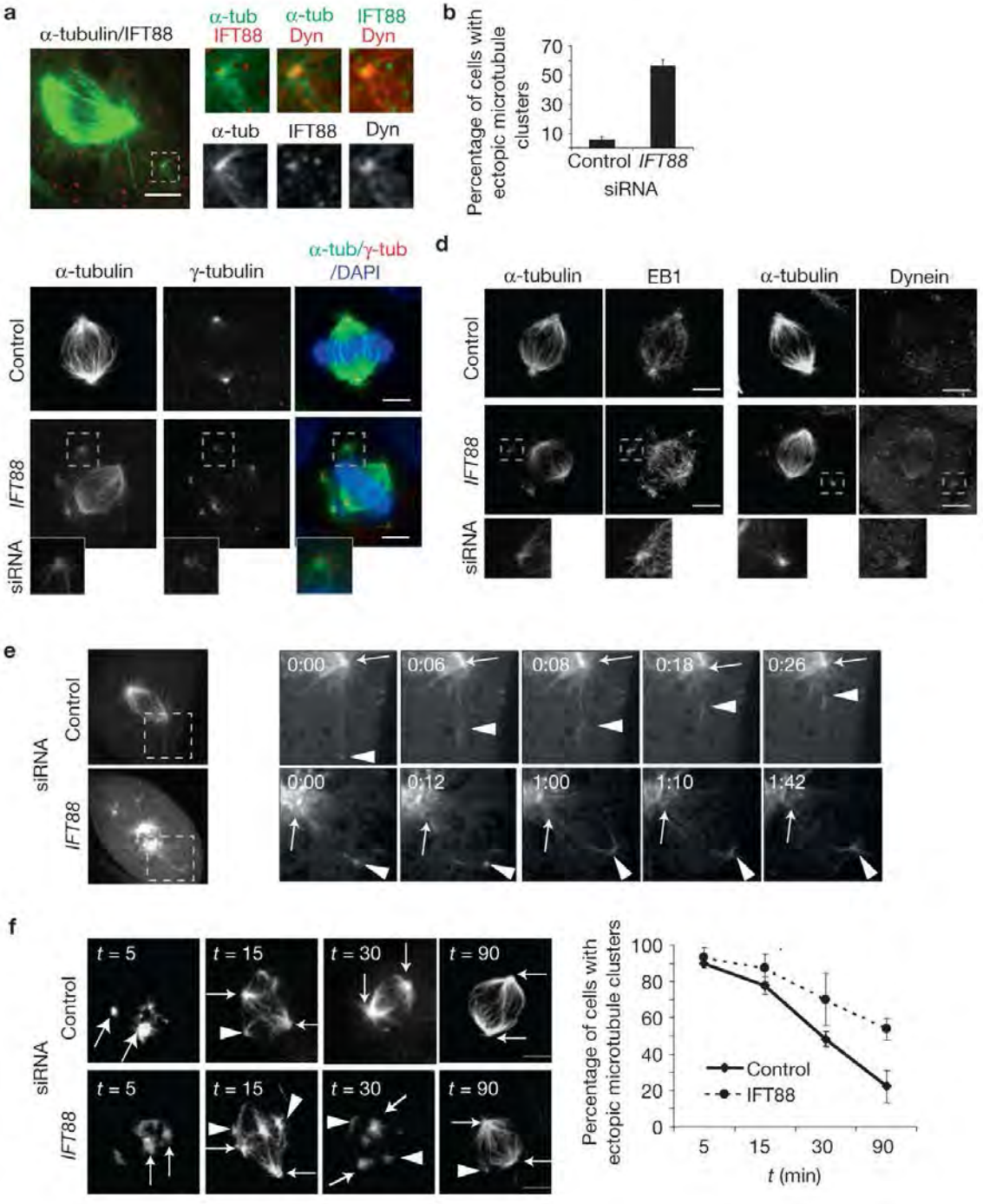
a
α-tubulin/IFT88
α-tub IFT88
α-tub Dyn
IFT88 Dyn
α-tub
IFT88
Dyn
b
Percentage of cells with ectopic microtubule clusters
70
50
30
10
Control
IFT88
siRNA
α-tubulin
γ-tubulin
α-tub/γ-tub /DAPI
Control
IFT88
siRNA
d
α-tubulin
EB1
α-tubulin
Dynein
Control
IFT88
siRNA
e
siRNA
Control
IFT88
0:00
0:06
0:08
0:18
0:26
0:00
0:12
1:00
1:10
1:42
f
siRNA
Control
IFT88
t = 5
t = 15
t = 30
t = 90
Percentage of cells with ectopic microtubule clusters
100
80
60
40
20
0
Control
IFT88
5
15
30
90
t (min)

Figure II-3

Figure II-3 IFT88 is required for the movement of peripheral microtubule clusters containing microtubule-nucleating components towards spindle poles in LLC-PK1 cells stably expressing GFP–α-tubulin.
(a) Immunofluoresence microscopy images showing IFT88 and dynein intermediate chain (Dyn) localizing to a peripheral microtubule cluster (GFP–α-tubulin) in a prometaphase cell. Pixel intensity range increased to visualize peripheral microtubule cluster. Scale bar, 5 μm. Inset, peripheral microtubule cluster. See Supplementary Fig. S4a for negative controls. **(b)** Quantification of GFP–α-tubulin LLC-PK1 metaphase cells with ectopic microtubule clusters following IFT88- or control- (lamin) siRNA treatment. *n* = 50 mitotic cells per experiment. **(c,d**) Immunofluoresence microscopy images of GFP–α-tubulin LLC-PK1 control or IFT88-depleted metaphase cells. γ-tubulin **(c)**, EB1 (**d**, left) and dynein (**d**, right) localize to ectopic microtubule clusters. Insets, ectopic microtubule clusters. Scale bar, 5μm. **(e)** Selected still images from time-lapse microscopy movies of GFP–α-tubulin LLC-PK1 cells. Control prometaphase, minus-end-directed motion of peripheral microtubule clusters towards spindle pole. In IFT88-depleted cells, peripheral clusters formed, but showed no movement towards spindle poles. Full cell (left); enlargement of spindle pole and microtubule cluster (right). Time (min); arrowhead, microtubule cluster; arrow, spindle pole. **(f)** Immunofluorescence microscopy images (left) and quantification (right) of the relocalization of microtubule clusters to spindle poles in a spindle reassembly assay (α-tubulin, microtubule regrowth following nocodazole washout). The decrease in cells with ectopic microtubule clusters over time correlates with their movement towards the poles. IFT88 depletion delays relocalization of microtubule clusters to poles. Arrows, spindle poles (localization confirmed with centrosome protein staining). Arrowheads, ectopic microtubule clusters. *n* = 40 mitotic cells per experiment per time point. *t* , time after nocodazole washout (min).

cytoplasmic foci (Figure II-4b). The IFT88 foci contained α-tubulin and singular or bundled microtubules as well as the newly characterized IFT88 mitotic interacting partners, γ-tubulin and EB1 (Figure II-4c,d). With time, the number of IFT88 foci decreased concomitant with an increase in the spindle pole fraction (Figure II-4e), indicative of translocation of the cytoplasmic foci to poles. Direct translocation of IFT88 to spindle poles was tested using GFP–IFT88- expressing LLC-PK1 cells (Figure II-4f). GFP–IFT88 localized to spindle poles and to cytoplasmic foci, confirming results with the endogenous protein. GFP–IFT88 foci exhibited vectorial movement towards poles (Figure II-4f and Supplementary Movie S5); anterograde movements were also observed (Figure II-4f, right). The speed of IFT88 retrograde movement (>1 μm s^{-1}) was consistent with dynein-mediated motility, indicating that polar transport of IFT88 was mediated by dynein (Figure II-4f, right), possibly in the form of a dynein–IFT88 complex. The common functions of IFT88 and dynein1 in astral microtubule organization, mitotic spindle orientation[55,68–70] (Figures II-1 and II-2a,b) and transport of microtubule clusters[62] (Figure II-3) supported this model.

To directly test for the presence of a mitotic IFT88 transport complex, we carried out a series of biochemical experiments. The approximate size of mitotic IFT88 complexes was determined by gel filtration chromatography (Figure II-5a). IFT88 was detected in fractions 16–20 (relative molecular mass M_r~2,000K–5,000K), where it partially co-eluted with dynein1; a separate peak of IFT88 appeared in fraction 26 (M_r of ~600K). Dynein co-eluted with dynactin components (fractions 16–22), indicating that the integrity of the dynein–dynactin complex was retained during gel filtration

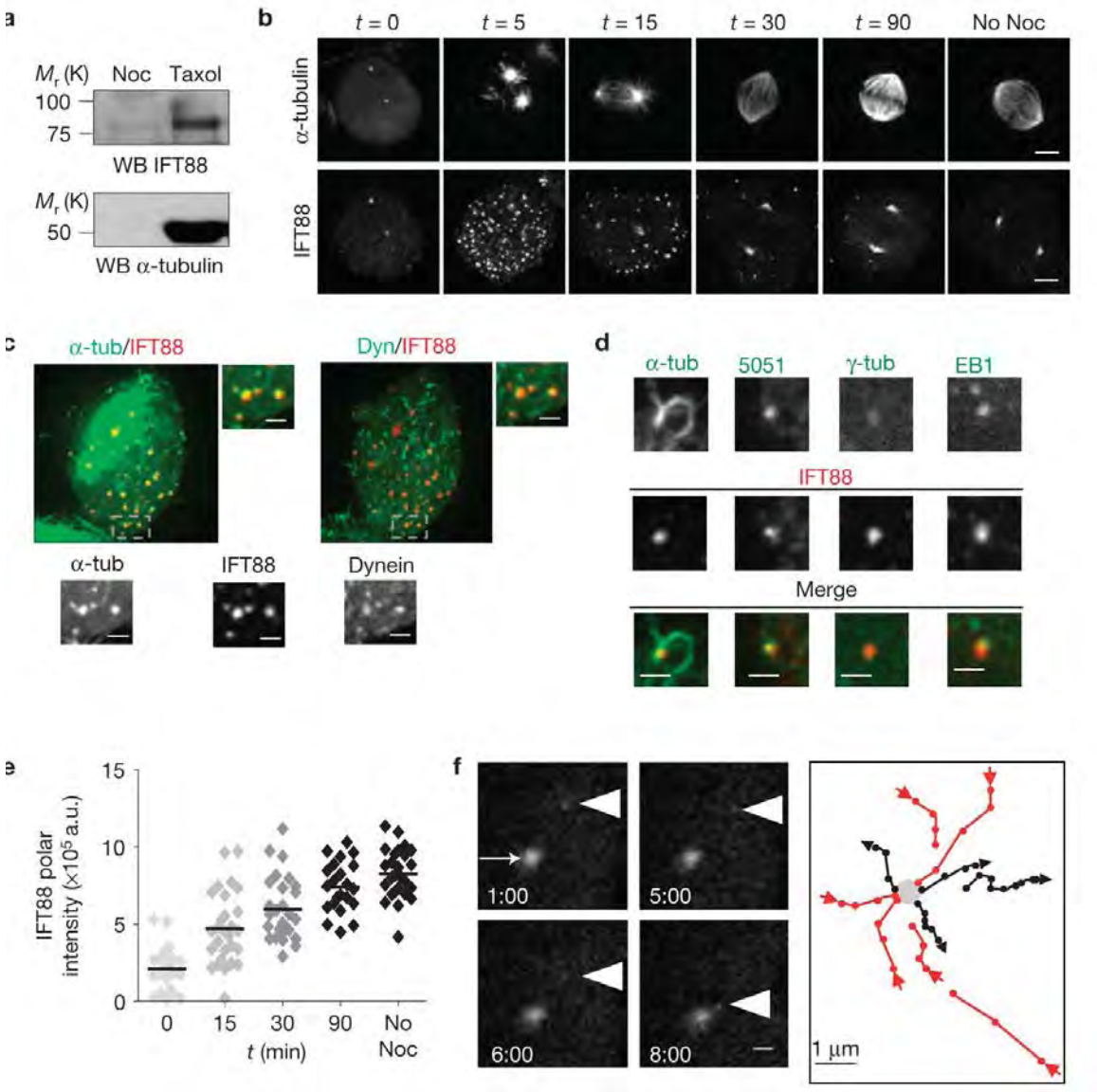
a
M_r (K) Noc Taxol
100
75
WB IFT88
M_r (K)
50
WB α-tubulin
b
t = 0
t = 5
t = 15
t = 30
t = 90
No Noc
α-tubulin
IFT88
c
α-tub/IFT88
Dyn/IFT88
α-tub
IFT88
Dynein
d
α-tub
5051
γ-tub
EB1
IFT88
Merge
e
IFT88 polar intensity (×10⁵ a.u.)
15
10
5
0
0
15
30
90
No Noc
t (min)
f
1:00
5:00
6:00
8:00
1 μm

Figure II-4

Figure II-4 IFT88 moves towards spindle poles and requires microtubules for its spindle pole localization.
(a) Microtubule pulldown assay shows that IFT88 co-pelleted with taxol-stabilized microtubules in mitotic HeLa cell lysates. Nocodazole (Noc), inhibition of microtubule polymerization used as negative control. α-tubulin, microtubules. **(b)** Immunofluoresence microscopy images showing IFT88 foci formation (lower panel) after nocodazole washout (α-tubulin, microtubule regrowth; upper panel) in HeLa cells. *t* , time after nocodazole washout (min). Control without nocodazole (no Noc). Scale bar, 5 μm. **(c,d)** Immunofluorescence microscopy images showing the molecular composition of IFT88 foci in HeLa cells. Maximum projection of a cell with IFT88 foci 5 min after nocodazole washout **(c)** showing that IFT88 foci co-stain for α-tubulin (α-tub) and dynein intermediate chain (Dyn). Enlargements, single plane of the outlined foci. Enlargements of IFT88 foci **(d)** showing that microtubule clusters (α-tubulin; α-tub) can be observed extending from some foci, and that IFT88 foci co-stain with microtubule-nucleating components (5051, centrosome protein marker; γ-tubulin; EB1). Pixel intensity range increased to visualize foci. Scale bar, 1 μm. **(e)** Quantification of IFT88 intensity at spindle poles of mitotic HeLa cells showing IFT88 recruitment to poles following nocodazole washout. t , time after nocodazole washout (min). Experiment shown is representative of three independent experiments. Bar, median. a.u., arbitrary unit. No nocodazole (No Noc), untreated cells. **(f)** Still images from time-lapse microscopy imaging of a GFP–IFT88 LLC-PK1 cell line (left) showing one of the GFP–IFT88 foci (arrowhead) moving towards the GFP–IFT88-labelled spindle pole (arrow). Time elapsed is shown in seconds. Scale bar, 1 μm. Schematic representation (right) of several GFP–IFT88 foci moving towards (red arrow) or away from (black arrowhead) the spindle pole (grey dot). Time between points, 1 s. Arrows indicate the direction of the movement.

chromatography (Figure II-5a). The partial co-elution of IFT88 and dynein indicated that a subfraction of IFT88 may interact with a subfraction of dynein in a large M_r~2,000K–5,000K complex (Figure II-5a). In fact, IFT88 and dynein co-immunoprecipitated from mitotic lysates (Supplementary Figure II-S4b,c). Immunoprecipitation experiments carried out on gel-filtration-chromatography fractions containing dynein confirmed that the interaction was maintained after gel filtration chromatography (Figure II-5a, right), providing further evidence for an IFT88–dynein1 complex in mitosis. Additional IFT proteins co-eluted with IFT88 in the M_r ~2, 000K–5,000K range and an interaction between IFT88 and IFT52 (another IFT B-complex component) was identified in mitotic cells (Figure II-5a and Supplementary Figure II-S4d,e). These data indicate that IFT88 and maybe other IFT proteins are part of a large dynein1-containing protein complex during mitosis.

To test for a role of dynein1 in the spindle pole localization of IFT88, dynein1 heavy chain was depleted by siRNA. An increase in mitotic index[70] and interphase defects[71] were observed (Supplementary Figure II-S5), validating the efficacy of the siRNA. In addition, dynein1 depletion induced a unique redistribution of IFT88 from its focused spindle pole position to a more diffuse region surrounding the poles (Figure II-5b–d), but did not markedly affect the centrosome localization of IFT88 in interphase as previously reported[25] (Supplementary Figure II-S6a). The IFT88 localization pattern was unlike other spindle pole proteins, which were lost from poles but not redistributed (Supplementary Figure II-S6b). This observation and the fact that IFT88 mislocalization occurred before major spindle disruption (Supplementary Figure II-S6c,d), indicated that

IFT88 mislocalization was not due to global perturbations of the spindle. The mitotic redistribution of IFT88 following dynein1 depletion was reminiscent of IFT88 accumulation at cilia tips following depletion of the cilia-associated dynein2 motor[53], an apparent consequence of net microtubule plus-end motor activity in the absence of minus-end activity (Figure II-5d). A similar redistribution of IFT88 was observed following depletion of p50 dynactin, which disrupts dynein function[70] (Supplementary Figure II-S6e–g). In contrast, depletion of the dynein2 motor, which is required for retrograde transport in cilia[1,53], did not affect mitotic index, spindle organization or the spindle pole localization of IFT88, despite its robust interphase and ciliary phenotypes[72] (Supplementary Figures II-S5 and II-S7). These data demonstrate a role for cytoplasmic dynein1 in the microtubule-dependent spindle pole localization of IFT88 and indicate that IFT88 functions as part of a previously uncharacterized dynein1-driven complex in mitotic cells.

To directly test the role of dynein1 in IFT88 transport to spindle poles, we examined the translocation of IFT88 foci from cytoplasm to poles during spindle reassembly (Figure II-5e,f). In dynein-depleted cells, IFT88 foci were delayed in their relocalization, as demonstrated by an increase in the number of IFT88 foci remaining in the cytoplasm after microtubule regrowth and a decrease in IFT88 at spindle poles (Figure 5e). More specifically, 30 min after nocodazole washout, most control cells (85%) lacked cytoplasmic foci and showed IFT88 at poles, whereas half of the dynein1-depleted cells still showed cytoplasmic IFT88 foci and weak pole staining (Figure II-5f). This demonstrates that dynein1 is required for the transport of IFT88 to spindle poles.

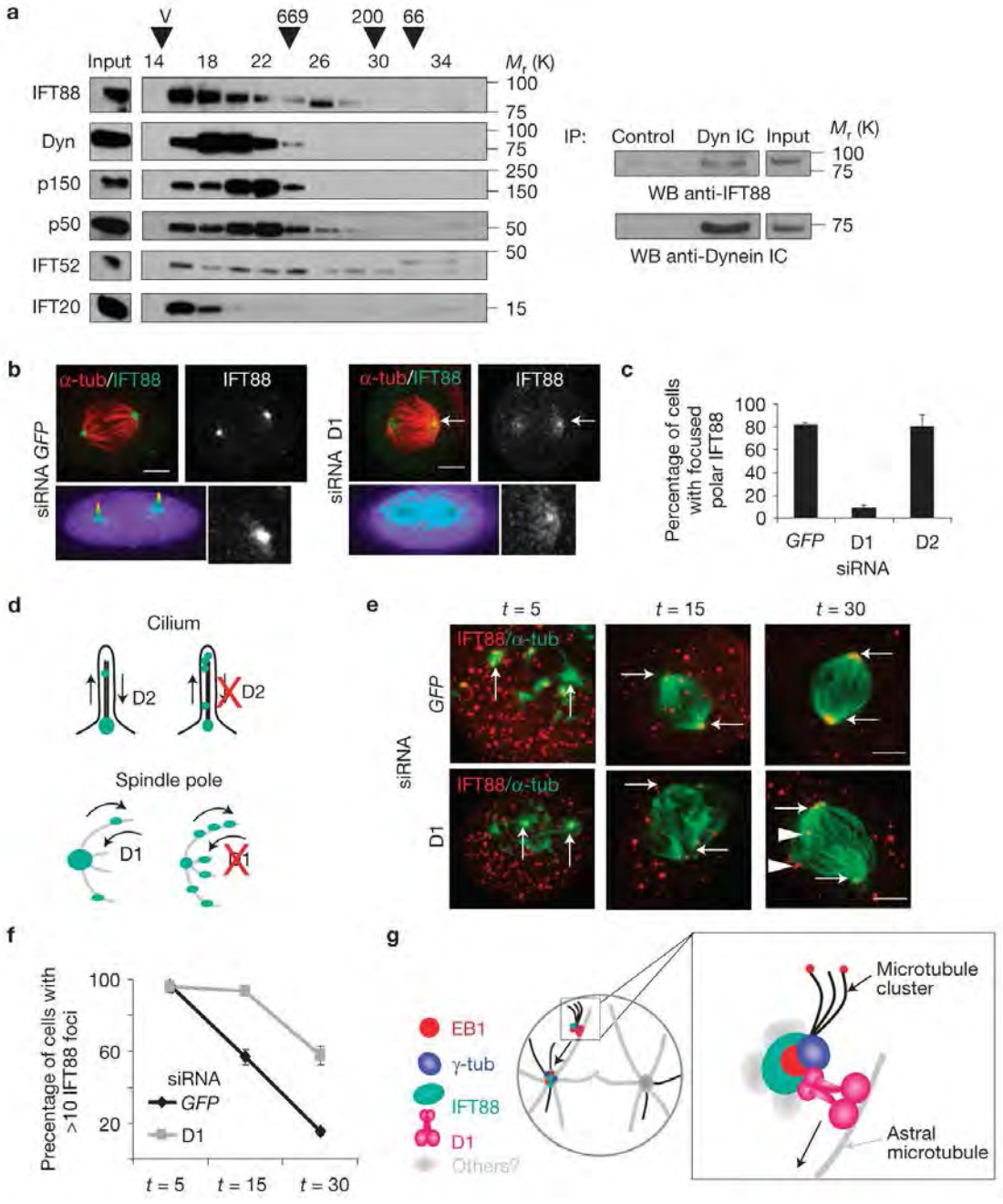
a
V
669
200
66
Input 14 18 22 26 30 34
M_r (K)
IFT88
Dyn
p150
p50
IFT52
IFT20
100
75
100
75
250
150
50
50
15
IP: Control Dyn IC Input
M_r (K)
100
75
WB anti-IFT88
75
WB anti-Dynein IC
b
α-tub/IFT88
IFT88
siRNA GFP
siRNA D1
c
Percentage of cells with focused polar IFT88
100
80
60
40
20
0
GFP
D1
D2
siRNA
d
Cilium
D2
D2
Spindle pole
D1
D1
e
t = 5
t = 15
t = 30
IFT88/α-tub
GFP
siRNA
D1
f
Precentage of cells with >10 IFT88 foci
100
60
20
siRNA
GFP
D1
t = 5
t = 15
t = 30
g
EB1
γ-tub
IFT88
D1
Others?
Microtubule cluster
Astral microtubule

Figure II-5

Figure II-5 IFT88 is part of a dynein1-driven transport complex in mitosis.
(a) Immunoblots (left) showing fractions of mitotic HeLa cell lysates obtained after gel-filtration fractionation and probed for IFT88, dynein intermediate chain (Dyn IC), dynactin p150/glued, p50 dynactin, IFT52 and IFT20. Input, total lysate before gel filtration chromatography. Arrowheads, peak elution fraction for calibration proteins: bovine serum albumin (M_r 66K), β-amylase (M_r 200K), thyroglobulin (M_r 669K). V, Void volume. Immunoprecipitation experiment (right) carried out on fractions 16–22 from gel filtration containing dynein. Immunoblots show that IFT88 co-immunoprecipitates with dynein (IC, intermediate chain) after gel filtration chromatography. For full scan of immunoblots, see Supplementary Fig. S8. **(b)** Immunofluorescence microscopy images of HeLa cells showing IFT88 redistribution from mitotic spindle poles to a more diffuse region surrounding the poles following dynein1 (D1) depletion, compared with control (GFP). α-tubulin; α-tub. Intensity profiles, lower left panels; spindle pole enlargement, lower right panels. Scale bar, 5 μm. **(c)** Percentage of cells with focused IFT88 localization at poles following dynein1- (D1) or dynein2 - (D2) siRNA treatment. n = 70 mitotic spindles per experiment. **(d)** Schematic representation of IFT88 (green) redistribution in cilia when dynein2 (D2) is depleted, and around mitotic spindle poles when dynein1 (D1) is depleted. **(e)** Immunofluorescence microscopy images showing that D1 depletion in HeLa cells delays IFT88 (red) relocalization to spindle poles in a spindle reassembly assay (α-tubulin, green). The decrease of cytoplasmic foci over time, observed in control (GFP) cells correlates with the relocalization of IFT88 from foci to spindle poles. Despite the formation of microtubule clusters in D1-depleted cells, several IFT88 foci remain in the cytoplasm 30 min after nocodazole washout. Arrows, spindle poles; arrowheads, IFT88 foci. **(f)** Percentage of cells with more than ten cytoplasmic foci. n = 40 cells per experiment per time point. t , time after nocodazole washout (min). **(g)** Molecular model for IFT88 function in mitosis. IFT88 is depicted as a component of a minus-end-directed dynein1-driven transport complex. This complex is required for transport of microtubule clusters and their associated nucleating components (EB1 and γ-tubulin) to spindle poles. IFT88 thus contributes to the formation of astral microtubule arrays and consequently spindle orientation. Adapted from [61].

This work identifies a role for an IFT protein in the formation of mitotic astral microtubule arrays and thus establishes a new molecular mechanism for a cilia protein in spindle orientation. These results, together with the previously established role of dynein1 in transporting peripheral microtubules[62] and centrosome components[73] to spindle poles, indicate that an IFT88–dynein1 complex transports peripheral microtubule clusters and associated microtubule-nucleating components to spindle poles (Figure II-5g). These microtubule clusters can be viewed as 'pre-fabricated' parts of the spindle pole, an observation reminiscent of 'pre-assembled' cilia components transported by motors along the cilia[1]. Integration of microtubule clusters into spindle poles instantly contributes to the astral microtubule population and the microtubule-nucleating components present in these structures (γ-tubulin, EB1) could contribute to microtubule nucleation at poles. Collectively, these events facilitate formation of astral microtubule arrays and subsequently spindle orientation. The IFT88-mediated spindle pole assembly pathway provides new insight into the underpinnings of fundamental processes including cystogenesis and asymmetric cell division[74].

As cilia disassemble before mitotic entry and HeLa cells are considered non-ciliated[75], the role of IFT88 in the formation of mitotic astral microtubule arrays represents a previously unknown cilia-independent function for this protein, in addition to its role in cilia formation[41], cell-cycle progression[25] and membrane trafficking[31]. The spindle pole localization of several other IFT proteins[24–27] and the mitotic interaction between IFT52 and IFT88 (Supplementary Figure II-S4d,e) indicate that other IFT proteins, and maybe other classes of cilia proteins, may function in dividing cells.

Moreover, the anterograde movement of IFT88 foci is indicative of a role for microtubule plus-end-directed motors in IFT88 mitotic transport (Figures II-4f and II-5d).

IFT88 depletion primarily affects a subset of microtubules in mitosis (astrals), consistent with the selective disruption of spindle function. The observed delay in mitosis, rather than a complete mitotic block, indicates that there are no major, potentially fatal defects in spindle function. IFT88 may thus operate selectively in cells, tissues and organisms that require astral microtubules for proper spindle orientation, such as the oriented cell divisions in an epithelial layer or the asymmetric division of stem cells[74]. This may explain why IFT88 disruption is not associated with more severe phenotypes in mouse, *Drosophila* or *Caenorhabditis elegans* embryos, such as lethality in the earliest embryonic stages[57,58,60].

Cystogenesis has been associated with cilia disruption and misoriented cell division[39]. Despite the appeal for a role of cilia in regulating the planar cell polarity[76], the molecular mechanism leading to misoriented cell division remains unclear. This work provides a likely mechanism for IFT88 function in oriented cell divisions. Further work is required to test whether the pathway outlined here for IFT88 can be applied to other cilia proteins involved in cystogenesis.

Supplemental Figures

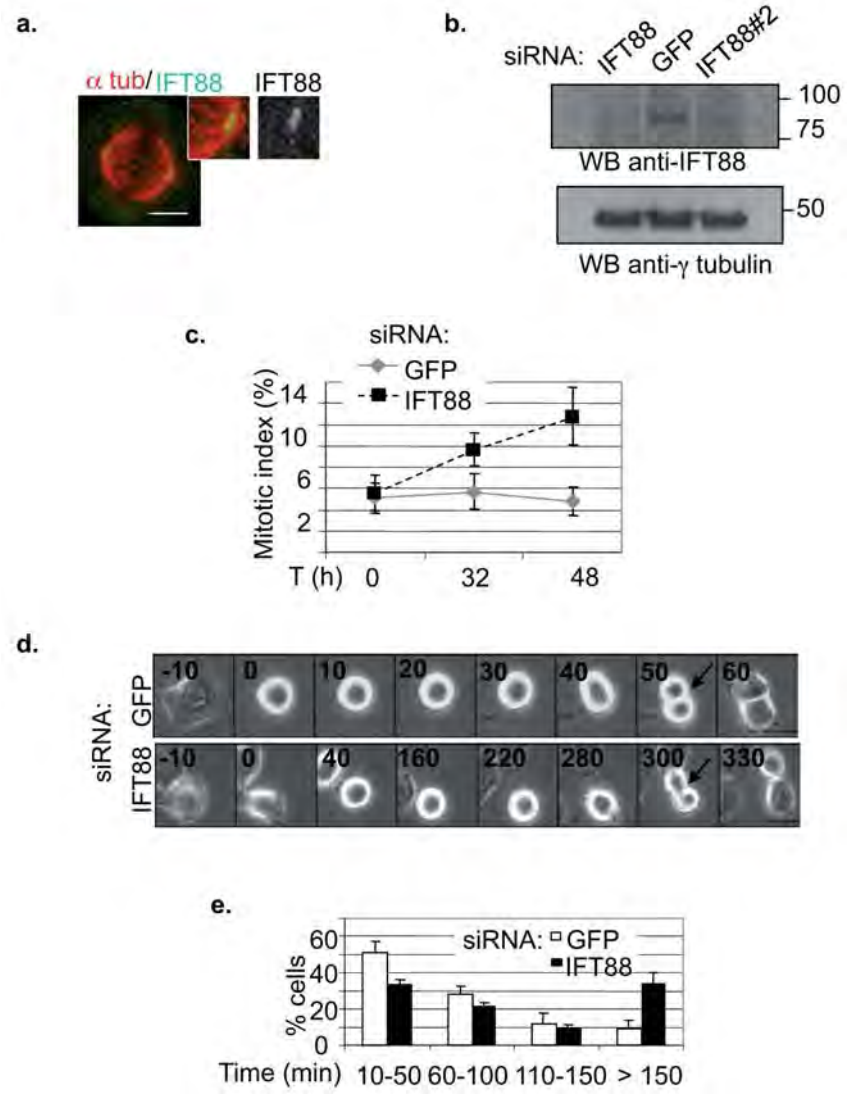

Figure II-S1 IFT88 depletion leads to mitotic defects in HeLa cells.
(a) Immunofluorescence images of IFT88 at spindle poles in a metaphase HeLa cell. Enlargements, spindle pole. Scale bar, 5µm. **(b)** Western blot showing IFT88 depletion in HeLa cells using two independent siRNAs. GFP, control siRNA; γ tubulin, loading control. **(c)** Manual counts of mitotic indices of control (GFP) and IFT88 depleted HeLa cells 0h, 32h and 48h after transfection. *n*=500 cells/experiment. h, hours. **(d, e)** Time-lapse imaging of HeLa cells **(d)** showing progression from nuclear envelope breakdown (NEB, 0 min) to anaphase onset (arrows, first frame following anaphase onset). siRNA treatment as indicated. Time in minutes (min). Graph **(e)**: Time required for cells to progress from NEB to anaphase onset, percentage of cells for each time interval. *n*=100 mitotic cells from two independent experiments.

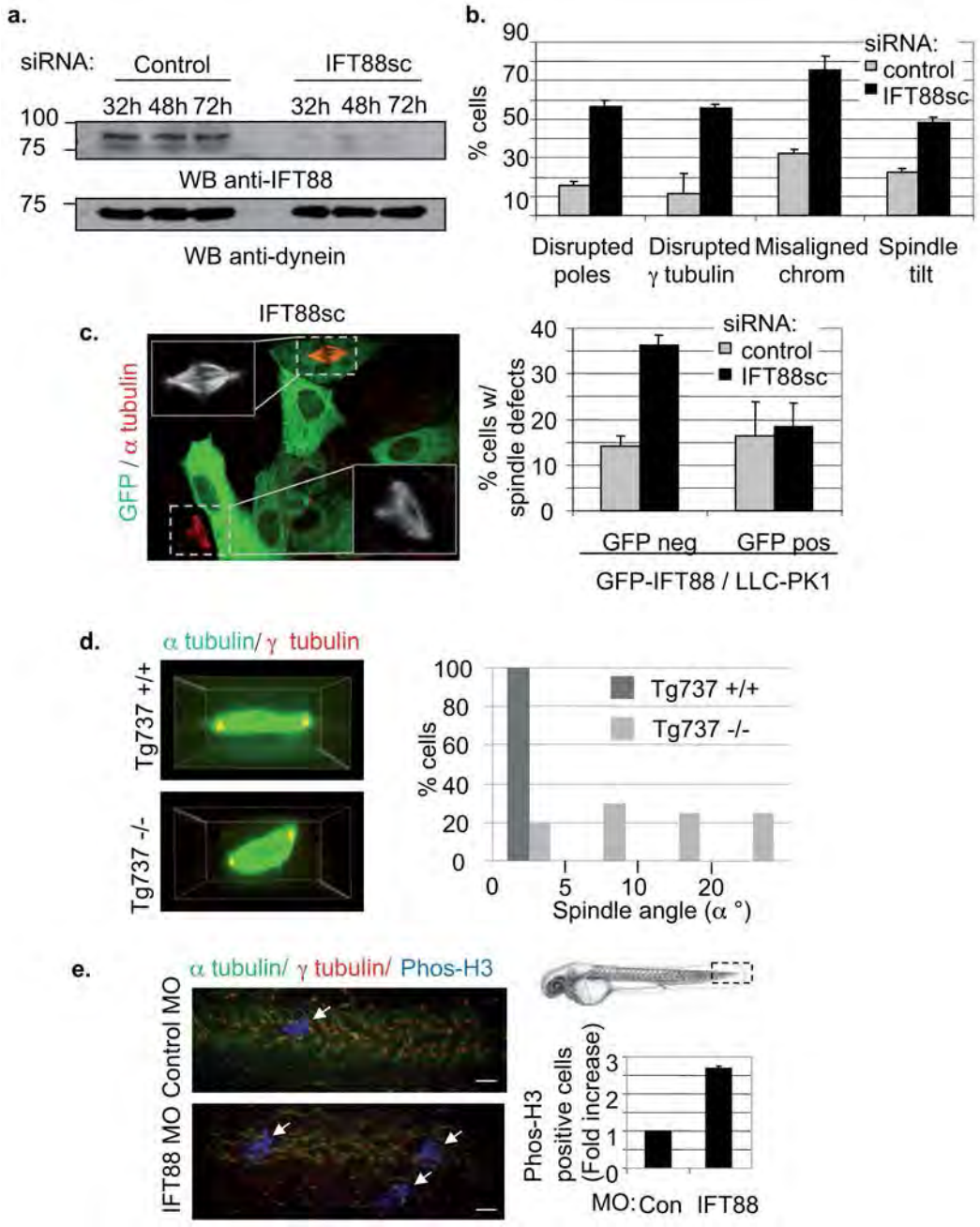
a.
siRNA: Control IFT88sc
32h 48h 72h 32h 48h 72h
100
75
WB anti-IFT88
75
WB anti-dynein
b.
% cells
siRNA:
control
IFT88sc
Disrupted poles
Disrupted γ tubulin
Misaligned chrom
Spindle tilt
c.
IFT88sc
GFP / α tubulin
% cells w/ spindle defects
siRNA:
control
IFT88sc
GFP neg
GFP pos
GFP-IFT88 / LLC-PK1
d.
α tubulin/ γ tubulin
Tg737 +/+
Tg737 -/-
% cells
Tg737 +/+
Tg737 -/-
Spindle angle (α °)
e.
α tubulin/ γ tubulin/ Phos-H3
Control MO
IFT88 MO
Phos-H3 positive cells (Fold increase)
MO: Con IFT88

Figure II-S2

Figure II-S2 IFT88 depletion leads to mitotic defects in kidney cells and zebrafish. **(a, b)** Western blot **(a)** showing IFT88 depletion in GFP-α tubulin LLC-PK1 cells. IFT88 siRNA designed against pig (IFT88sc, *Sus Scrofa*) IFT88 sequence. Dynein, loading control. Time, hours after siRNA transfection. Quantification **(b)** of GFP-α tubulin LLC-PK1 cells with mitotic defects following IFT88 or control (lamin) siRNA treatment. Defects include disrupted poles (α tubulin), disrupted γ tubulin, misaligned chromosomes (DAPI) or spindle misorientation (spindle tilt). *n*=70 mitotic cells/experiment. **(c)** Depletion of endogenous IFT88 (pig siRNA) in LLC-PK1 cells is rescued by the expression of GFP-IFT88 (mouse cDNA). Immunofluorescence images (left) of the GFP-IFT88 expressing LLC-PK1 cell line treated with IFT88sc siRNA. Normal spindle in a cell expressing GFP-IFT88; disrupted spindle in a GFP negative cell. Corresponding quantification (right) showing that, in the GFP-IFT88 LLC-PK1 cell line, depletion of endogenous IFT88 leads to an increase in spindle defects in cells that are GFP-IFT88 negative but not in cells that are GFP-IFT88 positive. Lamin, siRNA control. **(d)** Side views of three-dimensional reconstructed immunofluoresence images (left) show misoriented mitotic spindles in kidney cells derived from the IFT88 mouse mutant *Tg737*^{orpk} (*Tg737*-/-) compared to *Tg737*+/+ cells. Histogram (right) shows metaphase spindle angle distribution. n=35 mitotic spindles. **(e)** Immunofluorescence images of phos-H3 positive mitotic cells in tail buds of whole mount control or IFT88 depleted zebrafish embryos reveals an increase in mitotic cells. Schematic representation (top right) shows the corresponding tail bud region. Arrows, mitotic cells. MO, morpholino. Graph (right): Quantification by flow cytometry of mitotic phos-H3 positive cells obtained from dissociated embryos. *n*=30 embryos/experiment. *n*>20,000 total cells/experiment. For graphs in all panels: error bars, mean of at least 3 experiments ± SD unless otherwise specified.

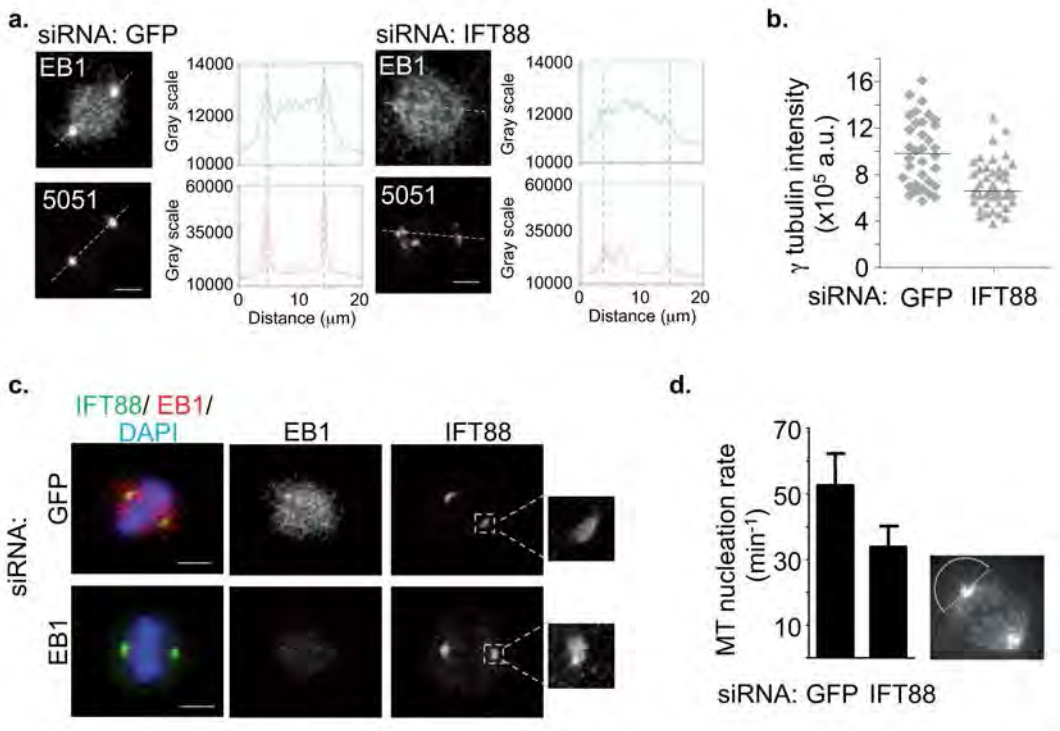

Figure II-S3 IFT88 depletion disrupts the spindle pole localization of EB1 and gamma tubulin thus decreasing MT nucleation at spindle poles, whereas EB1 depletion does not disrupt spindle pole localization of IFT88.
(a) Images of mitotic spindles and corresponding linescan histograms showing selective loss of EB1 from poles but not from spindles in IFT88-depleted HeLa cells versus control cells. **(b)** Quantification of γ tubulin intensity at spindle poles in GFP- and IFT88-siRNA treated HeLa cells. a.u., arbitrary unit. **(c)** Immunofluorescence images show that EB1 depletion does not affect IFT88 localization at spindle poles of HeLa cells despite EB1 loss from spindle (bottom panel, middle). Right, pole enlargements. **(d)** MT nucleation rate was measured in HeLa cells transiently expressing EB1-GFP by counting the number of EB1-GFP comets emerging from the centrosome over time. *n*= 8 cells for control; *n*=5 cells for IFT siRNA. Nucleation rate was measured for the astral side of the centrosome, as outlined by the white half-circle on the EB1-GFP image of a mitotic cell (right). Error bars, mean of at least 3 experiments ± SD.

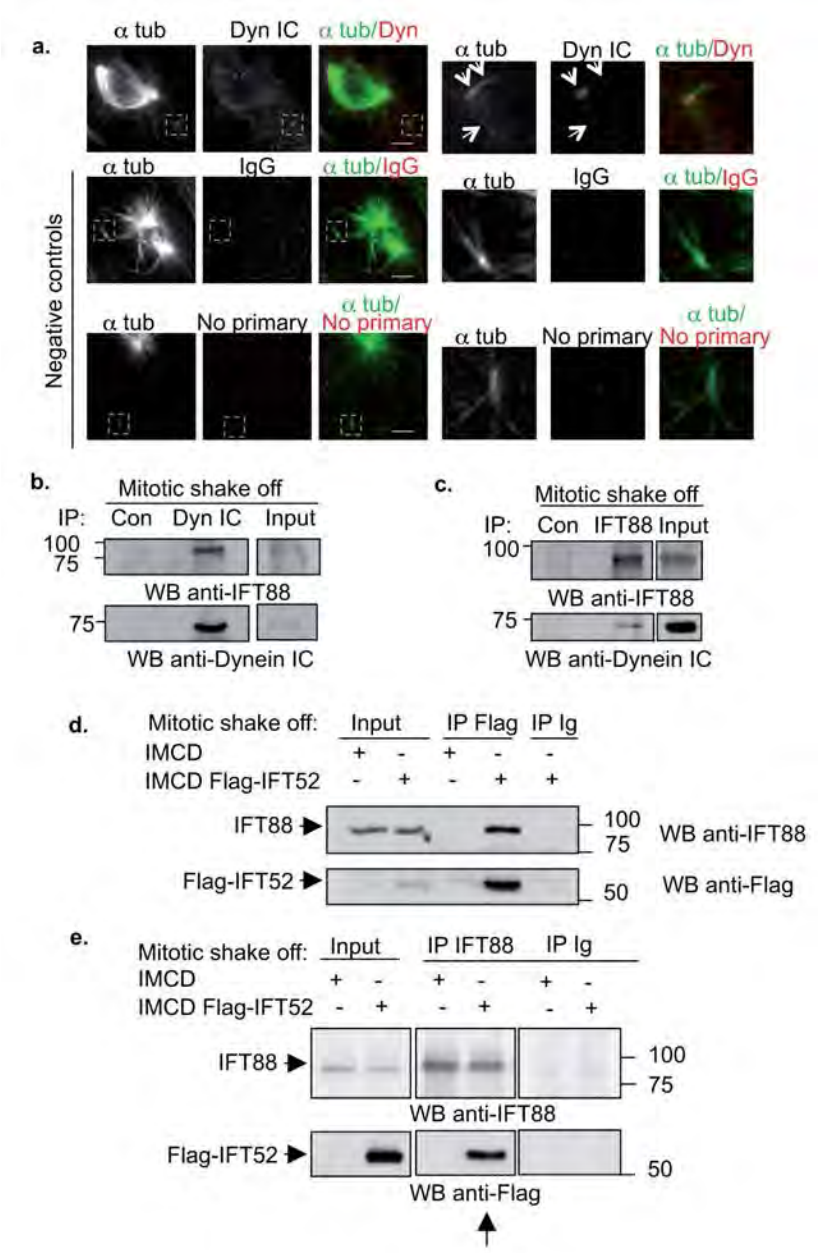
a.
α tub
Dyn IC
α tub/Dyn
α tub
Dyn IC
α tub/Dyn
α tub
IgG
α tub/IgG
α tub
IgG
α tub/IgG
Negative controls
α tub
No primary
α tub/
No primary
α tub
No primary
α tub/
No primary
b.
Mitotic shake off
IP:
Con
Dyn IC
Input
100
75
WB anti-IFT88
75
WB anti-Dynein IC
c.
Mitotic shake off
IP:
Con
IFT88
Input
100
WB anti-IFT88
75
WB anti-Dynein IC
d.
Mitotic shake off:
Input
IP Flag
IP Ig
IMCD
IMCD Flag-IFT52
IFT88
100
75
WB anti-IFT88
Flag-IFT52
50
WB anti-Flag
e.
Mitotic shake off:
Input
IP IFT88
IP Ig
IMCD
IMCD Flag-IFT52
IFT88
100
75
WB anti-IFT88
Flag-IFT52
50
WB anti-Flag

Figure II-S4

Figure II-S4 IFT88 colocalizes with dynein in MT clusters in prometaphase and interacts with dynein and Flag-IFT52 in mitotic cells.
(a) Immunofluoresence images showing dynein (intermediate chain, dynein IC) localizing at the minus end of a peripheral MT cluster and along the MTs of the cluster (arrows) in a prometaphase cell. Scale bar, 5μm. Inset, peripheral MT cluster. GFP-αtubulin, MTs. Negative controls, mouse IgG and no primary antibody. **(b-c)** Immunoblots showing that **(b)** IFT88 co- immunoprecipitates with cytoplasmic dynein intermediate chain from mitotic HeLa cells lysates, and **(c)** that cytoplasmic dynein intermediate chain co-immunoprecipitates with IFT88 from lysates of mitotic HeLa cells. Negative IP control (Con), Ig, mouse or rabbit antibody. Input, 5% of total lysate used for IP. **(d)** Immunoblots showing that IFT88 co-immunoprecipitates with Flag-IFT52 from mitotic lysates of inner medullary collecting duct (IMCD) cells stably expressing Flag-IFT52. Ig mouse antibody, negative IP control. Input, 5% of total lysate used for IP. **(e)** Immunoblots showing Flag-IFT52 co-immunoprecipitating with IFT88 from mitotic lysates of IMCD cells stably expressing Flag-IFT52. Ig, rabbit, negative IP control. WB, Western Blots as indicated. IP, immunoprecipitation. Input, 5% of total lysate used for IP. For full scan of immunoblots see Supplementary Fig. II-S8.

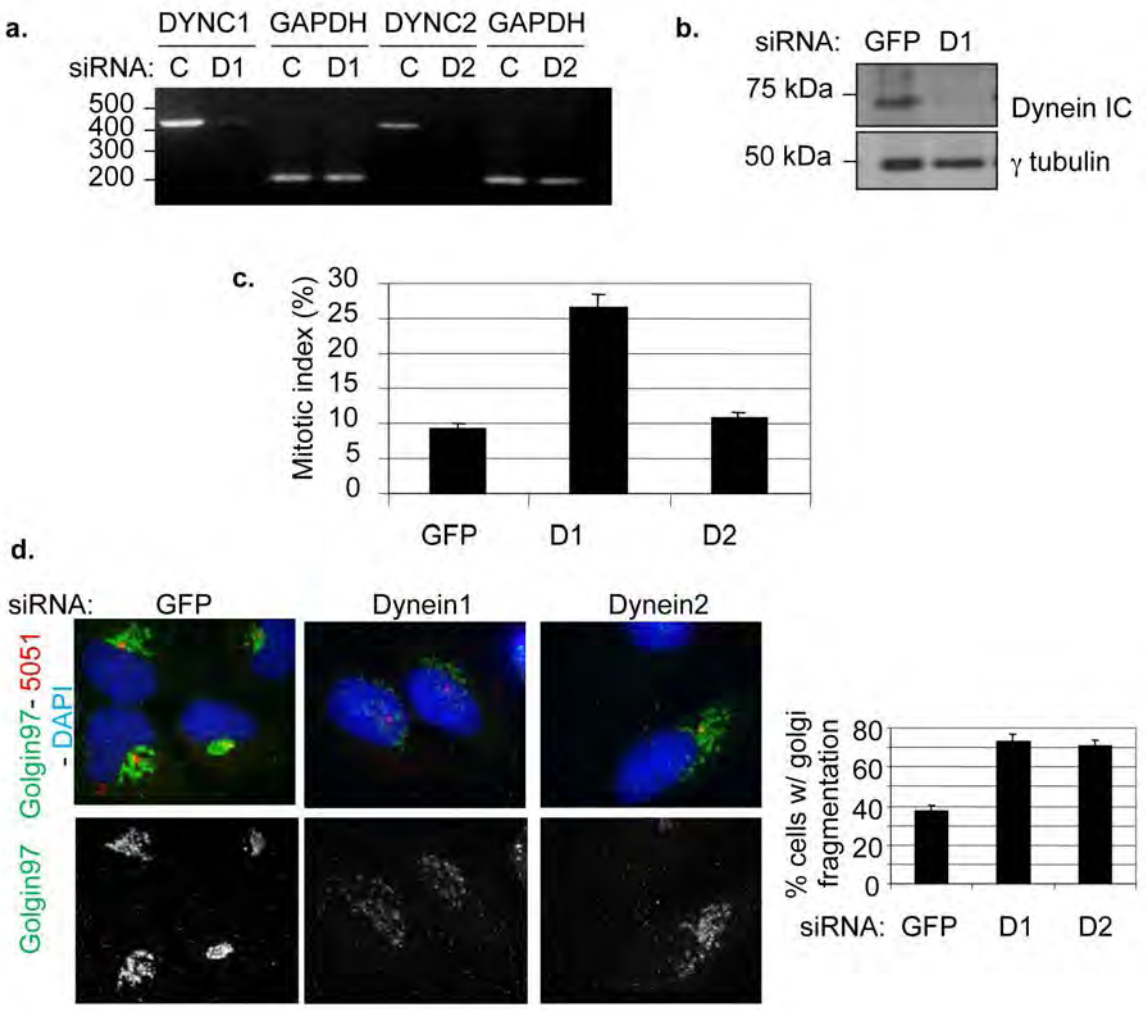
a.
DYNC1
GAPDH
DYNC2
GAPDH
siRNA: C D1 C D1 C D2 C D2
500
400
300
200
b.
siRNA: GFP D1
75 kDa
Dynein IC
50 kDa
γ tubulin
c.
Mitotic index (%)
30
25
20
15
10
5
0
GFP
D1
D2
d.
siRNA: GFP Dynein1 Dynein2
Golgin97 - 5051 - DAPI
Golgin97
% cells w/ golgi fragmentation
80
60
40
20
0
siRNA: GFP D1 D2

Figure II-S5

Figure II-S5 Depletion of dynein1 heavy chain but not dynein 2 disrupts mitosis whereas depletion of either disrupts interphase in HeLa cells.
(a) RT-PCR shows loss of cytoplasmic dynein1 mRNA (oligo, DYNC1) after siRNA depletion of the heavy chain of cytoplasmic dynein1 (D1) compared to GFP control (C) and loss of cytoplasmic dynein2 mRNA (oligo, DYNC2) after siRNA depletion of the heavy chain of cytoplasmic dynein2 (D2) compared to GFP control siRNA (C); GADPH, loading control. **(b)** Immunoblot from lysates of HeLa cells treated with cytoplamic dynein1 heavy chain (D1) siRNA shows decrease in the intermediate chain subunit of the complex (dynein IC) compared to control (GFP). γ tubulin, loading control. **(c)** Manual counting of mitotic indices after GFP, dynein1 (D1) or dynein2 (D2) siRNA in HeLa cells showing that dynein1 but not dynein2 depletion induces an increase in mitotic index. *n*=250 cells/ experiment. **(d)** Immunofluorescence images of dynein1 (D1) and dynein2 (D2) depleted HeLa cells show that both dynein1 and dynein2 depletion result in previously reported interphase phenotypes. The previously reported golgi fragmentation (golgin 97) following dynein depletion functionally confirms the efficacy of both siRNAs. Graph (right), quantification of cells with golgi fragmentation. Error bars, mean of at least 3 experiments ± SD, *n*=230 cells/ experiment.

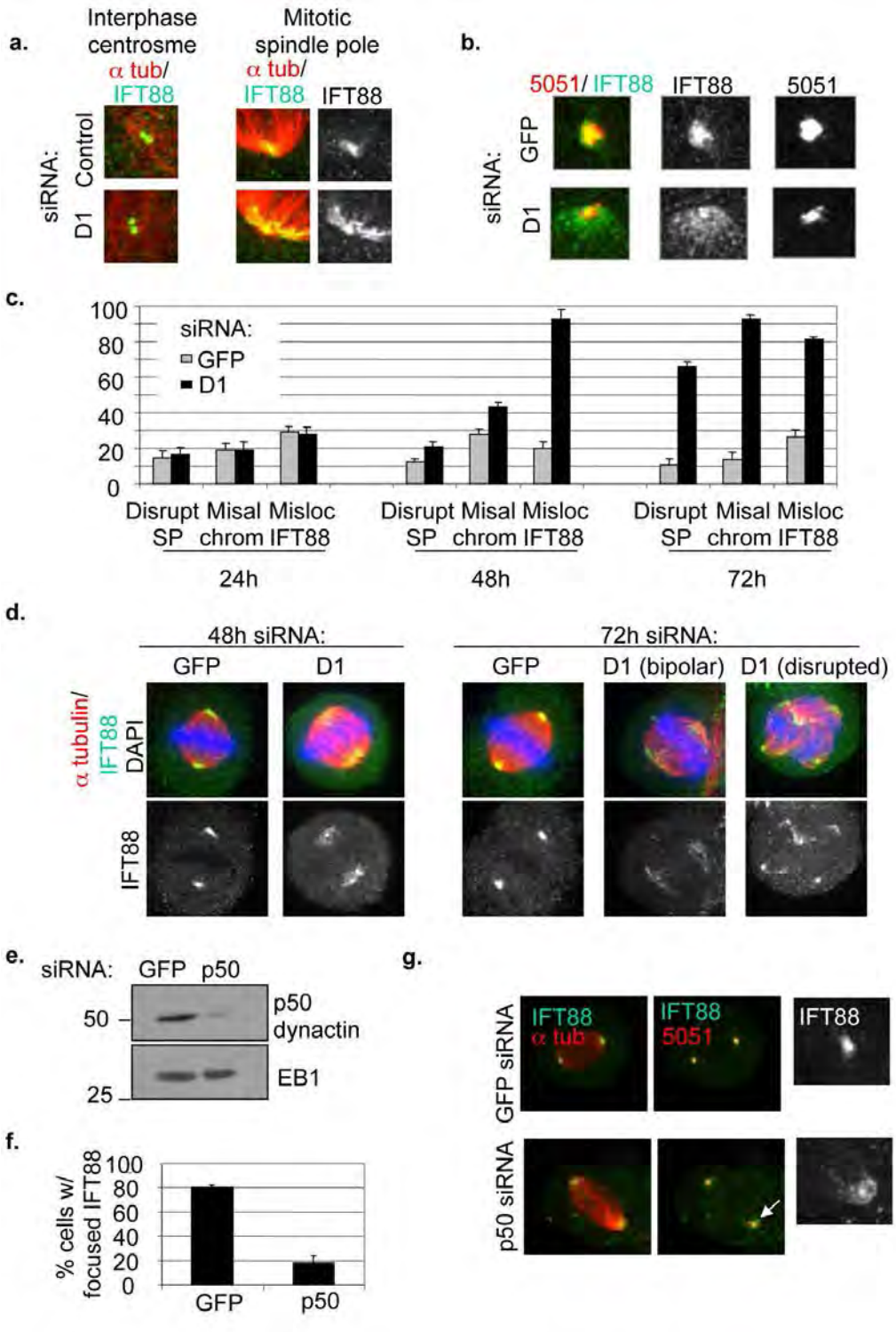
a.
Interphase centrosme
α tub/ IFT88
Mitotic spindle pole
α tub/ IFT88
IFT88
siRNA:
Control
D1
b.
5051/ IFT88
IFT88
5051
siRNA:
GFP
D1
c.
100
80
60
40
20
0
siRNA:
GFP
D1
Disrupt Misal Misloc SP chrom IFT88
24h
48h
72h
d.
48h siRNA:
72h siRNA:
GFP
D1
GFP
D1 (bipolar)
D1 (disrupted)
α tubulin/ IFT88 DAPI
IFT88
e.
siRNA: GFP p50
50
25
p50 dynactin
EB1
f.
% cells w/ focused IFT88
100
80
60
40
20
0
GFP
p50
g.
GFP siRNA
p50 siRNA
IFT88
α tub
IFT88
5051
IFT88

Figure II-S6

Figure II-S6 Dynein1 and p50 depletion disrupts the spindle pole localization of IFT88 in HeLa cells.

(a) Immunofluoresence images showing that Dynein1 (D1) depletion leads to major disruption of the localization of IFT88 at spindle poles (right panels) but no major disruption is observed at interphase centrosomes (left panels) as previously reported (Robert et al., 2007). **(b)** Immunofluoresence images showing that the centrosome marker 5051 is decreased but not defocused in D1 depleted mitotic cells demonstrating the specificity of IFT88 redistribution. **(c)** Early (24h, 48h after transfection) and late (72h after transfection) time points following D1 depletion reveal that IFT88 mislocalization (misloc.) occurs before major spindle disruption (disrupt SP) including misaligned chromosomes (misal. chrom.). **(d)** Corresponding immunofluorescence images. **(e)** Western blots showing loss of p50 dynactin 48h after transfection. GFP, siRNA control. EB1, loading control. **(f)** Quantification, % cells with disrupted IFT88 pole localization in p50 depleted cells compared to control (GFP). Average of 3 independent experiments ± SD. n=60 mitotic spindles. **(g)** Mitotic spindles (α tubulin) showing loss of focus of IFT88 at spindle poles (arrow) in p50 dynactin depleted HeLa cells. 5051, spindle pole. Enlargements, spindle poles.

a.

siRNA: / Functional assay:	GFP	D1	D2
Increased mitotic index	no	yes	no
IFT88 accumulation around spindle poles (unfocused staining)	no	yes	no
Golgi fragmentation	no	yes	yes
IFT88 accumulation at the tip of cilium	no	no	yes

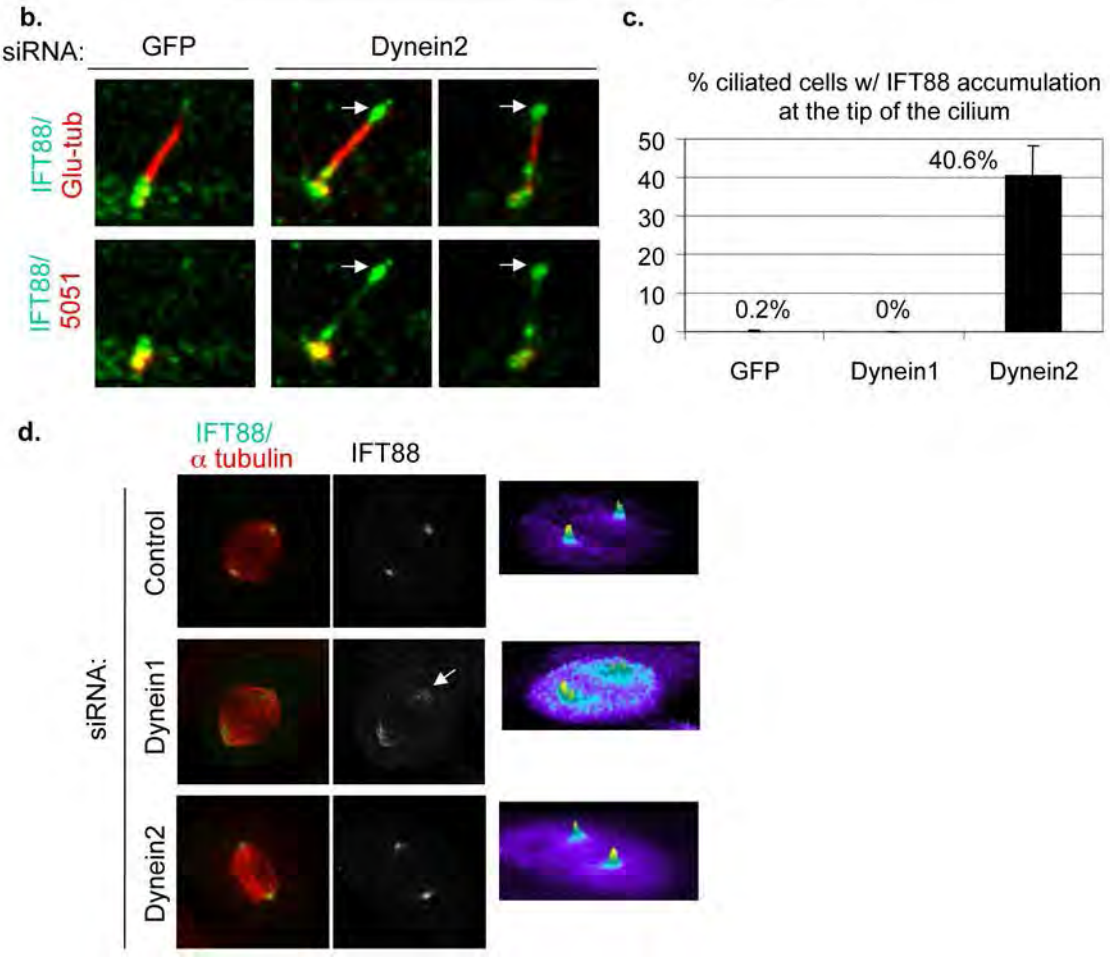

Figure II-S7

Figure II-S7 Dynein2 depletion causes IFT88 accumulation at tips of cilia but does not disrupt IFT88 localization at spindle poles.
(a) Summary table of dynein1 (D1) and dynein2 (D2) siRNA functional assays in mitotic cells (two top rows) and interphase cells (two bottom rows). **(b)** Immunofluoresence images showing redistribution and accumulation of IFT88 at the tip of the cilium (arrow) in RPE serum-starved cells following dynein2 depletion, functionally confirming the efficacy of the siRNA. Polyglutamylated tubulin, cilium. 5051, basal body. **(c)** Quantification of defects in ciliated RPE cells after GFP, dynein1 or dynein2 siRNA. Average of 3 independent experiments +/- SD, *n*=225 ciliated cells. **(d)** Mitotic spindles of HeLa cells stained for microtubules (α tubulin) and IFT88 showing disrupted IFT88 localization at spindle poles (arrow) in dynein1 but not dynein2 or control depleted cells. Inset (right), IFT88 intensity profiles.

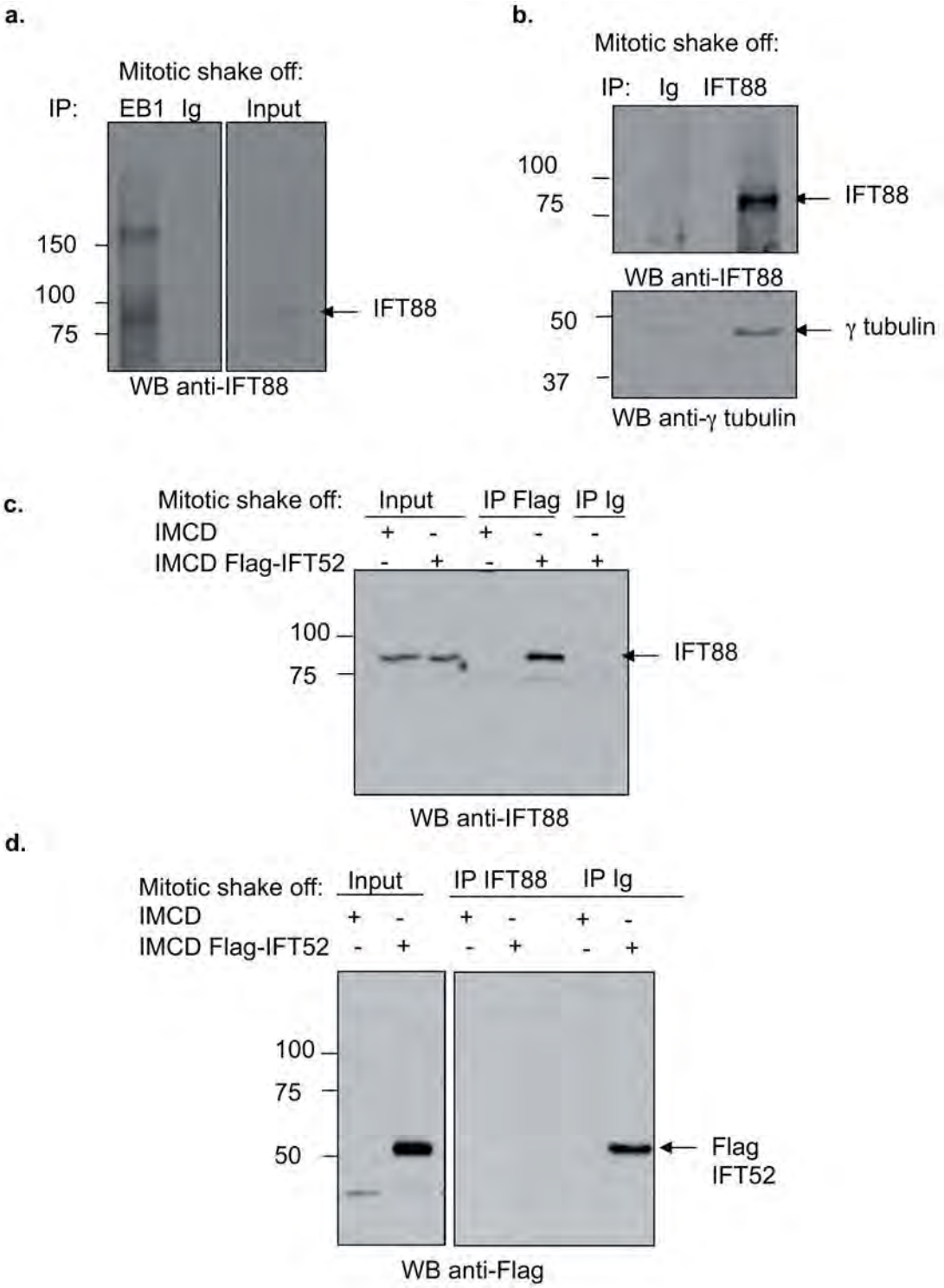
a.
Mitotic shake off:
IP: EB1 Ig Input
150
100
75
IFT88
WB anti-IFT88
b.
Mitotic shake off:
IP: Ig IFT88
100
75
IFT88
WB anti-IFT88
50
37
γ tubulin
WB anti-γ tubulin
c.
Mitotic shake off: Input IP Flag IP Ig
IMCD + - + - -
IMCD Flag-IFT52 - + - + +
100
75
IFT88
WB anti-IFT88
d.
Mitotic shake off: Input IP IFT88 IP Ig
IMCD + - + - + -
IMCD Flag-IFT52 - + - + - +
100
75
50
Flag IFT52
WB anti-Flag

Figure II-S8

Figure II-S8 Full scans of key immunoblots.
(a) IFT88 immunoblots of EB1 immunoprecipitation and total lysate (input). Shown in Fig. IIe. **(b)** γ tubulin and IFT88 immunoblots of IFT88 immunoprecipitation. Shown in Fig. IIe. **(c)** IFT88 immunoblot of Flag immunoprecipitation and total lysate (input). Shown in Supplementary information figure II-S4d. **(d)** Flag immunoblots of IFT88 immunoprecipitation and total lysate (input). Shown in Supplementary information figure II-S4e. **(e)** Immunoblots using antibodies as indicated of gel filtration fractions and input. Shown in Fig. II-5a. Dotted lines indicate where membrane was cut before blotting. **(f)** IFT88 and dynein IC immunoblots of dynein IC immunoprecipitation and total lysate (input). Shown in Fig. II-5a.

CHAPTER III

IFT88 AND IFT20 CO-REGULATE MITOSIS

Bright A and Doxsey S

Author contributions

Figures:
Contributions by Alison Bright
Figures III-1 through III-22 and Supplementary Figure III-S1

Abstract

Intraflagellar transport (IFT) proteins are key players in a bidirectional transport system required for ciliogenesis, and have been implicated in mitotic progression. Specifically, the IFT complex B member, IFT88, is part of a dynein1 driven mitotic transport complex required for spindle orientation[77]. However, it is unknown if IFT88 functions in concert with the remaining IFT B complex members during mitosis, as it does within cilia. We find that complex B members, IFT88, IFT57, IFT52, and IFT20 are in a mitotic complex with dynein-1, which localizes to the mitotic spindle pole. IFT88-depletion stalls mitotic progression, and causes disrupted spindle poles leading to spindle misorientation. Strikingly, depleting individual complex B members, IFT57, IFT52, or IFT20 did not disrupt mitotic progression, however depleting IFT20 (but not IFT52 or IFT57) simultaneously with IFT88 led to a rescue. Both the accumulation of dynein1 cargoes at spindle poles, as well as spindle orientation were rescued by concurrent IFT88 and IFT20 depletion. These findings are consistent with a model in which IFT88 negatively regulates IFT20, and IFT20 negatively regulates microtubule-based transport to the spindle pole, and thus mitotic progression. This work further suggests IFT complex B intrinsically self-regulates during mitosis, a capacity that may be conserved during ciliogenesis.

Introduction

Cilia are long, microtubule-based structures that emanate from the centrosome in non-cycling cells. They function in cell movement, sensation, and signaling[1,2]. Mitotic

spindles, another cellular structure composed of microtubules focused around centrosomes, set up the axis for cell division, and facilitate proper chromosome segregation during mitosis[3,4]. As discussed in Chapter I, cilia and spindles are both assembled and maintained via microtubule-based, motor-driven, transport systems (Figure I-1). The similarities between cilia and spindle assembly suggest proteins involved in one process may also function in the other.

Although cilia are resorbed prior to mitosis, IFT proteins are still expressed and several localize to spindle poles[24–27]. We demonstrated that IFT88, an IFT protein required for ciliogenesis[41], is also required for mitotic spindle orientation in non-ciliated, mitotic cells[77]. Like in cilia, IFT88 regulates a microtubule motor-driven transport process during mitosis. In this case IFT88 regulates the microtubule-based transport of dynein1-mediated cargo, including spindle pole components EB1 and γ-tubulin, as well as peripheral microtubule bundles, to the spindle pole during spindle assembly[77].

In cilia IFT proteins form two complexes: IFT complex A and IFT complex B, of which IFT88 is a member. The striking similarity between IFT88's mitotic and ciliary roles, and IFT88's co-localization with additional IFT complex B members at spindle poles suggests that IFT88 may function with IFT complex B during mitosis, like it does in cilia. In this manuscript we examined additional IFT complex B members in mitosis. Our results demonstrate that like IFT88, several additional IFT proteins interact with dynein1 during mitosis. Further we find that one additional IFT protein, IFT20, rescues the mitotic dysfunctions associated with IFT88-depletion when the two proteins are

depleted simultaneously, suggesting IFT88 and IFT20 function in the same genetic pathway and co-regulate microtubule-based transport during mitosis.

Results

Because IFT88 is known to function within IFT complex B during ciliogenesis, thus I propose that IFT complex B is functionally maintained during mitosis. IFT complex B is assembled in ciliated (interphase) cells, so lysate from unsynchronized (interphase) cells, or cells synchronized in mitosis by double thymidine block and release, was separated by size exclusion chromatography to identify IFT88-containing complexes. Fractions prepared for immunoblotting showed that as expected in interphase lysate, three IFT complex B members, IFT88, IFT52, and IFT20 co-eluted, indicating the presence of a 2-4 MDa IFT complex B. The mitotic elution profile was unchanged with IFT88, IFT52, and IFT20 again co-eluting (Figure III-1). The striking similarity between interphase and mitotic IFT protein elution profiles, and the known mitotic interaction between IFT88 and IFT52 (Figure II-S4d – II-S4e) suggests that IFT complex B is maintained during mitosis.

Size exclusion chromatography demonstrated a partial co-localization of IFT complex B proteins with dynein1 (Figure III-1), consistent with our previous finding that IFT88 interacts with dynein1 during mitosis (Figure II-5a). Based on this I tested whether IFT57, IFT52, and IFT20, also interact with dynein1 during mitosis by co-immunoprecipitation. Similar to IFT88, IFT57, IFT52, and IFT20 also co-

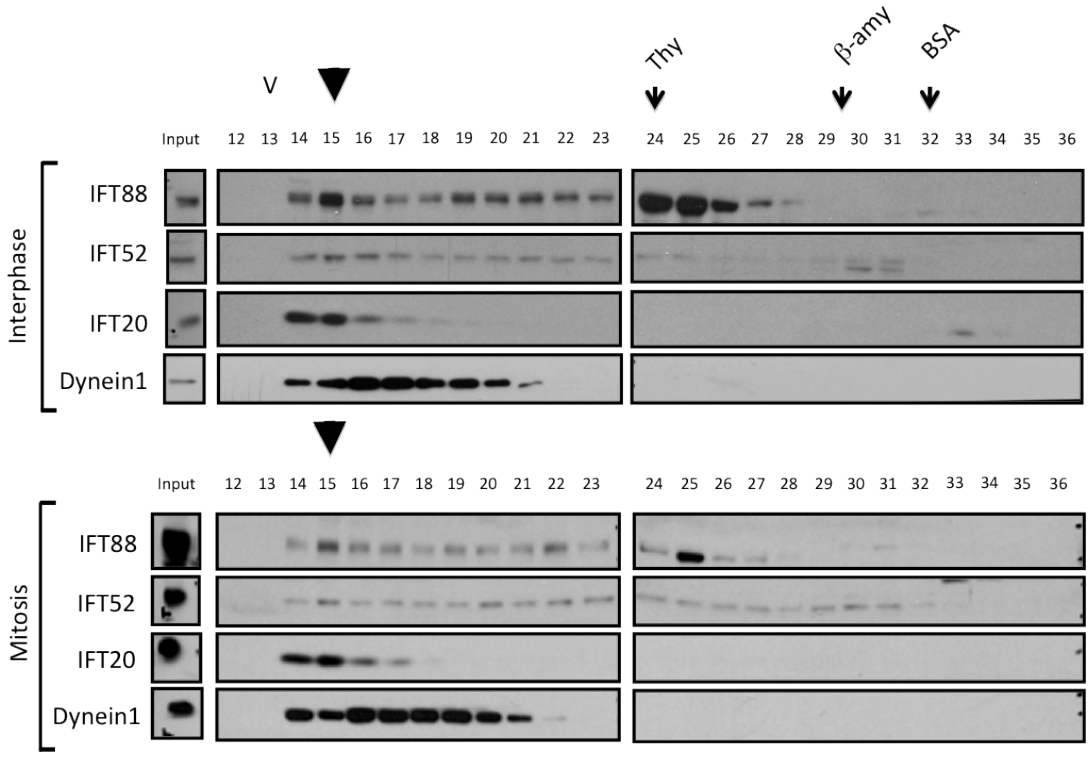

Figure III-1 IFT complex B is maintained during mitosis.
Top panel: Interphase HeLa cell lysate was separated using a superose 6 gel filtration column. Fractions were probed for IFT complex B proteins, IFT88, IFT57, and IFT20, and dynein1. Dynein1 antibody recognizes cytoplasmic dynein intermediate chain. Arrowhead, peak elution fraction for IFT complex B proteins. Arrows mark calibration protein elution: bovine serum albumin-66KDa (BSA), β-amylase-200KDa (β-amy), and thyroglobulin-669KDa (Thy). "V," void volume. Bottom panel: mitotic HeLa cell lysate was treated as described above. Arrowhead, peak elution fraction for IFT complex B proteins.

immunoprecipitated with dynein1 from mitotic lysate (Figure III-2). In addition, IFT88, IFT57, IFT52, and IFT20 all demonstrate consistent mitotic spindle pole localization (Figure III-3). Together these findings suggest that IFT88, IFT57, IFT52, and IFT20 maintain an IFT B complex during mitosis.

To characterize IFT complex B during mitosis I compared mitotic progression in cells depleted of IFT88, IFT57, IFT52, and IFT20 with Lamin-depleted control cells. Consistent with my previous finding, IFT88 depletion resulted in a 3-fold increase in mitotic cells compared to controls (Figure II-S1c; Figure III-4) and increased the amount of time IFT88-depleted cells take to complete mitosis (Figure II-S1d – II-S1e; Figure III-6). Although IFT complex B is maintained during mitosis, and IFT57, IFT52, and IFT20, like IFT88, interact with dynein1 during mitosis, the depletion of IFT57, IFT52, or IFT20 did not phenocopy IFT88 depletion. Despite effective siRNA depletion of IFT57, IFT52, or IFT20, cells did not accumulate in mitosis (Figure III-4). This result was recapitulated when each IFT protein was depleted using an additional siRNA sequence (Figure III-5). Furthermore, cells depleted of IFT57, IFT52, or IFT20 did not take longer than control cells to complete mitosis (Figure III-6).

To unmask the molecular mechanism between IFT complex B members during mitosis, simultaneous siRNA depletion of IFT88, IFT57, IFT52, and IFT20 was performed. Strikingly, whereas individual depletion of IFT57, IFT52, and IFT20 caused no mitotic defect, depletion of all three at the same time as IFT88 rescued the accumulation of cells in mitosis caused by IFT88 depletion alone (Figure III-7). Thus, I

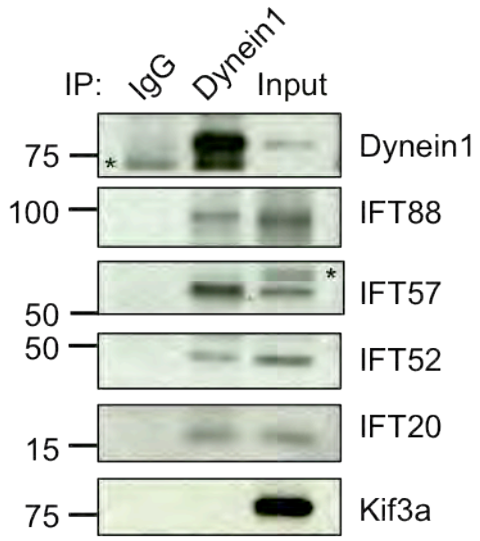

Figure III-2 IFT complex B members interact with dynein1 during mitosis. Endogenous dynein1 was immunoprecipitated from mitotic HeLa cell lysate using an antibody against dynein intermediate chain. Cells were synchronized using nocodazole. IFT complex B members, IFT88, IFT57, IFT52, and IFT20 co-immunoprecipitated with dynein1. Kif3a did not co-immunoprecipitate with dynein1, demonstrating the specificity of dynein1's interaction with IFT proteins. IgG, mouse antibody, negative immunoprecipitation (IP) control, * indicates non-specific band.

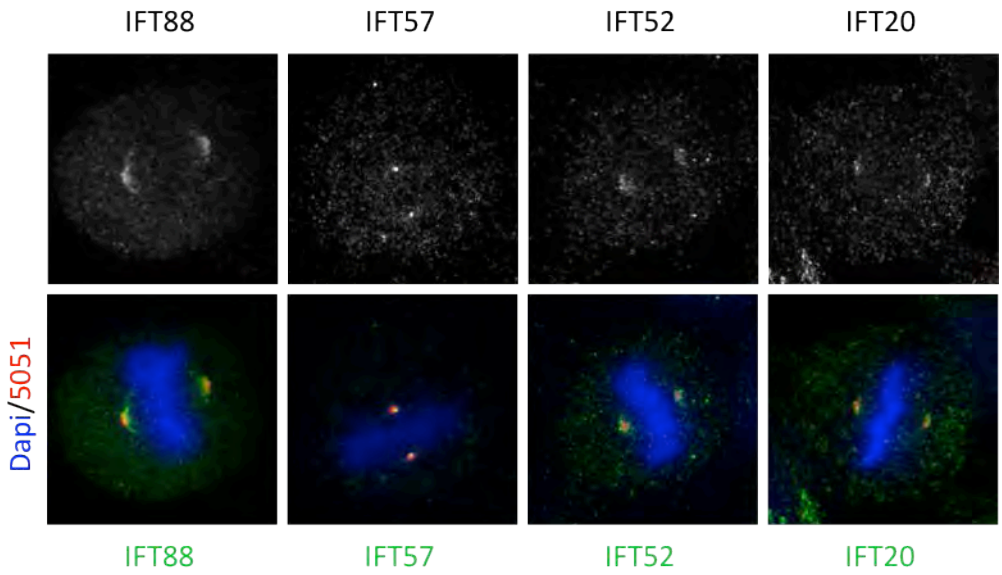

Figure III-3 IFT complex B proteins localize to mitotic spindle poles.
Immunofluorescence microscopy images of mitotic HeLa cells. Top panel stained for IFT complex B members: IFT88, IFT57, IFT52, and IFT20. Bottom panel, merge: IFT protein (green), spindle poles, 5051 (red), and chromosomes, Dapi (blue).

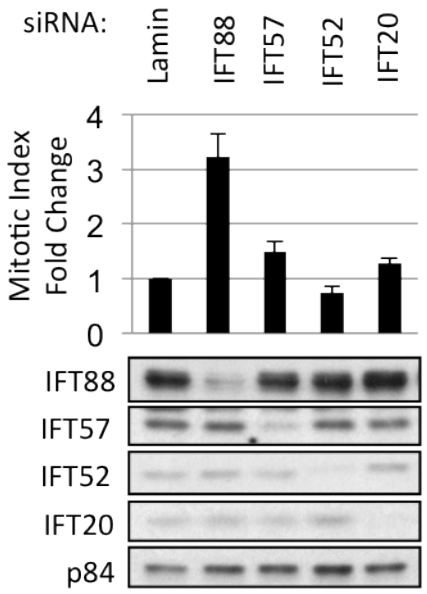

Figure III-4 Loss of IFT88, but not IFT57, IFT52, or IFT20 results in increased mitotic index. Mitotic index was calculated for HeLa cells depleted of indicated proteins. Top panel: quantification shows mitotic index fold change in populations depleted of indicated proteins compared to a lamin-depleted control population. (n=3 independent experiments, error bar is SE, >300 cells/bar). Bottom panel, immunoblot of lysates from mitotic cells depleted of indicated proteins. Loading control, p84.

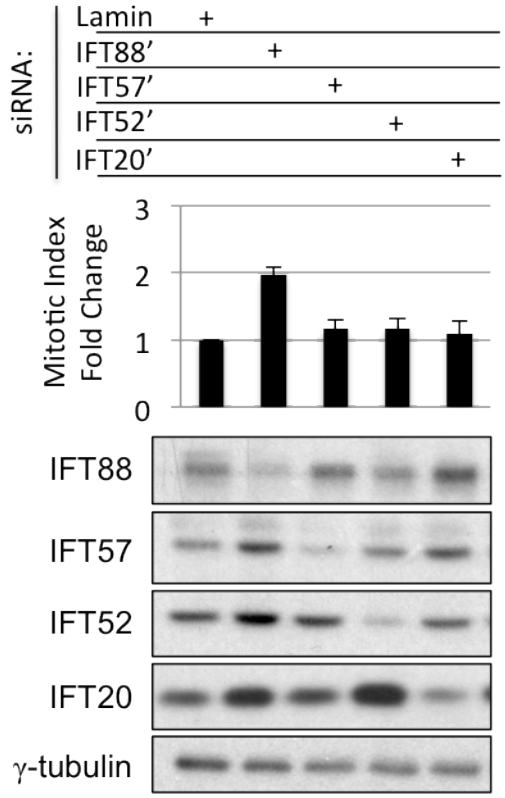

Figure III-5 Using an additional siRNA against each protein, loss of IFT88, but not IFT57, IFT52, or IFT20 results in increased mitotic index.
Mitotic index was calculated for HeLa cells depleted of indicated proteins. Top panel: quantification shows mitotic index fold change in populations depleted of indicated proteins compared to a lamin-depleted control population. (n=3 independent experiments, error bar is SE, >300 cells/bar/experiment). Bottom panel, immunoblot of lysates from mitotic cells depleted of indicated proteins. Loading control, γ-tubulin.

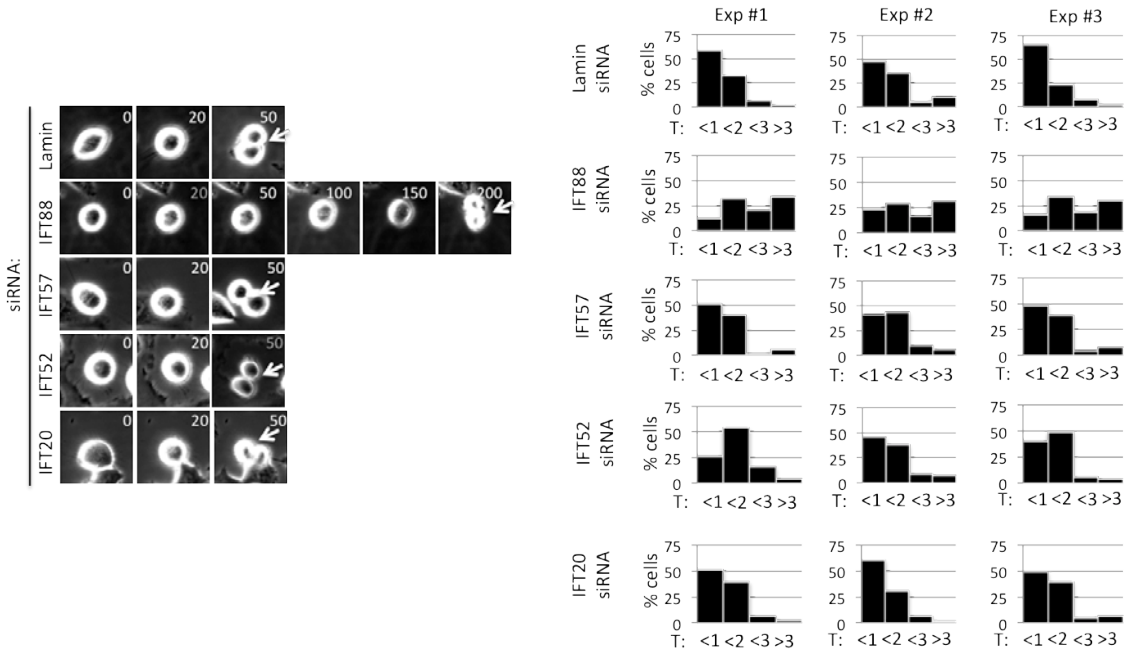

Figure III-6 Loss of IFT88, but not IFT57, IFT52, or IFT20 results in delayed mitotic progression.

Time-lapse imaging was performed to measure the pace at which HeLa cells progress through mitosis after depletion of indicated proteins. Left, images show cells depleted of indicated proteins progressing through mitosis. Arrows indicate cleavage furrow formation. Right, quantification shows the percentage of cells completing mitosis (nuclear envelope breakdown to daughter cell adhesion) within indicated time intervals. (Time, T, in hours, n=3 experiments, >100 cells/condition/experiment.)

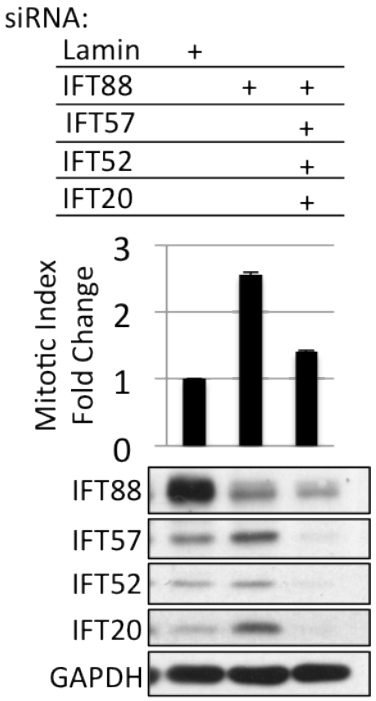

Figure III-7 Simultaneous depletion of IFT88, IFT57, IFT52, and IFT20 rescues mitotic index increase associated with IFT88-depletion alone.
Mitotic index was calculated for HeLa cells depleted of indicated proteins. Top panel: quantification shows mitotic index fold change in populations depleted of indicated proteins compared to a lamin-depleted control population. (n=3 independent experiments, error bar is SE, >300 cells/bar). Bottom panel, lysates from mitotic cells depleted of indicated proteins. Loading control, GAPDH.

propose that IFT88 co-functions with IFT57, IFT52, and/or IFT20. To determine which IFT protein was responsible for the rescue, IFT88 was depleted pairwise with IFT57, IFT52, or IFT20. Depletion of IFT20 at the same time as IFT88 was uniquely able to rescue the accumulation of cells in mitosis, while simultaneous depletion of IFT88 and IFT57, or IFT88 and IFT52, or IFT88 and a control protein (GFP) had no effect (Figure III-8). The rescue was also observed when IFT20 was depleted at the same time as IFT88, using a second siRNA sequence against IFT20 or a second siRNA sequence against IFT88 (Figure III-9 – III-10). Furthermore, simultaneous depletion of IFT88 and IFT20 partially rescued the delay in mitosis caused by IFT88 depletion alone, with ~75% of cells completing mitosis in under two hours, compared with ~90% of control cells (Figure III-11). The rescue induced by IFT88 and IFT20 co-depletion indicates the two proteins function in the same genetic pathway, and suggests a model in which IFT88 negatively regulates IFT20, which in turn negatively regulates mitotic progression (Figure III-12).

We examined the molecular mechanism causing IFT88/IFT20 co-depletion to rescue IFT88-depletion induced defects during mitotic spindle organization. We confirmed that IFT88 depletion, but not IFT20 depletion, disrupted metaphase plate congression, and further discovered that IFT88/IFT20 co-depletion rescued the metaphase plate congression defect caused by IFT88 depletion alone (Figure II-1a–II1b; Figure III-13 – III-14). We also confirmed that IFT88 depletion but not IFT20 depletion resulted in misoriented mitotic spindles. Neither control cells (lamin siRNA), nor IFT20-depleted cells displayed a defect in spindle orientation (~60% having a spindle pole axis

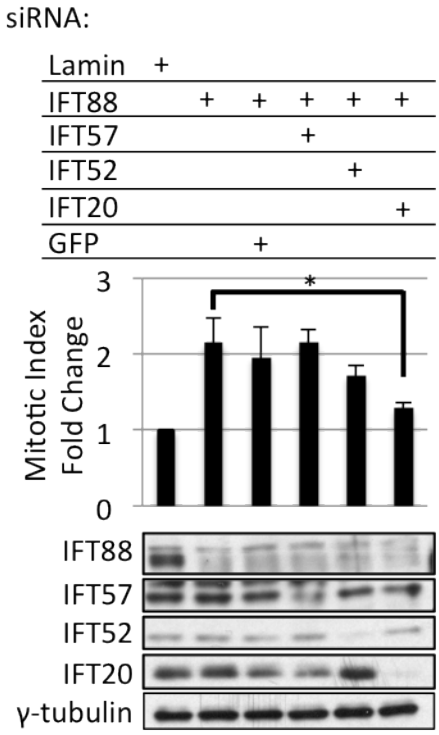

Figure III-8 Simultaneous depletion of IFT88 and IFT20 rescues mitotic index increase associated with IFT88-depletion alone.
Mitotic index was calculated for HeLa cells depleted of indicated proteins. Top panel: quantification shows mitotic index fold change in populations depleted of indicated proteins compared to a lamin-depleted control population. (n=3 independent experiments, error bar is SE, >300 cells/bar). Bottom panel, lysates from mitotic cells depleted of indicated proteins. Loading control, γ-tubulin. Statistics performed using Anova test.

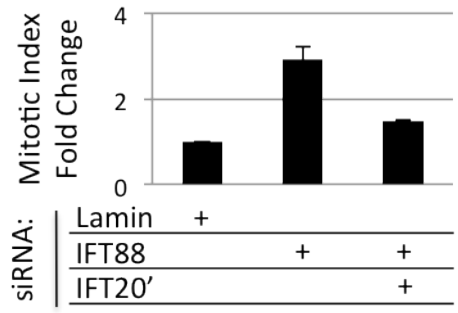

Figure III-9 Depletion of IFT20 at the same time as IFT88 (using a second siRNA sequence targeting IFT20) rescues the mitotic index increase associated with IFT88-depletion alone.
Quantification shows mitotic index fold change in populations depleted of indicated proteins compared to a lamin-depleted control population. (n=3 independent experiments, error bar is SE, >300 cells/bar/experiment).

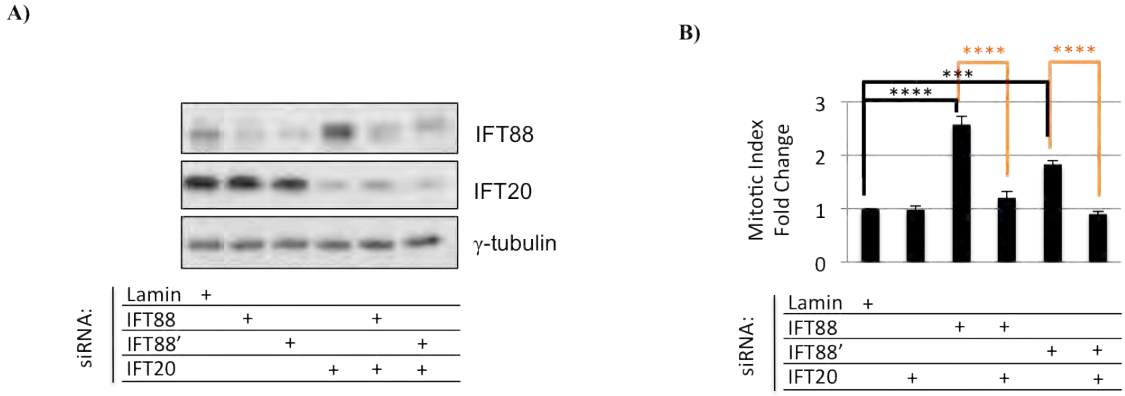

Figure III-10 Depletion of IFT20 at the same time as IFT88 (using either of two separate IFT88 siRNA sequences) rescues mitotic index increase associated with IFT88-depletion alone.

A) Lysates from cells depleted of indicated proteins. Loading control, γ-tubulin. B) Mitotic index was calculated for HeLa cells depleted of indicated proteins. Quantification shows mitotic index fold change in populations depleted of indicated proteins compared to a lamin-depleted control population. (n=3 independent experiments, error bar is SE, >300 cells/bar/experiment, statistics performed using Anova test).

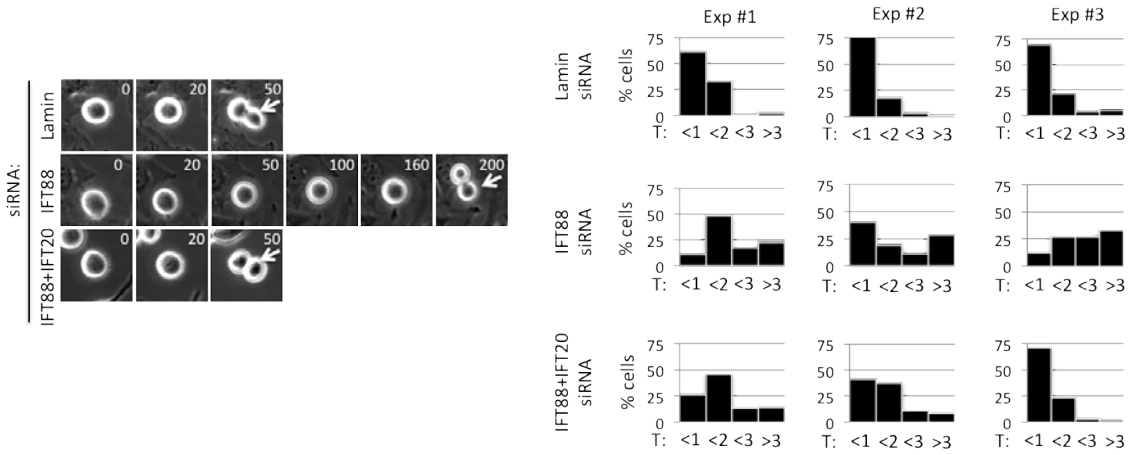

Figure III-11 Simultaneous depletion of IFT88 and IFT20 rescues delay in mitotic progression associated with IFT88-depletion alone.
Time-lapse imaging was performed to measure the pace at which HeLa cells progress through mitosis after depletion of indicated proteins. Left, images show cells depleted of indicated proteins progressing through mitosis. Arrows indicate cleavage furrow formation. Right, quantification shows the percentage of cells completing mitosis (nuclear envelope breakdown to daughter cell adhesion) within indicated time intervals. (Time, T, in hours, n=3 experiments, >100 cells/condition/experiment.)

Figure III-12 Model for IFT88 and IFT20 co-function in mitosis.
IFT20 is required for IFT88-depletion induced mitotic dysfunction, placing IFT20 downstream of IFT88 in a genetic interaction pathway during mitosis. Data suggests a model in which IFT88 negatively regulates IFT20, and IFT20 negatively regulates mitotic progression.

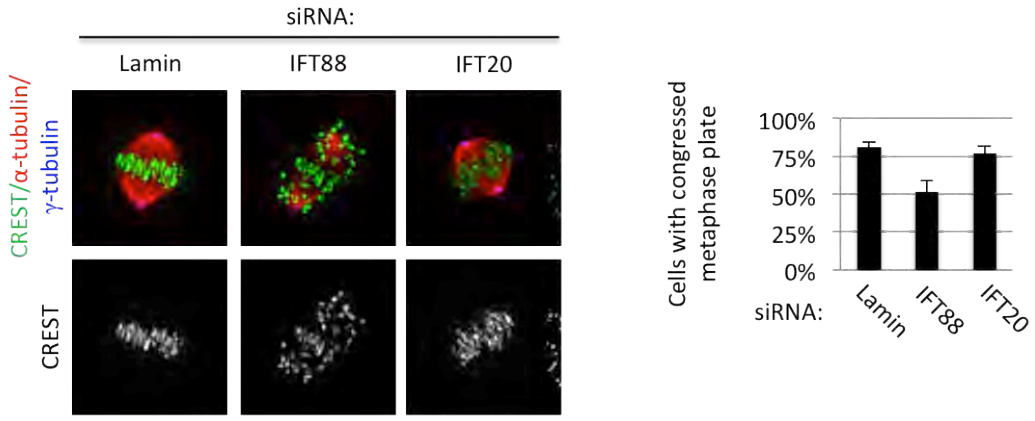

Figure III-13 Depletion of IFT88, but not IFT20 disrupts metaphase plate formation.
Left: immunofluorescence microscopy images of mitotic HeLa cells, spindles, α-tubulin (red), spindle poles, γ-tubulin (blue), and kinetechores, CREST (green). Right: quantification shows percentage of cells with proper metaphase plate formation after depletion of indicated proteins. (n=3 independent experiments, error bars are SE, >70cells/bar)

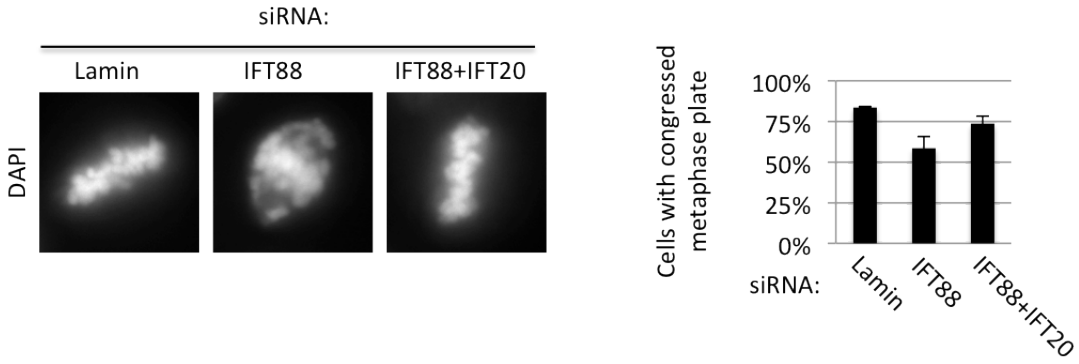

Figure III-14 Simultaneous depletion of IFT88 and IFT20 rescues metaphase plate formation.

Left: immunofluorescence microscopy images of mitotic chromosomes, (Dapi). Right, quantification shows percentage of HeLa cells with proper metaphase plate formation after depletion of indicated proteins. (n=3 independent experiments, error bars are SE, >70cells/bar)

at an angle of less than 10°), while in comparison only 30% of IFT88-depleted cells had spindle pole axes parallel to the substrate (Figure II-1c – II-1d; Figure III-15). Strikingly, IFT88/IFT20 co-depletion abolished the spindle misorientation defect caused by IFT88-depletion (Figure III-16). Spindle misorientation was also rescued by depleting IFT88 and a second siRNA against IFT20, confirming that the rescue was specific to IFT20 co-depletion with IFT88, and not a result off-target siRNA effects (Figure III-17). Based on these findings, I propose that together IFT20 and IFT88 coordinate the appropriate organization of the mitotic spindle to ensure symmetric division.

To understand how the co-depletion of IFT88 and IFT20 rescues mitotic spindle functionality, we tested if IFT20 along with IFT88 was required for the dynein1-mediated transport of spindle pole proteins. EB1 and γ-tubulin localization was compared between control cells and cells depleted of IFT88, IFT20, or IFT88 and IFT20 simultaneously. EB1 and γ-tubulin were disrupted at spindle poles in IFT88-depleted cells compared to control cells (Figure II-2c – II-2d; Figure III-18 – III-19). EB1 and γ-tubulin at spindle poles were unaffected in IFT20-depleted cells (Figure III-18 – III-19). Whereas, IFT88 and IFT20 co-depletion rescued EB1 and γ-tubulin localization (Figure III-20 – III-21), consistent with a proposed mechanism of IFT88 and IFT20 acting in consort to regulate dynein1-mediated transport of mitotic spindle pole cargoes (Figure III-22).

Discussion:

In summary we have demonstrated that four members of IFT complex B, IFT88, IFT57, IFT52, and IFT20 interact with dynein1 during mitosis. Of this complex, IFT20

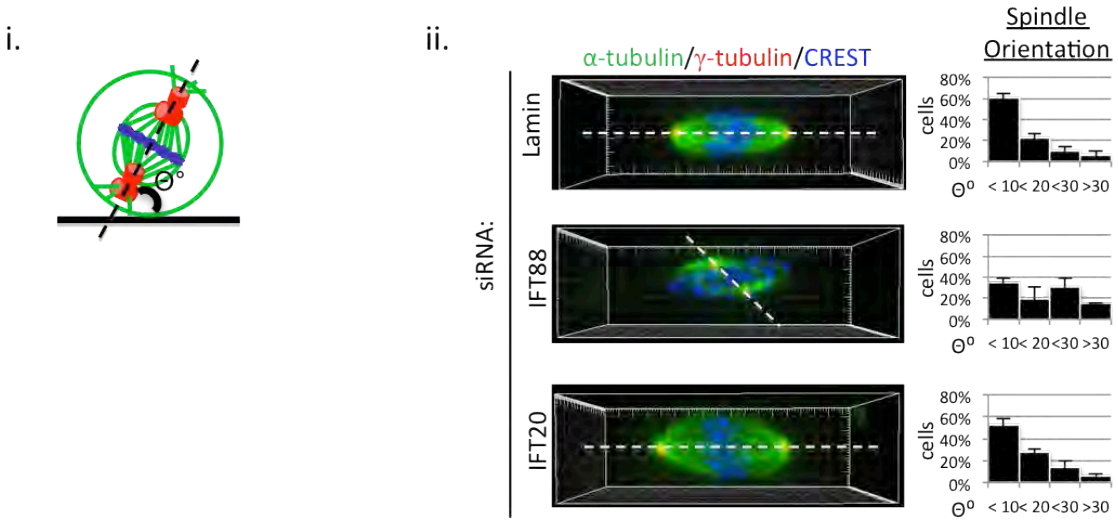

Figure III-15 Depletion of IFT88 but not IFT20 disrupts mitotic spindle orientation. (i) Cartoon depicting the angle (Θ°) between the spindle pole axis (dashed black line) and growth substrate (solid black line). (ii) Left: side views of 3-D reconstructed immunofluorescence images show spindle orientation relative to growth substrate in HeLa cells depleted of indicated proteins. Spindle, α-tubulin (green), spindle poles, γ-tubulin (red), kinetochores, CREST (blue). Dashed white line, spindle pole axis. Right: quantification of the angle (θ°) between the spindle pole axis and the growth substrate. Graphs show the distribution of metaphase spindle angles (θ°) in cells depleted of indicated proteins. (n=3 independent experiments, error bars are SE, >15cells/graph)

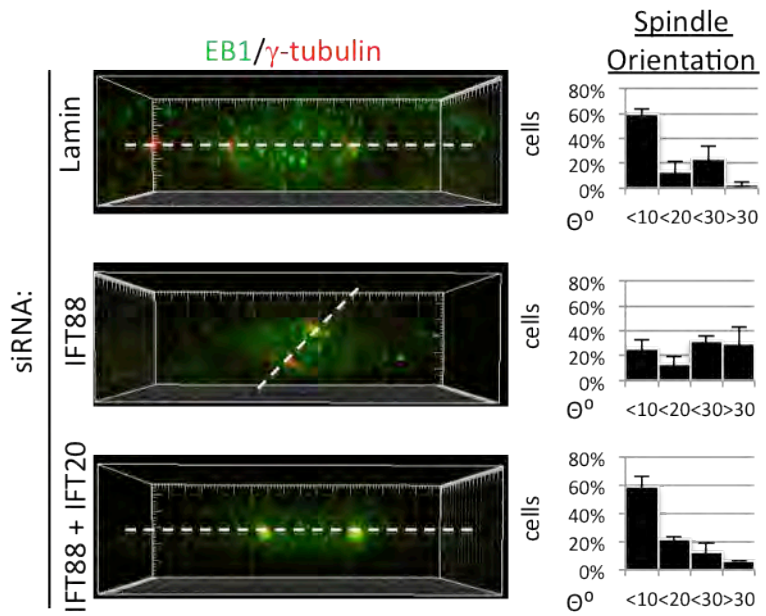

Figure III-16 Simultaneous depletion of IFT88 and IFT20 rescues mitotic spindle orientation.

Left: side views of 3-D reconstructed immunofluorescence images show spindle orientation relative to growth substrate in HeLa cells depleted of indicated proteins. Spindle, EB1 (green), spindle poles, γ-tubulin (red). Dashed line, spindle pole axis. Right: quantification of the angle (θ°) between the spindle pole axis and the growth substrate. Graphs show the distribution of metaphase spindle angles (θ°) in cells depleted of indicated proteins. (n=3 independent experiments, error bars are SE, >15cells/graph)

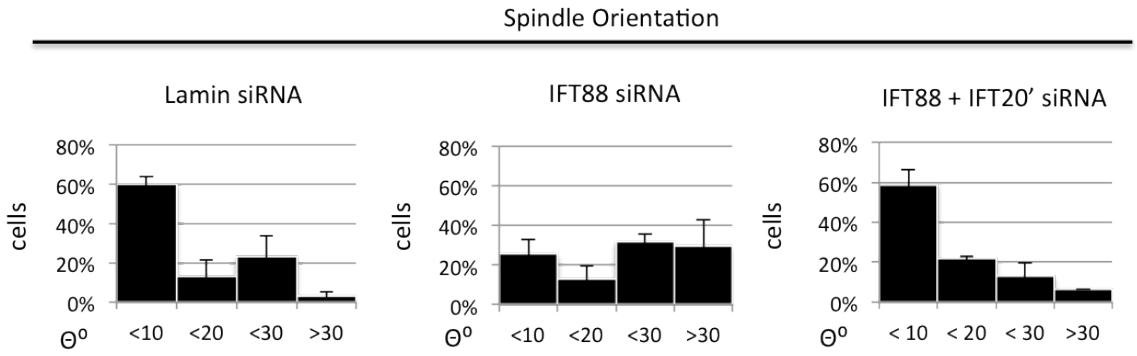

Figure III-17 Simultaneous depletion of IFT88 and IFT20 (using a second siRNA against IFT20) rescues mitotic spindle orientation.
Quantification of the angle (θ°) between the spindle pole axis and the growth substrate. Graphs show the distribution of metaphase spindle angles (θ°) in HeLa cells depleted of indicated proteins. (n=3 independent experiments, error bars are SE, >15cells/graph/experiment)

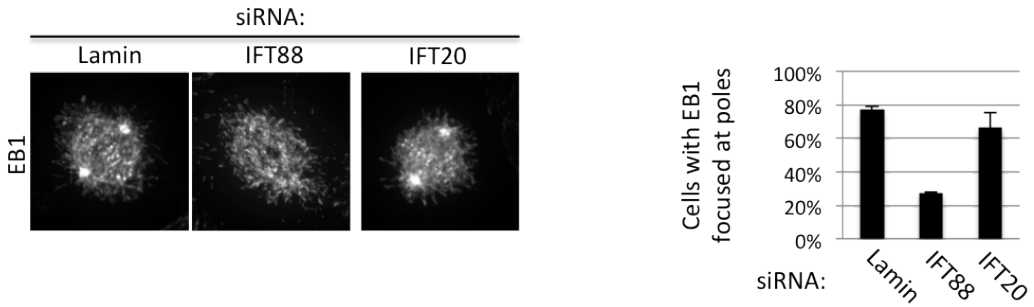

Figure III-18 Depletion of IFT88 but not IFT20 disrupts EB1 at spindle poles. Immunofluorescence microscopy images of mitotic HeLa cells stained for EB1. Quantification shows percentage of cells with focused EB1 at spindle poles after depletion of indicated proteins. (n=3 independent experiments, error bars are SE, >70cells/bar)

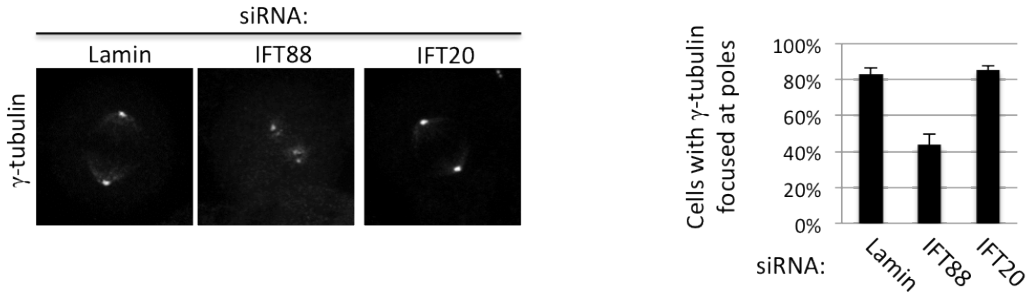

Figure III-19 Depletion of IFT88 but not IFT20 disrupts γ-tubulin at spindle poles. Immunofluorescence microscopy images of mitotic HeLa cells stained for γ-tubulin. Quantification shows percentage of cells with well-focused γ-tubulin at spindle poles after indicated proteins are depleted. (n=3 independent experiments, error bars are SE, >70cells per bar)

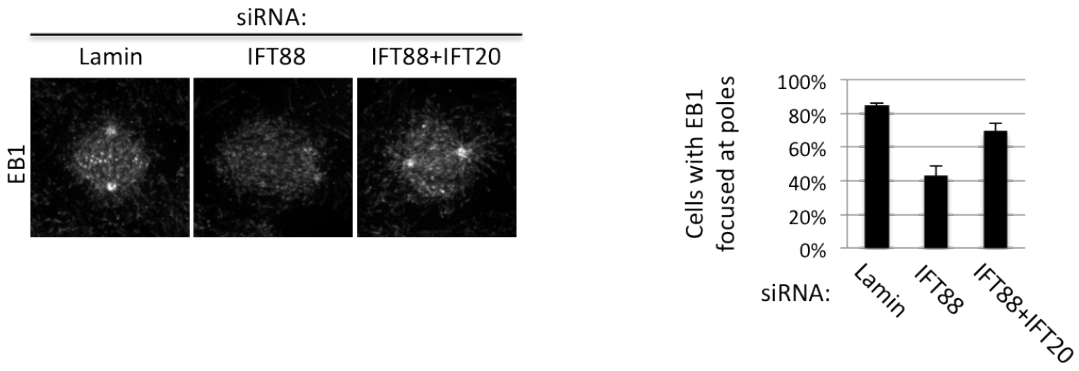

Figure III-20 Simultaneous depletion of IFT88 and IFT20 rescues EB1 at spindle poles.
Immunofluorescence microscopy images of mitotic HeLa cells stained for EB1. Quantification shows percentage of cells with focused EB1 at spindle poles, after depletion of indicated proteins. (n=3 experiments, error bars are SE, >70cells/bar)

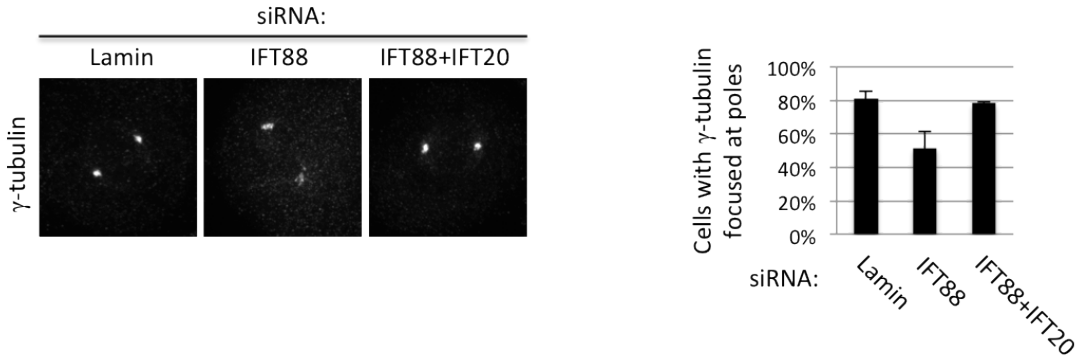

Figure III-21 Simultaneous depletion of IFT88 and IFT20 rescues γ-tubulin at spindle poles.
Immunofluorescence microscopy images of mitotic HeLa cells stained for γ-tubulin. Quantification shows percentage of cells with well-focused γ-tubulin at spindle poles after indicated proteins are depleted. (n=3 independent experiments, error bars are SE, >70cells per bar)

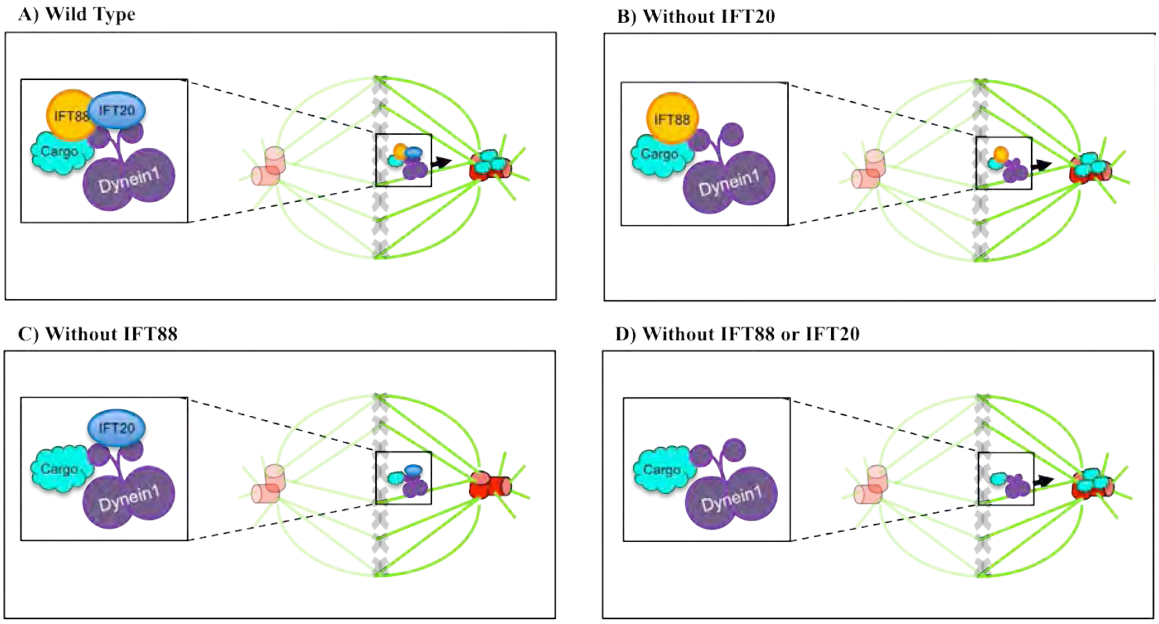

Figure III-22 Hypothetical model for IFT88 and IFT20 co-function during mitosis. IFT88 and IFT20 are regulatory members of a dynein1 driven transport complex. In wild type cells (A) IFT20 negatively regulates microtubule-based, dynein1-mediated, cargo movement toward spindle poles, but IFT88 negatively regulates IFT20, ensuring cargo delivery to poles. After IFT20 loss (B) cargo transport to spindle poles occurs without disruption. After IFT88 loss (C) IFT20 is no longer repressed and thus negatively regulates cargo transport to spindle poles. However, when IFT88 and IFT20 are both lost (D) transport is no longer negatively inhibited by IFT20, and dynein1 can move to spindle poles carrying the spindle pole components necessary for mitotic progression with it.

alone is able to specifically rescue the mitotic defects caused by IFT88 depletion when co-depleted with IFT88. We conclude that IFT20 and IFT88 act in consort to define spindle functionality (ie metaphase plate congression, and spindle orientation.) I propose a mechanism where IFT20 and IFT88 together regulate microtubule-based, dynein1-mediated cargo transport to spindle poles during mitosis (Figure III-18).

Within cilia contributions from individual IFT proteins to overall IFT complex function are just beginning to be understood. However, the structural relationships between IFT proteins have been more exhaustively studied. Biochemical studies carried out in *Chlamydomonas* flagella have characterized a set of core IFT complex B members that remain associated under high salt conditions, and a subset of peripheral IFT complex B members that are lost[78]. Direct interactions between several core IFT complex B proteins have been identified, including IFT88/IFT46/IFT52[79], IFT81/IFT74[78], IFT25/IFT27[80], and IFT70/IFT46[81]. However, no direct interactions have yet been found between core and peripheral IFT complex B members. It is intriguing therefore that our study identifies a regulatory relationship between IFT88, a core IFT complex B member, and IFT20, a peripheral IFT complex B member. Our results demonstrate that although IFT20 is structurally peripheral to IFT complex B, it is functionally important for the mitotic IFT complex that regulates microtubule-based transport to spindle poles. It remains to be seen if IFT88 and IFT20 directly interact during mitosis.

The mechanism behind IFT88 and IFT20's co-regulation of mitotic progression is yet to be elucidated. Interestingly, yeast two hybrid results demonstrate a direct interaction between IFT20 and kinesin-II, suggesting IFT20 may connect the ciliary

anterograde motor with IFT complex B[82]. We have shown bidirectional IFT88 movement during mitosis (Figure II-4f), although we have yet to identify the motor required for mitotic IFT complex B anterograde transport. One hypothesis is that like in cilia, IFT20 may directly regulate IFT complex B's interaction with an anterograde motor during mitosis. This relationship would explain why simultaneous depletion of IFT88 and IFT20 rescues the integrity of spindle pole cargoes at spindle poles. In this vein it will be interesting to test if IFT20-depletion increases the levels of EB1 and γ-tubulin at spindle poles. Future work will unravel the mechanism behind IFT88 and IFT20's co-regulation of mitotic progression, and may also provide insights into IFT protein relationships in cilia as well.

A host of human disorders, collectively termed ciliopathies, are associated with cilia protein disruption[38]. A well-studied mouse model for one ciliopathy, polycystic kidney disease, harbors a hypomorphic IFT88 mutation that results in cyst formation[41], thought to be caused by spindle misorientation[39], in developing kidney tubules. Recently, a null-mutation within IFT88 has also been found in human patients and fetuses with Meckel-Gruber and Jeune asphyxiating thoracic dystrophy ciliopathy syndromes[83]. My study, which demonstrates that IFT88 and IFT20 co-regulate mitotic progression, makes it clear that IFT proteins are not solely ciliary proteins. Thus, although ciliopathies have long been thought to result from cilia loss and dysfunction, our work suggests the important possibility that mitotic dysfunctions associated with IFT loss may also contribute to ciliopathy phenotypes.

CHAPTER IV

GENERAL DISCUSSION

IFT proteins have long been known to function in the bidirectional transport system called intraflagellar transport, required for the generation and maintenance of cilia. Chapter II describes work carried out by myself and others in the lab, demonstrating that one IFT protein in particular, IFT88, has an additional function outside of the cilium during mitosis. We identify a mitotic transport complex that contains IFT88 and dynein1. This complex mediates the movement of spindle pole components, such as EB1, γ-tubulin, and ectopic microtubule bundles, toward spindle poles, ultimately setting up the orientation for cell division. Chapter III details an investigation into the potential mitotic function of three additional IFT proteins, IFT57, IFT52, and IFT20. Here I show that when depleted with IFT88; IFT20, but not IFT57 or IFT52, rescues IFT88 mitotic dysfunctions. Not only does this illustrate a mitotic and additional non-ciliary function for another IFT protein, it also demonstrates a unique regulatory relationship between IFT88 and IFT20 that has yet to be described. Moreover, with mitotic functions defined for primary cilia associated proteins, a mitotic mechanism is now implicated in the etiology of ciliopathies.

IFT88's relationship with the cell cycle

As discussed in Chapter I, IFT88 has previously been described as a tumor suppressor[28]. Its depletion in non-ciliated HeLa cells has been shown to increase cell-

cycling, and its over-expression arrests cells between G_1 and S. The mechanism behind the G_1 arrest is IFT88's interaction with Che-1, which prevents Che-1 from interacting with the tumor suppressor, RB[25]. This frees Rb to repress E2F1, a transcription factor whose activation is required for the G_1/S transition.

In contrast to these studies, I present data in Chapters II and III demonstrating that IFT88 depletion delays cells as they progress through mitosis (Figure II-1f, Supplementary Figure II-S1d – e; Figures III-6 and III-11). Although initially these results seem contradictory, they are actually compatible. In fact, in the same time-lapse imaging experiments that demonstrate delayed mitotic progression in IFT88-depleted cells, we also observed increased numbers of cells entering mitosis compared to control populations. IFT88's pleiotropic effects on cell-cycling may be explained by the spindle misorientation associated with IFT88-depletion (Figure II-1c – d; Figures III-15 and III-16). Mitotic spindle orientation has been shown to regulate cell proliferation, particularly during development. For example, during neurogenesis mitotic spindle orientation can dictate whether a cell division event yields two symmetric stem (proliferative) daughter cells, or assymetric daughter cells, with one daughter cell maintaining stem (proliferative) qualities and one daughter cell becoming differentiated (nonproliferative) [84–87]. Based on IFT88's role in orienting mitotic spindles, it's possible that spindle misorientation in IFT88-depleted cells leads to an increase in symmetric (proliferative) cell division events in developing tissues, which could contribute to an increase in cell proliferation. Further investigation is required to identify all the ways IFT88 affects cell-cycle progression, and to understand the interplay between these mechanisms.

IFT20: required for spindle orientation, or not?

Our data also yield different results from previously published reports regarding IFT20 disruption. It has previously been published that IFT20 depletion in mice causes misoriented mitotic spindles and cystic kidneys[88]. However, we find that IFT20-depletion does not disrupt spindle orientation (Figure III-15). Furthermore, we find that when IFT20 is depleted at the same time as IFT88, the spindle misorientation associated with IFT88 depletion alone, is rescued (Figure III-16). The discrepancies between our results may be explained by cellular context. The previous study focused on cell divisions taking place inside kidney collecting ducts within a mouse model, while I measured spindle orientation in a fibroblast cell line. Perhaps additional mechanisms for spindle orientation exist within the kidney collecting duct that are not active in a HeLa epithelial cell line. Further investigation in mouse models mutant for both IFT88 and IFT20 would help clarify IFT20's role in spindle misorientation.

Directionality for IFT Complex A versus IFT Complex B

Although IFT complex A and B move together along the cilium, complex A is believed to contribute to microtubule minus end-directed transport (cilia tip to base), while complex B is thought to be more important for microtubule plus end-directed transport (cilia base to tip). This is based on deletion studies wherein cilia are unable to form after the disruption of IFT complex B proteins, while disruption of IFT complex A proteins yields short, stubby cilia. However this may be an over simplified view of IFT

complex function, as several observations contradict this model. For example two IFT complex B proteins, IFT88 and IFT20, have opposite affects on the ciliary accumulation of the membrane protein polycystin-2. When IFT20 is depleted, polycystin-2 is lost from the cilium, suggesting that IFT20 is important for the anterograde transport of polycystin-2 into the cilium, as expected for a member of IFT complex B[26]. Alternatively, IFT88 disruption in mouse and *Chlamydomonas* results in an increased concentration of polycystin-2 in the cilium, suggesting that IFT88 is involved in the retrograde traffic of polycystin-2 out of the cilium, a function that is canonically associated with IFT complex A[17,89]. These findings suggest that IFT complex B can affect both microtubule plus end-directed transport as well as microtubule minus end-directed transport in the cilia.

Our data for IFT complex B function in mitosis also contradicts the classical view of IFT complex directionality. We find that four IFT complex B proteins interact with dynein1 (a microtubule minus end-directed motor) during mitosis (Figure III-2), and that IFT88 and IFT20 co-regulate the dynein1-mediated transport of spindle pole cargo to microtubule minus ends anchored at the spindle pole. Future studies are required to test if additional IFT complex B proteins, as well as IFT complex A proteins contribute to microtubule minus end-directed transport of spindle pole cargo during spindle assembly. Interestingly, time-lapse imaging in Chapter II demonstrates that GFP-tagged IFT88 moves both toward and away from the spindle pole during mitosis (Figure II-4f), suggesting that IFT88 participates in bidirectional transport during mitosis, as it does in cilia. Further experiments are required to identify the motor responsible for microtubule plus end-directed transport of IFT88 away from the spindle pole, as well as the possible

contributions from IFT complex A or B proteins to microtubule plus end-directed movement during spindle assembly.

Potential roles for IFT proteins beyond cargo adaption

The intraflagellar transport system responsible for generating and maintaining cilia, relocates ciliary proteins synthesized in the cell body into the cilium. Within this system, IFT proteins are thought to function as cargo adaptors that link cilia motors, kinesin-II and dynein2, with the cilia cargo. Support for this idea are cilia cargoes, like TRPV channels and the BBS-4 protein, that move bi-directionally along the cilium at the same pace as IFT particles[90,91]. Furthermore, IFT proteins can interact simultaneously with IFT motors and another cilia cargo, radial spoke proteins, in *Chlamydomonas*[92]. However it remains to be seen if cilia cargoes and motors actually require IFT proteins in order to interact with each other, or affect one another's bidirectional movement within cilia.

I propose from evidence in Chapters II and III and Appendix A, additional possibilities for IFT protein function beyond cargo adaption. Like in cilia, IFT88 and IFT20 regulate microtubule-based, dynein-mediated cargo transport during spindle assembly. However, dynein1 cargoes, EB1 and γ-tubulin, are properly localized to spindle poles in cells simultaneously depleted of IFT88 and IFT20 (Figures III-16 and III-17), presumably by dynein1-mediated transport to the spindle pole, suggesting that IFT proteins are not necessary to link dynein1 with these cargoes. To confirm that spindle pole cargoes localize to spindle poles through the action of dynein1 in the absence of

IFT88 and IFT20, an acute inhibition of dynein1 using ciliobrevin[93] will be performed. Taken together these results suggest spindle pole cargoes including EB1, γ-tubulin, and ectopic microtubule clusters, can associate with dynein1 in the absence of IFT88 or IFT20. Because the IFT complex B core is still assembled in *Chlamydomonas* IFT88 mutants[94] and size exclusion chromatography suggests that IFT complex B is maintained during mitosis (Figure III-1), it is possible that after IFT88 and/or IFT20 depletion a partial IFT complex B is maintained that links spindle pole cargo to dynein1. However, it's also possible that IFT proteins have other functions, in addition to, or instead of linking cargo with motors.

One of these possible functions is that IFT88 may regulate dynein1 levels during mitosis. IFT88 depletion increases dynein1 intermediate chain specifically during mitosis (Figure A-1). Dynein1 intermediate chain expression is tightly co-regulated with that of dynein1 heavy chain, as siRNA depletion of dynein1 heavy chain also reduces protein levels of dynein1 intermediate chain (Supplementary Figure II-S5b). Dynein1 performs many roles during mitosis including recruiting spindle pole cargoes to the spindle pole[61,73,95], bundling microtubules to form the mitotic spindle[96], streaming checkpoint proteins off kinetochores after satisfaction of the spindle assembly checkpoint[97], and pulling the mitotic spindle to orient it properly within the cell[4,98,99]. Although dynein1 has to localize to different cellular structures, and interact with different sets of proteins in order to perform all of its mitotic functions, little is known about how this is regulated. One possibility is that IFT88, through direct or indirect regulation of dynein1 protein levels, prevents excess mitotic dynein1 from being in the wrong place at the wrong time.

Since IFT88 depletion induces an overabundance of dynein1 (Figure A-1) that is capable of binding microtubules (Figure A-2), I propose that “traffic jams” along the assembling spindle may occur. These “traffic jams” would prevent cargo from localizing to the spindle pole and prevent dynein1 from localizing appropriately for its many mitotic functions. Future experiments are required to determine where excess dynein1 localizes, and if the simultaneous depletion of IFT88 and IFT20 rescues the increase in dynein1 levels, as it does all other IFT88-depletion phenotypes tested so far. It will also be interesting to test if IFT88 regulates dynein2 levels in cilia.

Another intriguing, but highly speculative, possible IFT protein function is that of a compass for the “transport-complex” made up of IFT proteins, dynein1, and spindle pole cargo. For instance, IFT proteins either through their interacting partners or potential localization sequences may be responsible for positioning the transport-complex at the right place for incorporation into the assembling mitotic spindle. This model fits with data from Chapter III in the following way: IFT88 would be responsible for targeting the transport-complex to the mitotic spindle. IFT20 on the other hand, would drive the transport-complex somewhere else, preventing complex incorporation into the mitotic spindle. However, the IFT20 localization signal would be repressed unless IFT88 was depleted. This would explain both the mitotic defects observed after IFT88 depletion alone, and the rescue of mitotic dysfunctions incurred by simultaneous depletion of IFT88 and IFT20. In this context IFT88 and IFT20 could function as a switch between mitotic and ciliary IFT complex function, with IFT88 localizing the IFT complex for mitotic function, and IFT20 localizing the remaining IFT complex for ciliary function

after loss of IFT88. Future experiments are required to test for mislocalization of the remaining transport-complex after IFT88 depletion, and for correction of the remaining transport-complex (especially IFT proteins and dynein1, since cargo localization has already been examined (Figures III-20 and III-21)) after IFT88 and IFT20 co-depletion.

In conclusion, this work elucidates roles for cilia-associated IFT proteins in spindle assembly in non-ciliated, mitotic cells. All four IFT complex B proteins examined, IFT88, IFT57, IFT52, and IFT20, maintained their localization at the centrosome during mitosis, and interacted with the major mitotic, microtubule minus end-directed motor, dynein1. However, only IFT88 disrupted EB1, γ-tubulin, and astral microtubule arrays at spindle poles, indicating it regulates transport of dynein1-mediated cargo to spindle poles. Strikingly, depletion of IFT20 with IFT88 rescues mitotic dysfunction associated with IFT88 depletion alone, uncovering a unique regulatory relationship between IFT88 and IFT20. This regulatory pathway contributes to proper mitotic spindle orientation; highlighting the important possibility that mitotic dysfunction associated with cilia protein disruption can contribute to cystogenesis associated with ciliopathies. This work opens exciting new avenues of investigation into extra-ciliary functions for proteins traditionally associated with cilia, and into the etiology of ciliopathies.

APPENDIX A

IFT88 REGULATES MITOTIC LEVELS OF CYTOPLASMIC DYNEIN 1

Comparing cytoplasmic dynein1 levels in unsychronized (interphase) cells and mitotic cells reveals that during mitosis cytoplasmic dynein1 intermediate chain levels are reduced by half compared to interphase cells (Figure A-1). Further experiments are required to determine if other members of the cytoplasmic dynein1 complex undergo similar changes in expression level during mitosis. Interestingly, IFT88 depletion abrogated the reduction in dynein1 intermediate chain levels during mitosis, implicating IFT88 in the regulation of dynein1 particularly during mitosis (Figure A-1). To test if the overabundance of dynein1 intermediate chain was functional, a microtubule-pelleting assay was performed. An increased amount of dynein1 was pelleted with microtubules from IFT88-depleted mitotic cells compared to control (Lamin-depleted) mitotic cells suggesting that the excess dynein1 intermediate chain present in IFT88-depleted mitotic cells can functionally bind microtubules (Figure A-2). In future it will be important to test if mitotic dynein1 localization, speed, and processivity are also affected by IFT88-depletion.

This data suggests that IFT proteins, which are classically thought of as motor passengers, may also be motor regulators. Furthermore, it has interesting implications for the mechanism behind mitotic disruption that we observe after IFT88 depletion. Dynein1 is an important contributor to spindle orientation[100], and disruptions in cortical dynein result in misoriented spindles[98]. Perhaps the increased dynein1 present after IFT88

depletion localizes improperly to the cortex disrupting the cortical force generation required for spindle orientation, and contributing to the spindle misorientation phenotype we observe after IFT88 depletion. Alternatively, increased dynein1 that is competent to bind microtubules could cause “traffic jams” on microtubules, disrupting microtubule-based transport, and contributing to the disrupted spindle pole phenotype associated with IFT88 depletion.

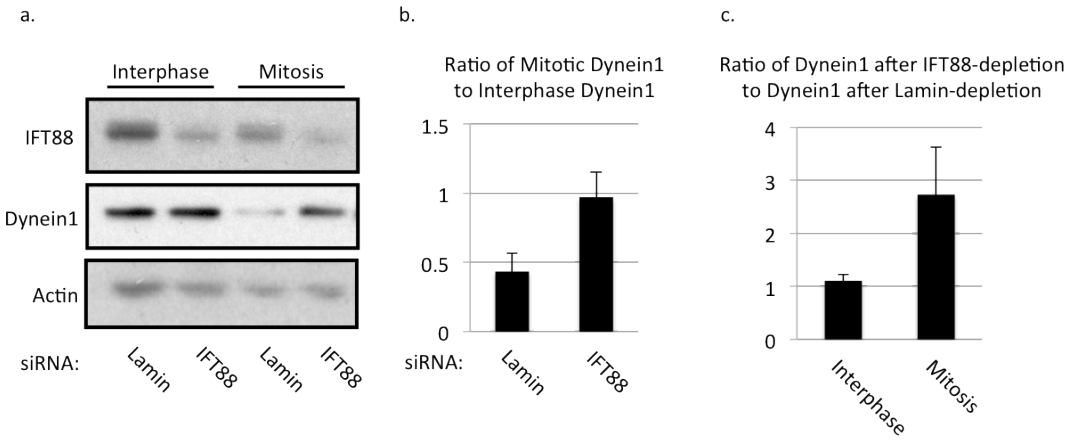

Figure A-1 IFT88 regulates dynein1 levels specifically during mitosis.
(a) Immunoblot of whole cell lysate from interphase (unsynchronized cells) or mitotic HeLa cells (harvested by mitotic shake-off), depleted of indicated proteins, and probed for IFT88, dynein1, and actin. Actin, loading control. Dynein1 antibody recognizes cytoplasmic dynein intermediate chain. **(b)** Quantification shows ratio of mitotic dynein1 level compared to interphase dynein1 level in control (lamin-depleted) or IFT88-depleted cells. (*n*=3 independent experiments, error bars are SE) **(c)** Quantification shows ratio of dynein1 level in IFT88-depleted cells compared to dynein1 level in control (lamin-depleted) cells in interphase or mitotic cells. (*n*=3 independent experiments, error bars are SE)

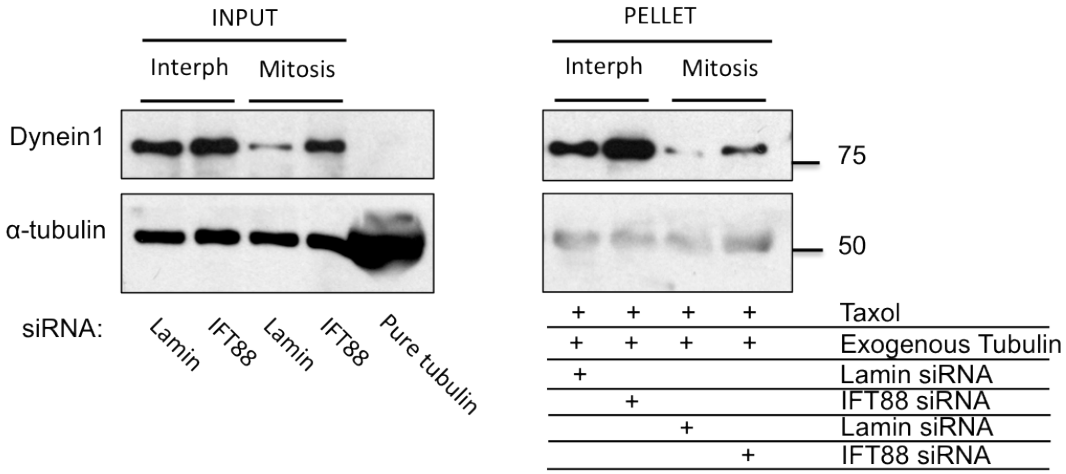

Figure A-2 Increased mitotic dynein1 resulting from IFT88-depletion binds microtubules.
Immunoblot from microtubule sedimentation assay. “Input” shows initial dynein1 levels in equal concentrations of lysate from interphase (unsynchronized) cells depleted of indicated proteins, or mitotic cells (harvested by mitotic shake-off) depleted of indicated proteins. “Pellet” shows concentrations of dynein1 co-sedimenting with polymerized microtubules from interphase or mitotic cells depleted of indicated proteins.

APPENDIX B

CHAPTER 2 MATERIALS AND METHODS

Cell culture, siRNAs and transfection. HeLa cells, hTert RPE-1 (Clontech) cells, GFP–α-tubulin LLC-PK1 stable cell line[61,62] (gift from P. Wadsworth, UMass, Amherst, USA), wild-type and Tg737−/− mouse kidney cells[17] and Flag–IFT52 IMCD[101] andGFP–IFT88LLC-PK stable cell line (gifts from G. Pazour, UMass Medical School, USA) were grown as described by the American Type Culture Collection. Targeted proteins were depleted with small-interfering RNAs (siRNAs) designed and ordered through Dharmacon and delivered to HeLa or LLC-PK1 cells using Oligofectamine, or RPE cells using Lipofectamine 2000 (Invitrogen) according to the manufacturers' instructions. Three siRNA sequences were used to target human and porcine IFT88: IFT88: 5'-CGACUAAGUGCCAGACUCAUU-3', IFT88#2: 5'-CCGAAGCACUUAACACUUA-3' previously published[25] and IFT88sc (Sus Scrofa): 5'-CCUUGGAGAUCGAGAGAAUU-3'. The efficacy of IFT88 knock-down was assessed by immunoblotting and immunofluorescence microscopy 48 h post-transfection. Functional loss of IFT88 was verified using a cilia formation assay in RPE cells[12]. A rescue experiment was carried out by depleting endogenous IFT88 (IFT88sc siRNA) in a porcine LLC-PK1 cell line expressing a mouse GFP‑IFT88 cDNA. EB1 siRNA (5'-GCCCUGGUGUGGUGCGAAA- 3'), p50 siRNA (5'-GACGACAGUGAAGGAGUCAUU-3') and siRNA specific for dynein1 or dynein2 (Dharmacon Smart Pool; sequences available on request) were also used. Control siRNA was described previously (GFP, lamin[12]). The efficacy of dynein1 and dynein2 knockdown was assessed by PCR with reverse transcription (DYNC1H1 forward: 5'-GGAAGTCAACGTCACCACCT-3'; DYNC1H1 reverse: 5'-CCAACCTCAGACCAACCACT-3'; DYNC2 forward: 5'-GTCAGCTGGAGGAAGACTGG-3'; DYNC2 reverse: 5'-GCACCAACAATTTTGTCACG-3'; glyceraldehyde 3-phosphate dehydrogenase (GAPDH) forward: 5'- CGACCACTTTGTCAAGCTCA-3'; GAPDH reverse: 5'-AGGGGAGATTCAGTGTGGTG-3') using a OneStep RT‑PCR kit (QIAGEN) for both dynein1 and dynein2 and by western blot for dynein1. Functional assays for loss of dynein1 and dynein2 were done 48 h and 72 h post-transfection and included Golgi fragmentation (dynein1 and dynein2) and mitosis-related (dynein1) or cilia assays (dynein2) previously described[12].

Zebrafish lines, morpholino injection and phenotyping. Wild-type zebrafish were raised according to standard protocols (ref 40). 1-phenyl-2-thiourea (PTU, Sigma) was used to suppress pigmentation when necessary, according to standard protocols (ref 40). Embryos were staged according to hours post-fertilization (hpf). IFT88 morpholino

antisense oligonucleotides (IFT88 morpholino oligonucleotides: 5'-CTGGGACAAGATGCACATTCTCCAT-3') were previously described[59] and standard control morpholino oligonucleotides were used. The efficacy of IFT88 morpholino oligonucleotides injection was assessed by changes in gross anatomical features (for example, curly trunk and pronephric duct defects, cyst formation) characteristic of IFT88 zebrafish mutants[50,59]. Gross anatomical defects and cyst formation were observed in 32 hpf and 52 hpf embryos, with a MZFLIII dissection microscope (Zeiss). One-cell-stage embryos were injected with 10 ng of control or IFT88 morpholino oligonucleotides as previously described[59]. Embryos at 52 hpf were used for whole-mount staining or flow cytometry (see below).

Antibodies. The following antibodies were used: IFT88 (from G. Pazour or Proteintech for biochemistry; western blot, 1:500, immunoprecipitation, 5 μg; or from C. Desdouets, Faculte de Medecine Rene Descartes, Paris; immunofluorescence 1:250); IFT20 (G. Pazour, western blot 1:500); IFT52 (western blot 1:500, Proteintech); IFT57 (western blot 1:500, Proteintech); polyglutamylated tubulin antibody (GT335, P. Denoulet, UMR7622, Paris, France and C. Janke, Institut Curie, France; immunofluorescence, 1:500); α- tubulin (DM1α, immunofluorescence, 1:250), FITC-conjugated α-tubulin (1:300), γ-tubulin (western blot, 1:500; immunofluorescence, 1:250), EB1 (immunofluorescence, 1:250; immunoprecipitation, 5 μg), BrdU (1:250), Flag (western blot, 1:500; immunoprecipitation, 5 μg) and acetylated tubulin (1:250) from Sigma; Ser 10 Phos-H3 (1:500, Upstate Biotechnology); EB1 (western blot, 1:300; immunofluorescence, 1:250), p150/glued (western blot, 1:1,000) and p50/dynactin (western, 1:500) from BD Biosciences; dynein intermediate chain 74.1 (immunofluorescence, 1:250; western blot, 1:500, immunoprecipitation, 5 μg, Santa Cruz Biotechnology); Golgin 97 (immunofluorescence, 1:250, Molecular Probes); and CREST (immunofluorescence, 1:250 anti-human centromere/kinetochore; Antibodies Inc.). 5051 (immunofluorescence, 1:500) has been described previously[12].

Lysates, cell synchronization, immunoprecipitation and gel filtration. Cell lysates were obtained from HeLa cells 48 h or 72 h post siRNA transfection. Lysis buffer: 50mM HEPES (pH 7.5), 150mM NaCl, 1.5mM MgCl2, 1mM EGTA, 1% IGEPAL CA-630 and protease inhibitors (Complete Mini, Roche Diagnostics). Protein concentration for lysate was determined using Bio-Rad protein dye reagent (Bio-Rad Laboratories), loads were adjusted, proteins were resolved by SDS–PAGE, and analysed by western blotting. Cell synchronization for biochemistry was achieved using double thymidine block in HeLa cells (2mM, 20h) and release (10 h) to achieve mitotic enrichment followed by mitotic shake off, or by using nocodazole synchronization (20ng/ml for 16 hrs). IMCD cell were synchronized in mitosis using R0-3306 inhibitor (reversibly arrests cells at the G2-M border, Enzo Life Sciences AG) overnight then released for 1h. For immunoprecipitation, antibodies were added to cell extracts and incubated at 4° C overnight, and then incubated for 45 min with protein G-PLUS agarose (Santa Cruz Biotechnology). Immunoprecipitated proteins were separated by SDS–PAGE and analysed by western blotting. For gel filtration, mitotic cell lysates (lysis buffer: 20mM HEPES at pH 7.6,

5mM MgSO4, 0.5mM EDTA, 50mM KCl and 1% NP-40; volume: 0.250 ml; protein concentration: 12 µg µl−1) were loaded onto a fast protein liquid chromatography Superose 6 gel-filtration column (GE Healthcare; 0.2 ml min−1 , equilibrated in extraction buffer), and 0.5 ml fractions were collected.

Flow cytometry. For flow cytometry, 52 hpf zebrafish embryos were grown in egg water and dechorionated by pronase treatment[102], rinsed for 15 min in calcium-free Ringer and passed several times through a 200 µl pipette tip to remove the yolk. Embryos were transferred into a 35 mm culture dish with 2 ml phosphate buffered saline (PBS, at pH 8) containing 0.25% trypsin and 1 mM EDTA and incubated for 30–60 min at 28.5° C. The digest was stopped by adding CaCl2 to a final concentration of 1 mM and fetal calf serum to 10%. Cells were centrifuged for 3 min at 300g , rinsed once with PBS and fixed and processed for flow cytometry. Cells were stained for flow cytometry experiments as previously described[12]. Phos-H3 staining (Ser 10 Phospho-Histone 3, Alexa Fluor 488 conjugate), was carried out according to manufacturers' instructions (Cell Signaling).

Microtubule regrowth assay. At 48 h post-transfection, microtubules were depolymerized in 10–25 µM nocodazole in culture medium for 1 h at 37° C. Cells were then washed and incubated in culture medium without nocodazole at 37° C to allow regrowth. Cells were fixed at different time intervals in methanol and processed for immunofluorescence microscopy to examine microtubule regrowth (α-tubulin) from spindle poles in metaphase cells.

Immunofluorescence experiments, microscopy and imaging software.
Whole embryos (48h) were processed for immunofluorescence by fixation in Dent's Fix (80% methanol/20% dimethylsulphoxide) at 4°C overnight, rehydrated, washed with PBS containing 0.5% Tween 20 (PBST), and blocked in 1× PBS-DBT (1% dimethylsulphoxide, 1% BSA, 0.5% Tween 20) at room temperature for 2 h. Primary and secondary antibody incubations were carried out in 1× PBS-DBT at 4°C overnight and 1h at room temperature, respectively, using 1× PBS-DBT washes between incubations. After rinsing in 1× PBS, the embryos were mounted and examined using a Perkin Elmer Ultraview spinning disc confocal microscope: Zeiss Axiovert 200M, ×100 Plan-Apocromat NA 1.4 Oil objective, or ×63 Plan- Apocromat NA1.4 Oil objective and Hamamatsu ORCA-ER camera. Images were processed on a MetaMorph workstation (Molecular Devices). Z stacks were acquired and used for creation of maximum projections or (3D) rendering (below). Immunofluorescence microscopy analysis of −20°C methanol-fixed cells was carried out as previously described[12] . Images were acquired using the spinning disc confocal microscope described above (×100 Plan-Apocromat NA 1.4 Oil objective). Z stacks were shown as 2D maximum projections (MetaMorph) or processed for 3D rendering (Imaris, Bitplane). Fluorescence range intensity was adjusted identically for each series of panels. Intensity profiles, linescan histograms and fluorescence intensity quantification were obtained from sum projections of Z stacks using MetaMorph. For fluorescence intensity quantification, computer-generated concentric circles of 60 (inner area) or 80 (outer area) pixels in diameter were

used to measure spindle pole (inner area) and calculate local background (difference between the outer and inner area) fluorescence intensity. Imaris 3D rendering software was used to visualize spindle orientation and to measure distances required to calculate spindle angle. Spindle angle measurements were carried out as previously described[56] .

Time-lapse microscopy imaging. Time-lapse microscopy imaging of cultured HeLa cells was carried out using the spinning disc microscope described above (×25 Plan-Neofluar NA 0.5, phase) using the scan stage tool (MetaMorph). Images were taken every 10 min from 32 h to 48 h post-transfection. For live microscopy of GFP–EB1 in metaphase HeLa cells, images were recorded every 5 s for 2 min using the spinning disc confocal microscope described above (×63 Plan-Apocromat NA1.4 Oil objective). Microtubule-nucleation rate was measured in GFP–EB1- expressing cells by manually counting the number of EB1–GFP comets emerging from the centrosome over time. For live microscopy of GFP–IFT88 in metaphase, single-plane images were recorded once per second using the spinning disc confocal microscope described above (×100 Plan-Apocromat NA1.4 Oil objective). The resulting movie is shown at 3 frames per second. Tracking of IFT88 foci was obtained using the track point application in MetaMorph. Live imaging of the GFP–α-tubulin LLC-PK1 cell line was carried out as previously described[62]. Resulting movies are shown at 10 frames per second.

Statistical analysis. The number of embryos or cells counted per experiment for statistical analysis is indicated in figure legends. For graphs in all figures: error bars, mean of at least 3 experiments ± s.d. unless otherwise specified; n, number of events per experiment. Images: scale bars, 5 μm unless otherwise specified. Graphs were created using GraphPad Prism software.

APPENDIX C

CHAPTER 3 MATERIALS AND METHODS

Cell culture, siRNAs and transfection. HeLa cells were grown as described by the American Type Culture Collection. Targeted proteins were depleted with small-interfering RNAs (siRNAs) designed and ordered through Dharmacon. siRNAs were delivered to HeLa cells using Oligofectamine according to the manufacturers' instructions. Two siRNA sequences were used to target human IFT88: IFT88: 5'-CGACUAAGUGCCAGACUCAUU-3' and IFT88': 5'-CCGAAGCACUUAACACUUA-3' previously published[25]. Lamin was used as a control siRNA, target sequence: 5'-CUGGACUUCCAGAAGAACAUU-3' previously published[12]. Two different siRNAs were used to target IFT57. One was a smart pool targeting the following sequences: 1) 5'-ACAAUCAGCUUGAGAAUUU-3', 2) 5'-GCACAGAAGUGGAAUUGAA-3', 3) 5'-GCCAAUAUACCCAGUAGAA-3', and 4) 5'-CGAUUAGGACUGACAAUAA-3'. The other IFT57 target sequence used was 5'-AGAAGAUGAUGCAGAAUUAUU-3'. Two different siRNAs were used to target IFT52 including 1) 5'-CAGGAGACAUCCACCUAAA-3' and 2) 5'- CAAUAAGUGUACUGAAGAAUU-3'. Two different siRNA sequences were used to target IFT20 including 1) 5'-GGAAGAGTGCAAAGA- CTTT-3', and 2) 5'- CCAUAGAGCUGAAGGAAGA-3'.

Antibodies. The following antibodies were used: IFT88 (from Proteintech Group for biochemistry; western blot, 1:500, or from C. Desdouets, Faculte de Medecine Rene Descartes, Paris; immunofluorescence 1:1000); IFT20 (from Proteintech Group for biochemistry; western blot, 1:500, from G. Pazour for immunofluorescence, 1:100); IFT52 (western blot 1:500, Proteintech Group), immunofluorescence 1:200); IFT57 (western blot 1:500, Proteintech Group, immunofluorescence 1:200); α- tubulin (FITC-conjugated α-tubulin (1:300)); γ-tubulin (GTU-88, sigma, western blot, 1:2000; AATR, immunofluorescence, 1:200); EB1 (immunofluorescence, 1:250); dynein intermediate chain 74.1 (immunofluorescence, 1:250; western blot, 1:500, immunoprecipitation, 5 μg, Santa Cruz Biotechnology); Kif3a (western blot, 1:500, Santa Cruz Biotechnology) CREST (immunofluorescence, 1:250 anti-human centromere/kinetochore; Antibodies Inc.); GAPDH (western blot, 1:2000, sigma) and 5051 (immunofluorescence, 1:500) has been described previously[12].

Lysates, cell synchronization, immunoprecipitation and gel filtration. Cell lysates were harvested from HeLa cells 48 hours after siRNA transfection. Lysis buffer: 50mM HEPES (pH 7.5), 150mM NaCl, 1.5mM MgCl2, 1mM EGTA, 1% IGEPAL CA-630 and protease inhibitors (Complete Mini, Roche Diagnostics). Protein concentration for lysate was determined using Bio-Rad protein dye reagent (Bio-Rad Laboratories). Cell synchronization for biochemistry was achieved using double thymidine block in HeLa cells (2mM, 20h) and release (10 h) to achieve mitotic enrichment followed by mitotic

shake off, or by using nocodazole synchronization (20ng/ml for 16 hrs). For immunoprecipitation, antibodies were added to cell extracts and incubated at 4° C overnight, and then incubated for 45 min with protein G-PLUS agarose (Santa Cruz Biotechnology). For gel filtration, mitotic cell lysates (lysis buffer: 20mM HEPES at pH 7.6, 5mM MgSO4, 0.5mM EDTA, 50mM KCl and 1% NP-40; volume: 0.250 ml; protein concentration: 12 µg µl−1) were loaded onto a fast protein liquid chromatography Superose 6 gel-filtration column (GE Healthcare; 0.2 ml min−1 , equilibrated in extraction buffer), and 0.5 ml fractions were collected.

Immunofluorescence experiments, microscopy and imaging software.
Cells were fixed in methanol, treated with primary and secondary antibody, then imaged using a Perkin Elmer Ultraview spinning disc confocal microscope: Zeiss Axiovert 200M, and a 100X Plan-Apocromat NA 1.4 Oil objective. Images were processed on a MetaMorph workstation (Molecular Devices). Z stacks were shown as 2D maximum projections (MetaMorph) or processed for 3D rendering (Imaris, Bitplane). Spindle angle measurements were carried out as previously described[56] .

Time-lapse microscopy imaging. Time-lapse microscopy imaging of cultured HeLa cells was carried out using the spinning disc microscope described above (20X Plan-Neofluar NA 0.5, phase objective) using the scan stage tool (MetaMorph). Images were taken every 10 min from 32 h to 48 h post-transfection.

Statistical analysis. The number of cells counted per experiment for statistical analysis is indicated in figure legends. For graphs in all figures: error bars, mean of at least 3 experiments ± SE unless otherwise specified; n, number of events per experiment. Graphs were created using Microsoft Excel.

APPENDIX D

BIBLIOGRAPHY

1. Rosenbaum, J. L. & Witman, G. B. Intraflagellar transport. *Nature Reviews Molecular Cell Biology* **3**, 813–825 (2002).

2. Ishikawa, H. & Marshall, W. F. Ciliogenesis: building the cell's antenna. *Nature reviews. Molecular cell biology* **12**, 222–234 (2011).

3. Walczak, C. E. & Heald, R. Mechanisms of mitotic spindle assembly and function. *International review of cytology* **265**, 111–158 (2008).

4. Siller, K. H. & Doe, C. Q. Spindle orientation during asymmetric cell division. *Nature cell biology* **11**, 365–374 (2009).

5. Schatten, H. The mammalian centrosome and its functional significance. *Histochemistry and cell biology* **129**, 667–686 (2008).

6. Doxsey, S. Re-evaluating centrosome function. *Nature reviews. Molecular cell biology* **2**, 688–698 (2001).

7. Bettencourt-Dias, M. & Glover, D. M. Centrosome biogenesis and function: centrosomics brings new understanding. *Nature reviews. Molecular cell biology* **8**, 451–463 (2007).

8. Pazour, G. J. & Witman, G. B. The vertebrate primary cilium is a sensory organelle. *Current Opinion in Cell Biology* **15**, 105–110 (2003).

9. Jurczyk, A. *et al.* Pericentrin forms a complex with intraflagellar transport proteins and polycystin-2 and is required for primary cilia assembly. *The Journal of cell biology* **166**, 637–643 (2004).

10. Doxsey, S. J., Stein, P., Evans, L., Calarco, P. D. & Kirschner, M. Pericentrin , a Highly Conserved Centrosome Protein Involved in Microtubule Organization. *Cell* **76**, 639–650 (1994).

11. Cole, D. G. *et al.* Kinesin-II–dependent Intraflagellar Transport (IFT): IFT Particles Contain Proteins Required for Ciliary Assembly in. **141**, 993–1008 (1998).

12. Mikule, K. *et al.* Loss of centrosome integrity induces p38-p53-p21dependent G1-S arrest. *Nature Cell Biology* **9**, 160–U49 (2007).

13. Barr, M. M. & Sternberg, P. W. A polycystic kidney-disease gene homologue required for male mating behaviour in C. elegans. *Nature* **401**, 386–389 (1999).

14. Yoder, B. K. The Polycystic Kidney Disease Proteins, Polycystin-1, Polycystin-2, Polaris, and Cystin, Are Co-Localized in Renal Cilia. *Journal of the American Society of Nephrology* **13**, 2508–2516 (2002).

15. Wang, S. The Autosomal Recessive Polycystic Kidney Disease Protein Is Localized to Primary Cilia, with Concentration in the Basal Body Area. *Journal of the American Society of Nephrology* **15**, 592–602 (2004).

16. Ward, C. J. *et al.* Cellular and subcellular localization of the ARPKD protein; fibrocystin is expressed on primary cilia. *Human molecular genetics* **12**, 2703–2710 (2003).

17. Pazour, G. J., San Agustin, J. T., Follit, J. A., Rosenbaum, J. L. & Witman, G. B. Polycystin-2 localizes to kidney cilia and the ciliary level is elevated in orpk mice with polycystic kidney disease. *Current Biology* **12**, R378–R380 (2002).

18. Zhang, J. *et al.* Polycystic kidney disease protein fibrocystin localizes to the mitotic spindle and regulates spindle bipolarity. *Human molecular genetics* **19**, 3306–3319 (2010).

19. Burtey, S. *et al.* Centrosome overduplication and mitotic instability in PKD2 transgenic lines. *Cell biology international* **32**, 1193–1198 (2008).

20. Battini, L. *et al.* Loss of polycystin-1 causes centrosome amplification and genomic instability. *Human molecular genetics* **17**, 2819–2833 (2008).

21. Gergely, F. & Basto, R. Multiple centrosomes: together they stand, divided they fall. *Genes & development* **22**, 2291–2296 (2008).

22. Castrillon, D. H. & Wasserman, S. a Diaphanous is required for cytokinesis in Drosophila and shares domains of similarity with the products of the limb deformity gene. *Development (Cambridge, England)* **120**, 3367–3377 (1994).

23. Rundle, D. R., Gorbsky, G. & Tsiokas, L. PKD2 interacts and co-localizes with mDia1 to mitotic spindles of dividing cells: role of mDia1 IN PKD2 localization to mitotic spindles. *The Journal of biological chemistry* **279**, 29728–29739 (2004).

24. Iomini, C., Tejada, K., Mo, W. J., Vaananen, H. & Piperno, G. Primary cilia of human endothelial cells disassemble under laminar shear stress. *Journal of Cell Biology* **164**, 811–817 (2004).

25. Robert, A. *et al.* The intraflagellar transport component IFT88/polaris is a centrosomal protein regulating G1-S transition in non-ciliated cells. *Journal of Cell Science* **120**, 628–637 (2007).

26. Follit, J. A., Tuft, R. A., Fogarty, K. E. & Pazour, G. J. The intraflagellar transport protein IFT20 is associated with the Golgi complex and is required for cilia assembly. *Molecular Biology of the Cell* **17**, 3781–3792 (2006).

27. Deane, J. A., Cole, D. G., Seeley, E. S., Diener, D. R. & Rosenbaum, J. L. Localization of intraflagellar transport protein IFT52 identifies basal body transitional fibers as the docking site for IFT particles. *Current Biology* **11**, 1586–1590 (2001).

28. Richards, W. G. *et al.* Oval cell proliferation associated with the murine insertional mutation TgN737Rpw. *The American journal of pathology* **149**, 1919–1930 (1996).

29. Isfort, R. J. *et al.* The tetratricopeptide repeat containing Tg737 gene is a liver neoplasia tumor suppressor gene. *Oncogene* **15**, 1797–1803 (1997).

30. Follit, J. a *et al.* The Golgin GMAP210/TRIP11 anchors IFT20 to the Golgi complex. *PLoS genetics* **4**, e1000315 (2008).

31. Finetti, F. *et al.* Intraflagellar transport is required for polarized recycling of the TCR/CD3 complex to the immune synapse. *Nature Cell Biology* **11**, 1332–U163 (2009).

32. Cemerski, S. & Shaw, A. Immune synapses in T-cell activation. *Current opinion in immunology* **18**, 298–304 (2006).

33. Brownlie, R. J. & Zamoyska, R. T cell receptor signalling networks: branched, diversified and bounded. *Nature reviews. Immunology* **13**, 257–269 (2013).

34. Qin, H., Wang, Z., Diener, D. & Rosenbaum, J. Intraflagellar transport protein 27 is a small G protein involved in cell-cycle control. *Current biology : CB* **17**, 193–202 (2007).

35. Vashishtha, M., Walther, Z. & Hall, J. L. The kinesin-homologous protein encoded by the Chlamydomonas FLA10 gene is associated with basal bodies and centrioles. *Journal of cell science* **109 (Pt 3**, 541–549 (1996).

36. Haraguchi, K., Hayashi, T., Jimbo, T., Yamamoto, T. & Akiyama, T. Role of the Kinesin-2 Family Protein , KIF3 , during Mitosis *. *Journal of Biological Chemistry* **281**, 4094–4099 (2006).

37. Miller, M. S. *et al.* Mutant Kinesin-2 Motor Subunits Increase Chromosome Loss. *Molecular Biology of the Cell* **16**, 3810–3820 (2005).

38. Gerdes, J. M., Davis, E. E. & Katsanis, N. The vertebrate primary cilium in development, homeostasis, and disease. *Cell* **137**, 32–45 (2009).

39. Fischer, E. *et al.* Defective planar cell polarity in polycystic kidney disease. *Nature Genetics* **38**, 21–23 (2006).

40. Fischer, E. & Pontoglio, M. Planar cell polarity and cilia. *Seminars in cell & developmental biology* **20**, 998–1005 (2009).

41. Pazour, G. J. *et al.* Chlamydomonas IFT88 and its mouse homologue, polycystic kidney disease gene Tg737, are required for assembly of cilia and flagella. *Journal of Cell Biology* **151**, 709–718 (2000).

42. Baena-López, L. A., Baonza, A. & García-Bellido, A. The orientation of cell divisions determines the shape of Drosophila organs. *Current biology : CB* **15**, 1640–1644 (2005).

43. Goodrich, L. V & Strutt, D. Principles of planar polarity in animal development. *Development (Cambridge, England)* **138**, 1877–1892 (2011).

44. Simons, M. *et al.* Inversin, the gene product mutated in nephronophthisis type II, functions as a molecular switch between Wnt signaling pathways. *Nature genetics* **37**, 537–543 (2005).

45. Gerdes, J. M. *et al.* Disruption of the basal body compromises proteasomal function and perturbs intracellular Wnt response. *Nature genetics* **39**, 1350–1360 (2007).

46. Corbit, K. C. *et al.* Kif3a constrains beta-catenin-dependent Wnt signalling through dual ciliary and non-ciliary mechanisms. *Nature cell biology* **10**, 70–76 (2008).

47. Ocbina, P. J. R., Tuson, M. & Anderson, K. V Primary cilia are not required for normal canonical Wnt signaling in the mouse embryo. *PloS one* **4**, e6839 (2009).

48. Badano, J. L., Mitsuma, N., Beales, P. L. & Katsanis, N. The ciliopathies: an emerging class of human genetic disorders. *Annual review of genomics and human genetics* **7**, 125–148 (2006).

49. Hildebrandt, F. & Otto, E. Cilia and centrosomes: A unifying pathogenic concept for cystic kidney disease? *Nature Reviews Genetics* **6**, 928–940 (2005).

50. Sun, Z. X. *et al.* A genetic screen in zebrafish identifies cilia genes as a principal cause of cystic kidney. *Development* **131**, 4085–4093 (2004).

51. Rieder, C. L., Faruki, S. & Khodjakov, A. The centrosome in vertebrates: more than microtubule-organizing center. *Trends in Cell Biology* **11**, 413–419 (2001).

52. Scholey, J. M. Intraflagellar transport motors in cilia: moving along the cell's antenna. *Journal of Cell Biology* **180**, 23–29 (2008).

53. Pazour, G. J., Dickert, B. L. & Witman, G. B. The DHC1b (DHC2) isoform of cytoplasmic dynein is required for flagellar assembly. *Journal of Cell Biology* **144**, 473–481 (1999).

54. Luders, J. & Stearns, T. Opinion - Microtubule-organizing centres: a re-evaluation. *Nature Reviews Molecular Cell Biology* **8**, 161–167 (2007).

55. O'Connell, C. B. & Wang, Y. L. Mammalian spindle orientation and position respond to changes in cell shape in a dynein-dependent fashion. *Molecular Biology of the Cell* **11**, 1765–1774 (2000).

56. Toyoshima, F. & Nishida, E. Integrin-mediated adhesion orients the spindle parallel to the substratum in an EB1-and myosin X-dependent manner. *Embo Journal* **26**, 1487–1498 (2007).

57. Murcia, N. S. *et al.* The Oak Ridge Polycystic Kidney (orpk) disease gene is required for left-right axis determination. *Development* **127**, 2347–2355 (2000).

58. Haycraft, C. J., Swoboda, P., Taulman, P. D., Thomas, J. H. & Yoder, B. K. The C-elegans homolog of the murine cystic kidney disease gene Tg737 functions in a ciliogenic pathway and is disrupted in osm-5 mutant worms. *Development* **128**, 1493–1505 (2001).

59. Kramer-Zucker, A. G. *et al.* Cilia-driven fluid flow in the zebrafish pronephros, brain and Kupffer's vesicle is required for normal organogenesis. *Development* **132**, 1907–1921 (2005).

60. Han, Y. G., Kwok, B. H. & Kernan, M. J. Intraflagellar transport is required in Drosophila to differentiate sensory cilia but not sperm. *Current Biology* **13**, 1679–1686 (2003).

61. Tulu, U. S., Rusan, N. M. & Wadsworth, P. Peripheral, non-centrosome-associated microtubules contribute to spindle formation in centrosome-containing cells. *Current Biology* **13**, 1894–1899 (2003).

62. Rusan, N. M., Tulu, U. S., Fagerstrom, C. & Wadsworth, P. Reorganization of the microtubule array in prophase/prometaphase requires cytoplasmic dynein-dependent microtubule transport. *Journal of Cell Biology* **158**, 997–1003 (2002).

63. Hannak, E. *et al*. The kinetically dominant assembly pathway for centrosomal asters in Caenorhabditis elegans is gamma-tubulin dependent. *Journal of Cell Biology* **157**, 591–602 (2002).

64. Rogers, S. L., Rogers, G. C., Sharp, D. J. & Vale, R. D. Drosophila EB1 is important for proper assembly, dynamics, and positioning of the mitotic spindle. *Journal of Cell Biology* **158**, 873–884 (2002).

65. Zimmerman, W. C., Sillibourne, J., Rosa, J. & Doxsey, S. J. Mitosis-specific anchoring of gamma tubulin complexes by pericentrin controls spindle organization and mitotic entry. *Molecular Biology of the Cell* **15**, 3642–3657 (2004).

66. Green, R. A., Wollman, R. & Kaplan, K. B. APC and EB1 function together in mitosis to regulate spindle dynamics and chromosome alignment. *Molecular Biology of the Cell* **16**, 4609–4622 (2005).

67. Tulu, U. S., Fagerstrom, C., Ferenz, N. P. & Wadsworth, P. Molecular requirements for kinetochore-associated microtubule formation in mammalian cells. *Current Biology* **16**, 536–541 (2006).

68. Walczak, C. E., Vernos, I., Mitchison, T. J., Karsenti, E. & Heald, R. A model for the proposed roles of different microtubule-based motor proteins in establishing spindle bipolarity. *Current Biology* **8**, 903–913 (1998).

69. Gaglio, T., Dionne, M. A. & Compton, D. A. Mitotic spindle poles are organized by structural and motor proteins in addition to centrosomes. *Journal of Cell Biology* **138**, 1055–1066 (1997).

70. Echeverri, C. J., Paschal, B. M., Vaughan, K. T. & Vallee, R. B. Molecular characterization of the 50-kD subunit of dynactin reveals function for the complex

in chromosome alignment and spindle organization during mitosis. *Journal of Cell Biology* **132**, 617–633 (1996).

71. Corthesytheulaz, I., Pauloin, A. & Pfeffer, S. R. CYTOPLASMIC DYNEIN PARTICIPATES IN THE CENTROSOMAL LOCALIZATION OF THE GOLGI-COMPLEX. *Journal of Cell Biology* **118**, 1333–1345 (1992).

72. Vaisberg, E. A., Grissom, P. M. & McIntosh, J. R. Mammalian cells express three distinct dynein heavy chains that are localized to different cytoplasmic organelles. *Journal of Cell Biology* **133**, 831–842 (1996).

73. Young, A., Dictenberg, J. B., Purohit, A., Tuft, R. & Doxsey, S. J. Cytoplasmic dynein-mediated assembly of pericentrin and gamma tubulin onto centrosomes. *Molecular Biology of the Cell* **11**, 2047–+ (2000).

74. Yamashita, Y. M., Mahowald, A. P., Perlin, J. R. & Fuller, M. T. Asymmetric inheritance of mother versus daughter centrosome in stem cell division. *Science* **315**, 518–521 (2007).

75. Wheatley, D. N. Primary cilia in normal and pathological tissues. *Pathobiology* **63**, 222–238 (1995).

76. Ross, A. J. *et al.* Disruption of Bardet-Biedl syndrome ciliary proteins perturbs planar cell polarity in vertebrates. *Nature Genetics* **37**, 1135–1140 (2005).

77. Delaval, B., Bright, A., Lawson, N. D. & Doxsey, S. The cilia protein IFT88 is required for spindle orientation in mitosis. *Nat Cell Biol* **13**, 461–468 (2011).

78. Lucker, B. F. *et al.* Characterization of the intraflagellar transport complex B core: direct interaction of the IFT81 and IFT74/72 subunits. *The Journal of biological chemistry* **280**, 27688–27696 (2005).

79. Lucker, B. F., Miller, M. S., Dziedzic, S. a, Blackmarr, P. T. & Cole, D. G. Direct interactions of intraflagellar transport complex B proteins IFT88, IFT52, and IFT46. *The Journal of biological chemistry* **285**, 21508–21518 (2010).

80. Wang, Z., Fan, Z.-C., Williamson, S. M. & Qin, H. Intraflagellar transport (IFT) protein IFT25 is a phosphoprotein component of IFT complex B and physically interacts with IFT27 in Chlamydomonas. *PloS one* **4**, e5384 (2009).

81. Fan, Z. *et al.* Chlamydomonas IFT70 / CrDYF-1 Is a Core Component of IFT Particle Complex B and Is Required for Flagellar Assembly. *Molecular Biology of the Cell* **21**, 2696–2706 (2010).

82. Baker, S. a, Freeman, K., Luby-Phelps, K., Pazour, G. J. & Besharse, J. C. IFT20 links kinesin II with a mammalian intraflagellar transport complex that is conserved in motile flagella and sensory cilia. *The Journal of biological chemistry* **278**, 34211–34218 (2003).

83. McIntyre, J. C. *et al.* Gene therapy rescues cilia defects and restores olfactory function in a mammalian ciliopathy model. *Nature medicine* **18**, 1423–1428 (2012).

84. Huttner, W. B. & Brand, M. Asymmetric division and polarity of neuroepithelial cells. *Current opinion in neurobiology* **7**, 29–39 (1997).

85. Kosodo, Y., Ro, K., Marzesco, A., Corbeil, D. & Huttner, W. B. Asymmetric distribution of the apical plasma membrane during neurogenic divisions of mammalian neuroepithelial cells. **23**, 2314–2324 (2004).

86. Haydar, T. F., Ang, E. & Rakic, P. Mitotic spindle rotation and mode of cell division in the developing telencephalon. (2002).

87. Noatynska, A., Gotta, M. & Meraldi, P. Mitotic spindle (DIS)orientation and DISease: cause or consequence? *The Journal of cell biology* **199**, 1025–1035 (2012).

88. Jonassen, J. a, San Agustin, J., Follit, J. a & Pazour, G. J. Deletion of IFT20 in the mouse kidney causes misorientation of the mitotic spindle and cystic kidney disease. *The Journal of cell biology* **183**, 377–384 (2008).

89. Huang, K. *et al.* Function and dynamics of PKD2 in Chlamydomonas reinhardtii flagella. *The Journal of cell biology* **179**, 501–514 (2007).

90. Qin, H. *et al.* Intraflagellar transport is required for the vectorial movement of TRPV channels in the ciliary membrane. *Current biology : CB* **15**, 1695–1699 (2005).

91. Lechtreck, K.-F. *et al.* The Chlamydomonas reinhardtii BBSome is an IFT cargo required for export of specific signaling proteins from flagella. *The Journal of cell biology* **187**, 1117–1132 (2009).

92. Qin, H., Diener, D. R., Geimer, S., Cole, D. G. & Rosenbaum, J. L. Intraflagellar transport (IFT) cargo: IFT transports flagellar precursors to the tip and turnover products to the cell body. *The Journal of cell biology* **164**, 255–266 (2004).

93. Firestone, A. J. *et al.* Small-molecule inhibitors of the AAA+ ATPase motor cytoplasmic dynein. *Nature* **484**, 125–129 (2012).

94. Richey, E. a & Qin, H. Dissecting the sequential assembly and localization of intraflagellar transport particle complex B in chlamydomonas. *PloS one* **7**, e43118 (2012).

95. Dictenberg, J. B. *et al.* Pericentrin and gamma-tubulin form a protein complex and are organized into a novel lattice at the centrosome. *The Journal of cell biology* **141**, 163–174 (1998).

96. Heald, R. *et al.* Self-organization of Microtubules into Bipolar Spindles Around Artificial Chromosomes in Xenopus Egg Extracts. *Nature* **382**, (1996).

97. Whyte, J. *et al.* Phosphorylation regulates targeting of cytoplasmic dynein to kinetochores during mitosis. *Journal of Cell Biology* **183**, 819–834 (2008).

98. Kotak, S., Busso, C. & Gönczy, P. Cortical dynein is critical for proper spindle positioning in human cells. *The Journal of cell biology* **199**, 97–110 (2012).

99. Kiyomitsu, T. & Cheeseman, I. M. Chromosome- and spindle-pole-derived signals generate an intrinsic code for spindle position and orientation. *Nature cell biology* **14**, 311–317 (2012).

100. Lu, M. S. & Johnston, C. a. Molecular pathways regulating mitotic spindle orientation in animal cells. *Development* **140**, 1843–1856 (2013).

101. Follit, J. A., Xu, F., Keady, B. T. & Pazour, G. J. Characterization of Mouse IFT Complex B. *Cell Motility and the Cytoskeleton* **66**, 457–468 (2009).

102. Westerfield, M. *The Zebrafish Book; A Guide for the Laboratory Use of Zebrafish (Brachydanio rerio)*. (University of Oregon Press: Eugene, 1993).